Dissipation of vibration energy using viscoelastic granular materials

A thesis submitted to the University of Sheffield for the degree of Doctor of Philosophy in the Faculty of Engineering

Babak Darabi

Department of Mechanical Engineering

University of Sheffield

April 2013

Abstract

This work addresses the way in which a viscoelastic granular medium dissipates vibration energy over broad ranges of frequency, amplitude and direction of excitation.

The viscoelastic properties (modulus and loss factor) of polymer particles are obtained experimentally both by deriving the master curve of the material and by measuring the stiffness of these spherical particles at different frequencies using a test rig designed for this purpose. Three dimensional Discrete Element Method (DEM) is used to develop a numerical model of the granular medium and is validated by comparison with experimental results. Despite the simplifications the model was found to be in good agreement with experiments under vertical and horizontal vibrations with different numbers of particles over a range of frequencies and amplitudes of excitation.

The study is extended to investigate different phases that occur under vibrations of granular materials. The low amplitude vibrations when the particles are permanently in contact without rolling on each other is called solid phase. In this phase, most energy is dissipated internally in the material. A theoretical/numerical approach is considered for this phase and it is validated by experiment. At higher amplitude vibrations when the particles start to move and roll on each other (the convection phase) there is a trade-off between energy dissipation by friction and viscous/viscoelastic effects. Energy dissipation is relatively insensitive to the damping of individual particles. At extremely high amplitude vibrations particles spend more time out of contact with each other (the particles are separated from each other – gas region). It can be seen the particles with lower damping reach the gas region earlier because they are less sticky and more collisions can happen so although the damping for each individual particle it less, the total damping increases.

The effect of parameters of particles on energy dissipation is also studied using sensitivity analysis. The benefit of doing this is to better understand how each parameter influences the total system damping.

Acknowledgments

First of all I would like to express my deepest gratitude to my supervisors, Dr. Jem Rongong and Professor Keith Worden, for invaluable guidance, support and encouragement throughout the course of my research.

This thesis would not have been possible without the support of many people. My warmest thanks extend to all the friends of the Dynamic Research Group and in particular, Dr. Charles Eric Lord for his help and advice during my research.

Lastly, I would like to thank my parents, sister and brother. Their moral support was always there in the form of well wishes for my PhD.

Thank you all!

Table of Contents

List of Figures

List of Tables

Nomenclature

A	Area in contact of cylindrical test specimen
a	Radius of contact area of particles
b	Length of the container of particles
c	Viscous damping constant
C_{eq}	Equivalent damping constant
C_{eff}	Wave speed in the homogenous solid
d	Diameter of spherical particle
d_i	Material incompressibility
d_o	Overlap of two entities (particle-particle or particle-wall)
E	Young's modulus
E_o	Young's modulus at temperature T_o
E^*	Effective Young's modulus in contact of two entities
E_{eff}	Effective Young's modulus of the homogenous solid
F	Force
f	Frequency of excitation in Hz
f_r	Reduced frequency in master curve
G	Shear modulus
G_n	Shear modulus for n^{th} element of viscoelastic model
G_{rel}	Relaxation modulus in time domain
G^*	Complex shear modulus
G_{real}	Real part of shear modulus
G_{img}	Imaginary part of shear modulus
G_e	Equilibrium or long-term shear modulus
G_0	instantaneous (initial shear) modulus
g_n	Dimensionless form of shear modulus
g	Acceleration due to gravity

h	Depth of granular materials
h_0	Initial depth of granular materials
I	Moment of inertia
$\bar{I}$	Deviatoric strain invariant
K	Bulk modulus
K_r	Redirection factor in the granular medium
k_{bs}	Stiffness of bias spring
k	Stiffness of particle
l	Gap clearance of particles' container
L	Length of cylindrical test specimen
m	Mass of particle
m_{eff}	Effective mass of entities in contact
p	pressure
P	Power dissipated
R	Radius of particle
R^*	Effective radius in contact of two entities
S	Shape factor
T	Temperature
t	Time
U	Strain energy
W	Energy dissipated
w	Width of the container of particles
X	Displacement amplitude of excitation
$x, \dot{x}, \ddot{x}$	Displacement, velocity and acceleration
τ	Relaxation time in viscoelastic model
ε	Strain
σ	Stress
υ	Dynamic viscosity
ν	Poisson's ratio
v	Contact velocity of two entities
Γ	Dimensionless acceleration
α	Displacement of each particle after static loading

δ	Displacement approach of two particles in contact
ϕ	Packing fraction of spheres
η	Loss factor
μ	Coefficient of friction
ρ	Density of particle
ρ_{eff}	Effective density of the homogeneous solid
ζ	Damping ratio
$\omega, \dot{\omega}$	Angular velocity and acceleration

1 Introduction

It is often desirable to reduce the weight of structures and machines for performance and economic reasons. However, reducing the weight can, at times, cause vibrational problems. The control of vibrations is therefore vital in designing many structures. Failure to address vibrations issues can lead over a period of time, to catastrophic failure due to fatigue. To eliminate or reduce the vibrations to an acceptable level, damping may be added to a structure to remove energy from the system and dissipate it as heat.

There are many passive vibration reduction techniques available. Vibration isolation is one of the techniques used to reduce vibrations between structures and vibrations source. The airplane landing gear is an example of vibration isolation, however it needs the source of the vibrations to be separated from the body which is not possible in all cases. Vibration absorption technique is another technique that stores the energy in a separate mass-spring system and applies to discrete frequencies. An absorber requires tuning and if the system moves away from the target frequency, the absorber may amplify the vibrations. The use of viscoelastic material layers attached to structures is another technique which is used to increase damping. In this technique, bending deformations of the base structure cause deformations in the viscoelastic material that dissipate vibration energy [1]. However applying layer damping treatments to large surface areas can be expensive, add weight to the structures and require complex shapes for practical applications. In some cases, the

high strain areas may not be accessible making the use of viscoelastic layer dampers difficult.

Particle dampers are an alternative technique for damping structural vibrations and are particularly suitable for hollow structures. A particle damper comprises a granular material (e.g. polymer spheres or metallic beads) enclosed to the structure. Figure 1.1 is an example of a spacecraft structure with integrated particle dampers that were located at the points of highest acceleration.

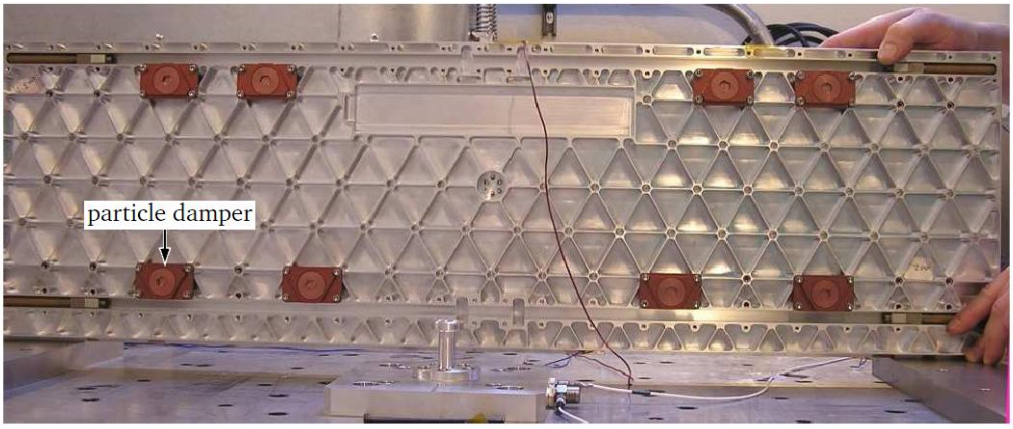

Figure 1.1: Spacecraft structure with integrated particle dampers [2, 3].

Granular materials are found in a variety of forms and are used in many applications. In a general sense, the term granular refers to several discrete particles. Unlike other materials, the behaviour of granular materials, when excited, often resembles various thermodynamic phases (solids, liquids and gases) [4, 5]. Therefore, it is complicated to describe their behaviour. During the various phases, different levels of elastic and plastic interactions and frictional contact occur. Vibration energy is dissipated through these inelastic collisions and also from the friction between the particles making them suitable for damping of vibrationally excited structures.

One particular advantage to granular materials is their level of compliance. Because they possess fluid-like properties, they can easily be used for filling structures with complex geometries such as by placing them within the voids in honeycomb and cavities in hollow structures. To extend this, they can easily be removed too making them serviceable. Using granular materials as dampers can also increase damping without significant compromise to the design or increasing total mass of the structure.

Damping strategies that use granular materials to attenuate structural vibrations generally rely on one of two very different mechanisms for dissipating energy. For low vibration amplitudes, where particles remain in contact and do not slip relative to one another, damping depends on the ability to maximise energy dissipation within individual particles [6, 7]. However, if the excitation is such that separation and slip between particles does occur, optimisation of the energy loss at the contact points becomes important and even particles with low internal loss, for example steel ball bearings, can give vibration suppression exceeding that of the material with high loss factor. Traditionally, particle dampers utilise low-loss hard spheres, such as metal particles, that are small in diameter. These dampers generally work well for large temperature ranges since the material is not as sensitive to temperature as viscoelastic materials [8-10].

In practice, it is often desirable to have good damping performance over a wide range of amplitudes. For low amplitude vibrations, the most effective particles tend to be made from low modulus materials with a high loss factor.

Viscoelastic materials (VEM) are widely used as amplitude-independent damping elements in engineering structures. It has been shown that viscoelastic particles are effective as granular fillers for low amplitude vibrations for hollow structures. One of the advantages for this kind of filler is that they are low density, minimising the added weight to structures. At low vibration amplitudes, a granular viscoelastic medium behaves as a highly flexible solid through which stress waves travel at low velocity. A filler of this kind reduces the resonant vibrations in the structure over frequency ranges in which standing waves are generated within the granular medium. A characteristic of particle dampers is that noise can be produced from the collisions of the particles. When metal spheres are used this has been shown to be higher than for viscoelastic particles. This also holds for the reception of acoustic noise [11, 12].

It is necessary to study the dynamic behaviour of viscoelastic particle dampers (PD) as they have high levels of damping and their properties change with frequency. Very little information is currently available for systems based on moderately large particles made from materials with significant internal energy dissipation capacity.

This thesis will focus on the behaviour for VEM particles under different excitation levels and under vertical and horizontal excitations. In this work, experiments are performed and validated using simulations. The simulations are based on the Discrete Element Method (DEM). DEM is a numerical method to simulate this medium and is based on the application of Newton's Second Law to the particles and force-displacement law at the contacts.

1.1 Aims and Objectives of this Research

The current research aims to understand the behaviour of granular systems comprising viscoelastic particles within a structure subjected to sinusoidal vibration excitation.

The main objectives of this research are listed below.

- Investigate existing methods for predicting and measuring the vibration damping performance of viscoelastic granular systems at low vibration amplitudes where the medium behaves as a solid.
- Design and manufacture a test rig to measure the properties of individual viscoelastic particles.
- Use the Discrete Element Method to develop a model that predicts the energy dissipation of a granular medium consisting of spherical polymeric particles.
- Investigate the behaviour of viscoelastic granular systems at higher amplitudes, where the particles collide with each other.
- Consider the sensitivity of the power dissipated by a granular medium to physical parameters.

1.2 Brief Summary of Chapters

This thesis is structured as follows:

Chapter 2

In Chapter 2, the available literature on the topic is reviewed. Research on granular materials in different scientific fields such as physics and agriculture are briefly mentioned. Benefits and limitations and also different parameters which are effective

in the behaviour of existing granular materials as particle dampers are addressed followed by different applications in the structures. A modelling strategy of this medium by using the Discrete Element Method is described. As this research ultimately utilises polymeric particle dampers (high-loss), recent developments in this field are explained. At the end, the use of polymeric particles as a low density and low-wave speed medium is reviewed.

Chapter 3

Different models for viscoelastic materials are discussed. The viscoelastic properties namely, Young's modulus and loss factor of the principal polymer to be studied in this work are extracted by experiment at different frequencies and temperatures. The Master curve for properties is developed. A suitable Prony series model to represent viscoelastic behaviour is fitted to the data. Two different approaches for measuring of damping of the granular systems and individual particles which were used in this thesis are also explained.

Chapter 4

Chapter 4 provides the understanding regarding the effect of low-amplitude excitation on the energy dissipation of viscoelastic granular medium. In this case it has been shown that the medium can be approximated as a solid homogenous material attached to the host structure. Energy is dissipated by the generation of internal standing waves within the granular medium. A theoretical/numerical approach was taken. In this approach the equivalent elastic properties of the medium were estimated and then used in conjunction with finite element analysis. In low-amplitude vibration the particles are in contact without sliding and behave as an equivalent solid zone. In this case properties of medium change significantly over the frequency range considered. This chapter is concluded by drawing a comparison between approach taken including numerical analysis and experiment is presented.

Chapter 5

The stiffness contact properties in both normal and tangential direction for individual spherical particles are further explored by using finite element analysis and compared with related theories. The models were validated using impact/rebound

and steady-state tests. A test rig was designed to measure the properties of spherical particles. This chapter is concluded by measurement of the dynamic stiffness and damping for individual particles which are used for the numerical modelling of the granular medium in Chapter 6.

Chapter 6

A numerical approach based on Discrete Element Method (DEM) is introduced to identify the behaviour and energy dissipated of granular medium. The three-dimensional DEM used here is based on the commercial software, PFC3D v4.1. All steps in order to build the model are explained. This chapter is concluded by simulating the granular medium which was validated by experiments in Chapters 4 and 7 and further discussion by parametric studies.

Chapter 7

The purpose is to understand the performance of high-loss granular fillers at higher amplitude vibrations. The approach taken involves experimental and numerical studies and relates observed behaviour to existing understanding. Validation of the numerical model for predicting energy dissipation in vertical vibration (same direction as gravity) of a granular medium comprising several hundred particles is described. The validated model is then used to investigate the importance of different parameters and discussed on results. Finally, new conclusions regarding the behaviour of this type of granular system are presented.

Chapter 8

A sensitivity approach is taken to investigate the effectiveness of particle properties including, stiffness, damping ratio and friction coefficient on energy dissipation of the granular medium. Furthermore to understand of the behaviour and effects of friction better, a simple SDOF sliding system is modelled. It was shown that the power dissipated of the system is more sensitive to very low friction coefficient and damping ratio.

Chapter 9

Comprehensive conclusions are detailed, and areas for the future work are recommended.

The main contributions to the knowledge:

- Understanding of the behaviour of a granular damper made from viscoelastic particle and excited at different frequencies and amplitudes.
- Development of the DEM to model this type of damper.
- Investigation on theory/numerical approach of viscoelastic granular medium when it is subjected to *low amplitude vibration* (the particles are permanently in contact and without any rolling on each other).
- Understanding of effective particle properties (coefficient of friction, loss factor and stiffness) on the energy dissipation of the granular medium.

2 Literature Review

2.1 Aspects of a Granular Medium

Granular materials consist of grains in contact and surrounding voids [13]. These grains can be made of nearly any material and can be nearly any morphology. Materials in granular form are widely employed in various industries such as mining, pharmaceutics and agriculture. The study of granular materials has long been an active area of research. In 1895 when considering grain silos, Janssen [14] proposed a model based on a coefficient describing the redirection of gravity-induced forces toward the wall and derived an equation for the relationship between pressure on the walls and depth of grains. Describing the flow of the granular material has been a consistent problem that still persists [15, 16]. The mechanics of granular materials is often studied by formulating the macro-behaviour in terms of micro-quantities [16], where the dynamic behaviour is derived from the analysis of individual particles. Researchers have studied the granular medium for different purposes – some important topics are described in this section.

2.1.1 Segregation, bed depth, heaping and arching forms

Granular materials display several phenomena when exposed to dynamic loading, such as: segregation, heaping and arching. Segregation occurs when materials of either varying size or densities exist and the materials with like sizes and densities are attracted to one another. The first recorded explanation of the segregation

phenomenon in three-dimensions was provided by Oyama [17]. He studied two granular materials differing by their density, shape and size to find the fundamental laws governing the physics of the segregation process. Wassgren [18, 19] investigated the different behaviour of granular materials under vertical vibrations. He identified different behaviours in deep particle beds. In his work, a deep bed was defined as,

$$\frac{h_0}{d} > 4 \tag{2-1}$$

where h_0 is initial depth and d the diameter of particles. He also found that the particle bed behaved differently at different levels of dimensionless acceleration, defined as,

$$\Gamma = \frac{X\omega^2}{g} \tag{2-2}$$

where X is the displacement amplitude, ω is the excitation frequency in *rad*/*s* and g is the acceleration due to gravity. Where $\Gamma \approx 1.2$ a phenomenon known as heaping was observed. Heap formation results from the convection flow of particles as shown schematically in Figure 2.1. As Γ was increased to 2.2 (this value changes slightly depending on the bed depth value) small-amplitude surface waves began to appear on the slope of the heap. Increasing Γ further causes the heap to disappear and surface waves become clearer. As Γ approached 3.7, the sections of the particle bed could oscillate out-of-phase producing the behaviour known as arching where nodes and antinodes appear on the bed.

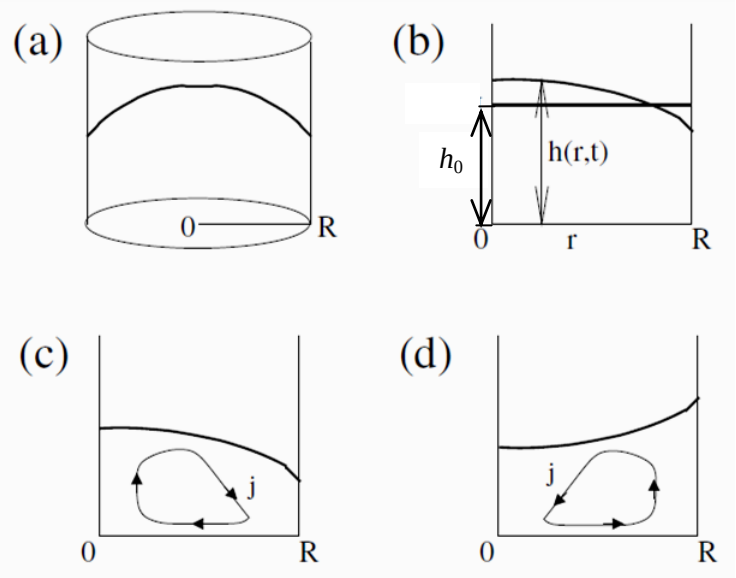

Figure 2.1: Heap and the convection roll of a vibrated container, a) cylindrical container. b) Initial height h_0 and *h(r,t)* is height of pattern formation at any position and time. c) Downward heap and convection current profile. d) Upward heap and convection current profile [20].

2.1.2 Phases in granular material beds

Some researchers have identified different phases in granular material beds subjected to vibration – it is anticipated that similar phases may be present in particle dampers. The subject of the onset of fluidization for vertically vibrated granular materials was presented by Renard *et al.* [21]. They proposed that there are several phases in granular materials subjected to vertical vibration. The first phase is similar to a solid that moves as a block with one layer surface in contact with the container. This occurs when $\Gamma < 1$. As Γ increases, the bulk of the bed will remain nominally solid but some of the particles on the surface may begin to fluidise. The next phase is a bouncing bed where the particle bed leaves the lower surface exciting the bed and is temporarily airborne. In this phase, critical dimensionless acceleration is defined as,

$$\Gamma_c = \frac{\pi(1-\varepsilon_p)}{(1+\varepsilon_p)} \qquad (2\text{-}3)$$

where ε_p is the coefficient of restitution for collisions with the container. The next phase reported is a granular gas, where the particles in the bed move about randomly in relation to one another [4,5, 22].

The phases in horizontally excited granular beds are less clearly defined because particles are under different static pressures along the plane perpendicular to the direction of excitation. This results in different behaviour at different vertical positions in the particle damper under excitation. The first reported phase is a glassy solid phase which occurs when $\Gamma << 1$. The second phase transition is to a liquid like phase where convection occurs. It is not entirely clear whether this is a phase in itself or just a transition between solid and gas phases. The final phase is a gas phase which the particles move randomly in relation to one another [8, 23, 24].

Tennakoon *et al.* [25, 26] also performed experimental observations of the onset of flow for a horizontally vibrated granular system. They observed in convection flow that grains rise up in the middle of the container and flow transversely along the surface towards the side walls and then sink at the wall boundaries giving the top surface of the liquefied layer a dome shape. They showed that the initial acceleration for transition depends on whether vibration is increasing or decreasing. If, when increasing vibration level, a critical value Γ_1 is reached, a dome is formed. Reduction in amplitude reduces the height of this dome but does not remove it until the amplitude drops below a second critical value Γ_2 after which flow stops. They explained that this phenomenon happens because the onset of flow must occur by the breaking static friction.

Tennakoon and Behringer [27] studied the flow characteristics that appear in a granular bed subjected to simultaneous horizontal and vertical sinusoidal vibrations. The heap formation and the onset of flow are captured. They showed that, for instance, in the case that there is no phase difference in horizontal and vertical vibrations as Γ_h (horizontal dimensionless acceleration) is increased at fixed $\Gamma_v = 068$ (vertical dimensionless acceleration). In this case the vertical acceleration is less than 1; therefore no convective flow occurs due to purely vertical shaking. Static heap is gradually formed between $0.39 < \Gamma_h < 0.6$ when Γ_h exceed from 0.6,

the top layer along the slope liquefies and starts to decreasing the average slope. A simple Coulomb friction model was used to capture the features observed in experiments. The friction model simply considered a block static friction coefficient which is placed on a surface inclined at a heap angle. King [28] investigated the stability conditions of the surface of a granular pile under horizontal and vertical harmonic vibrations and the relation between the effective coefficient of friction and the slope angle. The experimental findings were interpreted within the context of a Coulumb friction model that showed that there are deviations from the predictions of the Coulumb model at higher frequencies and small grains (75-150 micron). From this, a parameter was introduced that is a function of the frequency. This parameter is used as a factor to reduce the effective magnitude of the horizontal and vertical forces.

2.1.3 Packing and bulk density

One of the key parameters controlling the performance of a granular medium is its packing density. Often, this can be approximated by sphere packing theories – studied in many fields including; condensed mater physics [29], to investigate the different configurations due to crystals; computer science and mathematics on group/number theory [30,31]. From this, it has been shown that a random arrangement results in an amorphous structure with a packing factor of 0.64 [32] or less while crystalline packing results in higher density with face-centred cubic (FCC) structures (See Figure 2.2) achieving a packing factor as high as 0.74.

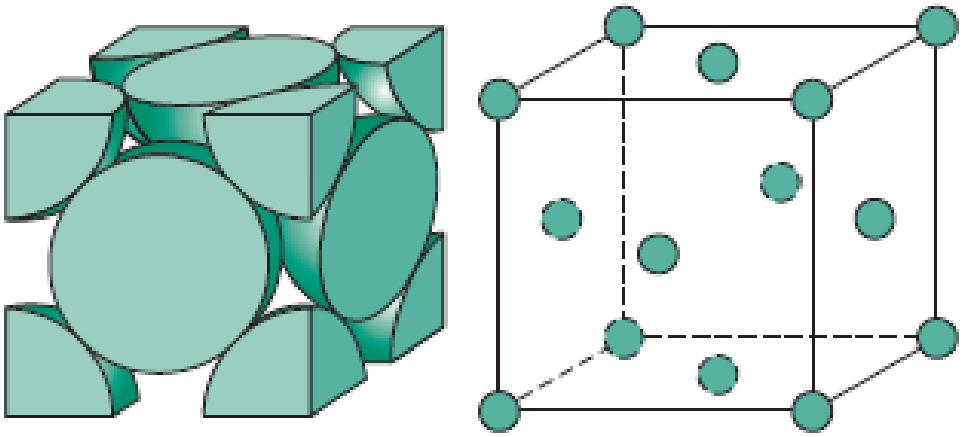

Figure 2.2: Face-centred cubic (FCC) lattice, this is the highest fraction of space occupied by spheres, theoretically is equal to 0.74 [33].

The arrangement of particles in a granular medium affects the bulk density of the medium. This is important in industries that involve transportation and packing. The identification of the factors that affect bulk density is important. A common way to increase bulk density is to employ vibration. Knight and Nowak [34, 35] considered that the way in which the density of a vibrated granular system slowly reaches a final steady-state value. They found an experimental equation that explained the related bulk density of the granular medium to the amplitude and frequency of acceleration which were applied to the container. Zhang and Rosato [36] showed that for a vessel filled deeply with acrylic spheres, when the ratio of excitation amplitude to the diameter of spheres is between 0.06 and 0.1, the maximum in bulk density is achieved using $5 < \Gamma < 7$ with improvement more than 5%. By increasing Γ, the improvement in the bulk density slightly decreases.

2.1.4 Other applications

Due to the similarities of flowing granular materials to fluids, some researchers use hydrodynamic models such as conservation of energy and constitutive models (relation between stress field and energy flux) to deal with granular material behaviours [37, 38]. Some researchers model granular gases by hydrodynamic equations of motions. Analogous to definitions of different phases for granular materials, in the case of molecular gases/liquids, the macroscopic field also has been defined by expressions such as granular temperature. Granular temperature is defined as the ensemble average of the square of the fluctuating velocity of the particles [39].

2.2 Traditional dampers containing metal spheres

An important application of granular materials is in passive damping of vibration. A particle damper comprises a granular material enclosed in a container that is attached to or is part of a vibrating structure. There are two types of dampers: an impact damper and a particle damper. An impact damper is composed of a container with

one large mass whereas particle dampers consist of a large number of smaller masses – see Figure 2.3.

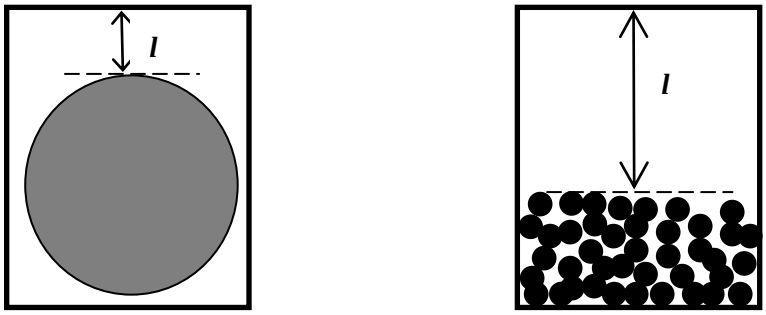

Figure 2.3: Impact damper (left) and particle dampers (right), ***l*** is the gap inside the container [40].

There has been considerable research attention given to amplitude-dependent behaviour in particle dampers where the granular material is in the form of small metal spheres [41-43]. The main advantage of metal spheres is temperature independence and they can be used in harsh environmental conditions. However, metal spheres can increase the total weight of the system and during the impact process the impact loads transmitted between the particles and the walls can cause high levels of noise. These also can create large contact forces resulting in material deterioration and plastic deformation.

2.2.1 Impact damper

Impact dampers are used in special applications. They should be tuned for a specific frequency and specific amplitude of excitation [40]. Because of this limitation, this type of damping rarely is used especially for applications in which operating conditions change.

The impact of a single particle, in a container with a ceiling, under the influence of gravity and harmonically base excited was studied by Ramachandran *et al*. [44]. The effects of various parameters such as the gap clearance (Figure 2.3) on damping were investigated. It was concluded that the damping increases by increasing the gap. However for higher gap values, the dynamics of the particle becomes very complex and damping decreased. There is an intermediate range with optimum high loss

factors. Popplewell et al [45] discussed analytically on the effectiveness of damping in a SDOF system (host/primary structure) using an impact damper. The procedure for an optimum impact damper showed that under sinusoidal excitation, damping increases by increasing the mass of the damper and also by decreasing the damping ratio of the host structure. Li [46] studied the effect of an impact damper in MDOF primary system. One of his results showed that only for the first mode, the higher mass ratio is better for damping performance while for the second mode, it is worse, in contrary with an SDOF system.

2.2.2 Metal particle dampers and their applications

Particle dampers can be added to a structure by attaching them to the outer surface or, for hollow structures, by filling voids. The first method is a quick-fix [10] solution for an existing design and the latter method saves space and does not compromise the structural integrity.

Honeycomb structures are convenient for use with particle dampers as they have large number of voids that can be filled. Vibration attenuation was achieved without significantly shifting the natural frequency of a laminated honeycomb cantilever beam [47]. It was concluded that in order to avoid increasing mass, particles should be inserted into particular cells where the maximum amplitude normally occurs. In sandwich structures, partial filling with sand within the honeycomb core achieved increase by factor of 10 in the damping, although weight increased about 75% [48].

Simonian *et al.* [49-51] employed more standard applications of particle dampers by mounting a hollow base plate to a structure. The base plate had machined cylindrical cavities that were filled by different type of particles. It was shown that there is an optimum fill ratio for particles and effectiveness, which drops at very high frequencies (>1000 Hz). Tungsten powder generally showed better performance than 2mm tungsten spheres. As another application analogous to SDOF systems, a piston-base particle damper under free vibration was studied [52]. In this case the piston was attached to the system from one side, and the other side was submerged in a container consisting of particles. It was concluded that the piston immersion depth was a crucial parameter for damper design and that there is a critical length above which its effect on the damping is less significant. It was also found that nanometre

size particles showed a poor damping because the piston displacement caused a hole in this medium during vibration due to adhesion effects (Van der Waals forces) and the particles could not flow properly.

2.2.3 Metal particle dampers and design procedures

There are many studies for characterization of particle dampers and design procedures. Papalou and Masri [53-55] studied key parameters such as container dimensions and the level of excitation. They introduced design procedures based on an equivalent single particle damper, under random excitation. One of their results showed that the response amplitude reduces by increasing the distance between walls which are perpendicular to the direction of excitation although there is an optimum for this clearance.

A design methodology for particle dampers was recommended by Fowler *et al.* [56]. They showed that, particle mass has a significant effect on the damping, but coefficient of friction does not. Also modelling and analytical techniques of particles as vibration control devices (vibro-impact dynamics) have been considered [57]. The optimum design strategy for maximizing the performance (i.e., response attenuation capability) of particle damping under different excitations was discussed and showed that properly designed particle dampers (vertical and horizontal) can significantly attenuate the response of lightly-damped primary systems (SDOF and MDOF) [58].

2.2.4 Metal particle dampers under vertical excitation

Hollkamp *et al* [59] performed experimental work on a cantilever beam with 8 holes along its length and filled with particles. Their findings showed that the value of damping strongly depends on the excitation amplitude. The damping increased with amplitude to a maximum and then decreased by a further increase in amplitude. The optimal location of the particles is the area of highest kinetic energy and it is not linearly cumulative so that the summation of damping which obtained from placing particles individually in chambers is not comparable to that obtained those same chambers are simultaneously filled.

Extensive analysis of the behaviour of particle dampers was performed by Friend and Kinra [60-61]. An analytical approach was derived for a cantilever beam with particle dampers attached at the tip. The performance also was estimated as an SDOF model. It was found that the damping was highly nonlinear, amplitude dependent and depends on the clearance (particle fill ratio) inside the enclosure on the particle dampers. It was shown from three different clearances that the higher clearances gives higher damping (total mass was kept constant and $1 < \Gamma < 25$). The previous work was extended and investigated on different materials (steel, lead and glass with similar diameter and clearance) and showed that the normalised specific damping capacity with total particle mass is independent of those materials [62].

The Power Flow method was first used by Yang to find damping from experimental analysis of particles in an enclosure under vertical excitation [40]. In this application, the average power dissipated as active power (terms borrowed from electrical engineering) and maximum power trapped (e.g. kinetic energy of particles) named as reactive power, by the vibrating particle damper can be estimated directly by cross spectrum of the force and response signal of the particle dampers [10].

2.2.5 Metal particle dampers under horizontal excitation

Experimental work on small metal spheres in a disc shape container whose axes were horizontal and parallel to the applied sinusoidal vibration was carried out by Tomlinson *et al* [63,64]. They examined the behaviour of particles in a damper attached to a SDOF system under different amplitudes of excitation. It was observed that by increasing the excitation level, the damping rises dramatically and the resonance frequency of the SDOF system shifts gradually towards that measured with the empty particle damper (dashed line − Figure 2.4). It also can be seen that at the very low amplitude level ($0.1g$) the particles behave as an added mass and therefore the resonance frequency of the system decreases from around 246 Hz (empty container) to 234 Hz. It was shown that the cavity geometry has a very important role in the particle behaviour. By increasing the aspect ratio (length divided by the diameter of the cylindrical damper container) particle fluidisation appeared at a lower excitation level and so more FRF curves shifted from left to right

(see Figure 2.4). Also it was shown that for smaller aspect ratio, higher excitation amplitudes cause better damping and conversely at higher aspect ratio, smaller excitation amplitude could give better damping. Nonlinear behaviour of metallic particle dampers also observed experimentally in the literature [65].

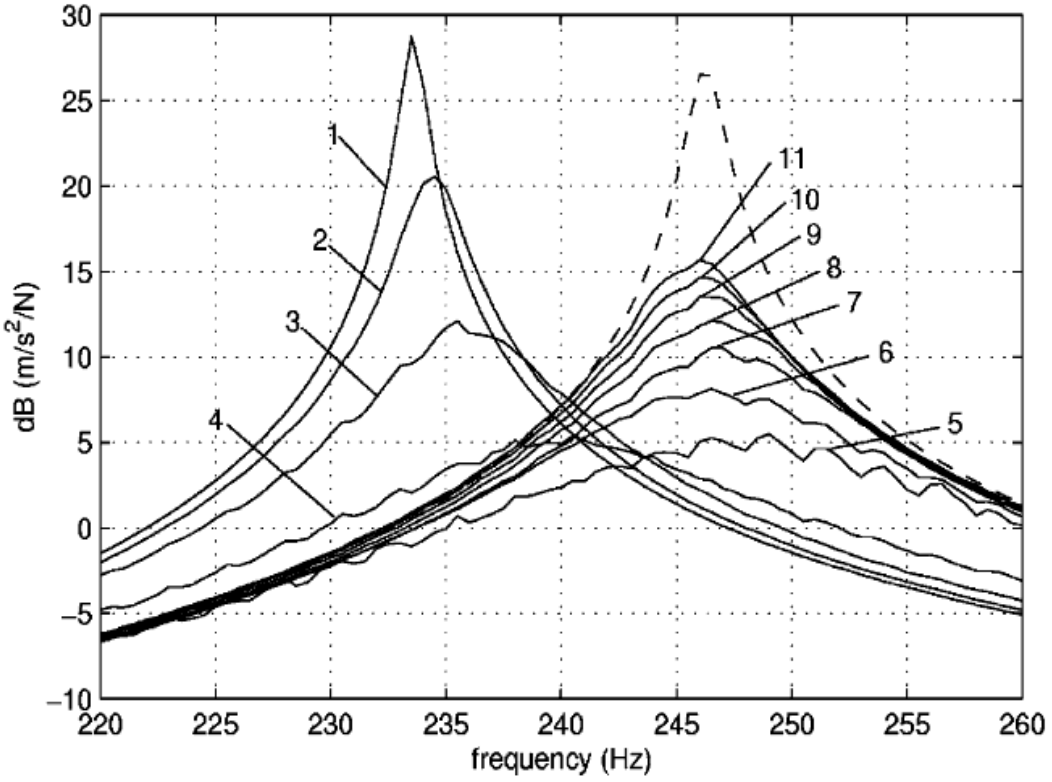

Figure 2.4: Dynamic behaviour of SDOF system with a PD, FRF marked 1-11 shows different acceleration amplitude from 0.1*g* to 40*g* and aspect ratio 0.4, [63]

The influence of mass ratio and container dimensions of particles were studied in multi-unit cylindrical containers (vertically seated on a primary support – as a base – which has horizontal harmonic motion). The results showed that in containers with a smaller radius, when the mass ratio of the particles is lower, better damping in the system appears. This happens because for the higher mass ratio it is more difficult for the granular particles to move as the cavity radius decreases. It was also shown that there is an optimum cavity radius [66]. In transient vibrations on a cantilever beam with particle dampers attached on the tip, it was concluded that the damping capacity significantly increase for $0.25 < \Gamma < 1$ and decreases for greater than 1 [67].

A new concept named effective momentum exchange (EME) was used to quantitatively characterise some of the physics of particle dampers. It was shown that lower damping ratios lead to less reduction of the primary system's response in small-size container and more reduction in large-size container, compared to higher damping ratio. This phenomenon also can be seen in this thesis that in gas region (particles moving completely separated – analogy to large-size container) particles with lower damping ratio give higher total damping [9].

2.2.6 Metal particle dampers under centrifugal excitation

Some researchers considered particle damping for applications where high centrifugal loads exist such as turbine and fan blades. The performance parameters of particles under centrifugal loads were investigated [2,68]. A rotating cantilever beam filled with steel particle dampers in an aluminium container attached at the tip was tested. The tip of the beam was remotely activated vertically with a cam (the beam was in a free decay vibration mode) [2]. It was concluded that the ratio between the peak vertical vibration acceleration and the centrifugal acceleration is a fundamental property of the performance of particle dampers under centrifugal loads. It was shown that there are two zones of damping for low and high damping factor which these zones depend on that ratio. Zones are limited in terms of centrifugal loading beyond which the particles can not operate if the vibration amplitude is fixed.

2.3 Numerical Modelling for granular medium

There are many reasons for simulations of granular materials. One of the main reasons is that there is no comprehensive analytical theory on granular materials for example to reliably predict the behaviour of machinery in powder technology before they are produced. Experiments are expensive, time consuming and even sometimes dangerous [69]. Many researchers have studied the simulations of granular medium.

2.3.1 Event-Driven Method

The Event-Driven method in particle dynamic simulation methods uses the hard spheres model where particles are assumed rigid. In fact an event driven method is

used so that the particles undergo an undisturbed motion under gravity until an event (collision, particle-particle or particle-wall) occurs [70]. This method does not consider contact mechanics and the only needed properties are the coefficient of restitution for particle-particle and particle-wall impact and the mass and size of spheres. This method is useful where the typical duration of a collision is much shorter than the mean time between successive collision of a particle [69] and particles are only contact not more than one other particle, for example very dilute or granular gases. The principal assumption for using this method is at any time instant in the system one collision occurs of infinitesimal duration. By this method the simulation speed can significantly be increased. However only in cases where the assumption of isolated instantaneous collision can be justified can this method be applied.

2.3.2 Discrete Element Method

The Discrete Element Method (DEM) which attempts to replicate the motion and interaction of individual particles [71,72] has increasingly been used to analyse particle damper behaviour.

The calculations performed in the DEM alternate between the application of Newton's second law to the particles and a force-displacement law at the contacts.

Contact conditions used in DEM studies can vary in complexity. For calculation speed and simplicity, linear spring and dashpot representations and simple Coulomb friction elements have usually been used to describe the normal and tangential contacts between metal particles [8-10]. There is some evidence to show that appropriate linearization of the elastic contact forces does not significantly affect the calculated power dissipation [10].

For small metal spheres, DEM has been used to simulate damper performance under different vibration excitations.

In the steady-state vibration, two-dimensional DEM performed to simulate power dissipated in a granular medium consisting of beads up to 1mm in diameter and are compared with experiment. It was reported that the DEM simulation was able to

qualitatively reproduce major features found in the experimental data. However, quantitative agreements between experimental and DEM values were only possible within a small range of accelerations – high accelerations, and suggested that it is required further investigation [73]. The influence of mass ratio, particle size and cavity dimensions were investigated in horizontal excitation by DEM [74]. Other researchers also studied on particle dampers performance using three-dimensional DEM under steady-state vibrations [9,10, 75].

In transient vibration also simulations were performed on dissipation mechanisms of non-obstructive particle damping (NOPD) by using DEM and showed that how energy dissipated during inelastic collision due to momentum exchanged of particles and friction between them. NOPD is a vibration damping technique where placement of numerous loose particles inside any cavity built-in or attached to a vibrating structure at specific locations, based on finite element analysis to find energy dissipation through momentum transfer and friction [43]. The particles will damp the vibration for specific mode(s). The results showed great adaptability of NOPD to a wide frequency band. Also, they showed that for very small particle size, most of energy was dissipated by friction however for greater size (0.2 mm and same packing ratio) the impact energy dissipation is more than friction. They explained that the reason for the above phenomenon is that with the particle size increasing, the number of particles and, therefore, the number of contacts between particles and host structure and between particles has to decrease. This would cause lesser friction energy dissipation. Meanwhile, with the size increasing, according to the momentum principle, the impact force will increase [76]. Also by using three-dimensional DEM, simulations provided information of particle motions within the container during different regions and help explain their associated damping characteristics during transient vibration under different excitation amplitude [77].

Many researchers have used DEM for granular medium for other purposes. Two-dimensional DEM was used to simulate in a quasi-static granular flow in order to find pressure on walls of a silo during filling and discharge [78]. The flow pattern during filling and discharge in a silo with a hopper was predicted by DEM and velocity at different levels and pressure distribution on the walls was evaluated. Observations showed the importance of particle interlocking to predict a flow pattern and that was similar to real observations. Two types of particles, single-sphere and

paired-sphere (formed by clustering two spheres with aspect ratio1.5) were used. One of the results showed that paired-sphere produced flow pattern closer to the ones observed in the experiments [79-81]. The behaviour of particle interaction level is increasingly popular [82,83]. Determination of parameters of grains which are required for simulation in DEM was performed [84]. The volume of grains approximated to a regular geometrical shape and mechanical properties of grains measured by designing different apparatus and explained the uncertainty due to irregular particle shapes.

Studying and investigation of the damage to particles and segregation phenomenon in granular medium are other applications that researchers used simulation by three-dimensional DEM [85-89].

2.4 Vibration of granular materials comprising high-loss polymer particles

Viscoelastic polymers are widely used as amplitude-independent damping elements in engineering structures [90]. Figure 2.5 shows the behaviour of a general viscoelastic material whose properties change with frequency and temperature. At high temperature, the internal energy of the molecules allows them to move more freely, making the material softer. Softening also occurs at low frequency, because larger scale molecular deformation can occur. Conversely, at low temperature the internal energy and hence the mobility of molecules is low, resulting in high values of modulus. At high frequency, the modulus is also high because there is not sufficient time for large scale deformations to occur. In the transition zone, the loss factor is high because the modulus changes quickly and the material is unable to respond at the same rate as the excitation and a significant phase lag occurs. Therefore this transition zone is the best operating region for high damping viscoelastic material.

Commonly used treatments such as free and constrained layer damping for continuous or distributed mass structures are designed to operate in the transition region for optimum effectiveness [91]. However, dampers based on single or multiple surface layers perform less well on hollow tube and box sections because

effectiveness requires the damping layer to have significant stiffness in comparison to the substrate which is difficult to achieve [12]. Instead for such structures, high levels of damping can be achieved using high loss, flexible granular fillers [92].

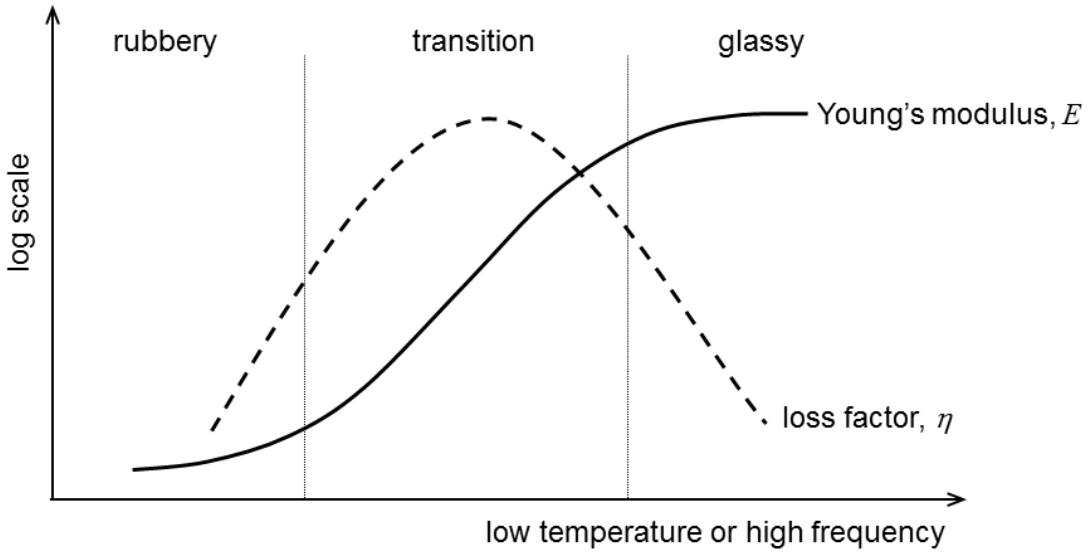

Figure 2.5: Variation in complex modulus of a typical viscoelastic material

Significant damping of structural vibration can be obtained by using viscoelastic spheres especially in hollow structures. One of the main advantages of the polymeric particles (fillers) is very low weight added to the host structure. Test results for box section beams filled with viscoelastic spheres have also been presented by Pamley *et al.* [11] and Oyadiji [93] and have shown to match theoretical predictions [12]. Oyadiji measured experimentally inertance frequency response functions of the beam in horizontal and vertical directions under free boundary conditions. This measurement was performed both with the cavity empty and with the cavity filled with different sizes of viscoelastic spheres. When the cavity was empty, the modal loss factors of the hollow steel beam were found to be between 0.2% and 1%. However when it was filled with the viscoelastic spheres the modal loss factor increased to a range of 2% to 31% .

For low amplitude vibrations (when the particles are in contact permanently), the most effective fillers tend to be made from low modulus materials with high loss factor [6]. Rongong [12] performed an experimental test on polymeric particle

dampers filled in a long glass tube (glass material because of small background damping). It was shown that at very low amplitude, the damping is high. However when the amplitude exceeds 1*g*, the decompaction of particles occur (causing the particles to lose contact with one another temporarily) and the damping drops significantly. At these higher amplitudes, interface friction becomes an important loss mechanism allowing the use of harder materials with low internal loss such as metals.

Walton [94] derived an analytical method to find the effective elastic modulus and effective Poisson ratio of a random packing for identical elastic spheres when they are in contact permanently (analogous to low amplitude vibration). The results are applicable for initial boundary conditions which cause compressive forces between any spheres in contact, this could include hydrostatic compression. The results are for two types of spheres, rough or perfectly smooth.

Viscoelastic granular fillers can also be used to absorb airborne noise. It was shown that the use of low-density granular materials can reduce structure borne vibrations. Granular materials utilise the effect of low sound speed in these structures without the problems of heavy added weight. [95].

2.4.1 Damping using low-density and low-wave speed medium

Experiments indicate that low-density materials can provide high damping of structural vibration if the wave speed in the material is sufficiently low.

Cremer and Heckel [96] discussed the transmission of waves in granular materials. They showed that using sand as a granular material and filled within an structure, it can be modelled as a continuum material and damping can be changed by adjusting dimensions so that standing waves happens in the granular medium at the resonant frequencies of the structure. Richard [97] performed experiments on sand-filled structures and studied the influence of different directions and amplitude of excitation. He also showed that maximum damping can be obtained at frequencies where resonances occur in granular particles. An aluminium beam coupled with low density foam layer under impact showed that the loss factor as high as 5% can be

obtained [98]. Another experiment performed with hollow beam filled with powder (average diameter 65 micron) showed high damping performance [7].

At low vibration amplitudes, a granular viscoelastic medium behaves as a highly flexible solid through which stress waves travel at low speeds. A filler of this kind can reduce resonant vibrations in the host structure dramatically over frequency ranges in which standing waves are generated within the damping medium [1,98]. Exploiting the flexible solid analogy, House [6, 99] used viscoelastic spheres in this way to damp vibrations in freely suspended steel beams. He explained that damping effect of viscoelastic layers is affected by motion of the layer in its thickness direction and can be improved by increasing the layer thickness or increasing the density of layers (reducing the wave velocity in viscoelatic material). This can also be achieved by reducing the effective modulus of the viscoelastic layer (making the layers as foam).

2.5 Summary

The key findings in the literature survey shows that granular medium has different patterns and different phases such as solid, fluidization and gas phases during vibrations which depend on the amplitude and direction of vibrations. Packing density is also one of the parameters that controls the performance of the medium. Granular particles can have effects on the damping of structural vibrations. DEM is one of the powerful numerical approaches that are used for modelling the granular medium. Viscoelastic particles as low weight added to the host structure and as a high level of damping in hollow structures have been proposed and used by a few researchers although with different methods and ways than this thesis [6,12,93]. At low amplitude vibrations, it is shown that viscoelastic particles behave as highly flexible solid which can cause high level of damping in the structures.

This thesis studies the amplitude-dependent energy dissipation of a granular system composed of moderately large polymeric spheres that display significant viscoelasticity. Its purpose is to understand the performance of granular dampers whose properties lie between those of classical particle dampers and high-loss

granular fillers. The prediction of power dissipated is studied when the granular medium is at low amplitude excitation (steady-state horizontal excitation) where the particles are randomly dropped in a container. As the vibration amplitude increases, particles in granular systems temporarily lose contact or slide relative to each other and the flexible solid analogy no longer holds. In these conditions, it has been demonstrated that experimentally, damping levels decrease significantly. To date however, there has been no methodical study that explains the important parameters controlling such behaviour. The approach taken involves experimental and numerical studies and relates observed behaviour to existing understanding. The three-dimensional DEM model has been created to predict the behaviour of such medium.

3 Viscoelasticity and Damping

3.1 Introduction

In this chapter different viscoelastic models are discussed. Two particular methods for measuring the damping (power dissipated and hysteresis loop methods) which are used in next chapters are explained. As viscoelastic properties of the material of spherical particles are needed in the next chapters, therefore the procedure for master curve extraction is discussed. In order to measure the viscoelastic properties of particles and extraction the master cure, a sample from particle's materials is made and insert in Dynamic Mechanical Thermal Analysis (DMTA) equipment, the procedures are discussed thereafter. By using the master cure one can obtain the viscoelastic properties (Young's modulus and loss factor) at any temperature and any frequency. The Prony series which are fitted to material properties of the viscoelastic sphere are derived. Those Prony series are used for Finite Element modelling of spheres in Chapter 5.

3.2 Viscoelastic properties of materials

A material is termed viscoelastic if it can simultaneously store and (through viscous forces) dissipate mechanical energy. Most common damping materials displaying viscoelastic behaviour are polymers such as plastics and rubbers, however significant viscoelasticity can also be detected in ceramics such as glass at high temperatures. Deformation of a viscoelastic material causes the dissipation of vibrational energy as heat.

A polymeric material consists of a carbon atomic structure which is connected together firmly as long molecular chains. The damping arises from relaxation and recovery of these chains after deformation and is related to frequency and temperature.

By attention to the selected temperature and frequency zones the proper viscoelastic material for specific application can be manufactured.

3.2.1 Constitutive equation – Boltzmann equation

A constitutive equation expresses the behaviour of a material and specifies the properties of the material in a manner which is independent of the geometry of the body and depends only on its material nature.

In general, the response of a viscoelastic material to loading at any time is not only affected by the current conditions, but also by any previous load or deformation history. Boltzmann's principle of superposition in integral form can be used to define the relationship between the stress $\sigma(t)$ at the current time t and each individual strain $\varepsilon(\tau)$ applied at a historic time τ [100].

$$\sigma(t) = \int_{-\infty}^{t} G_{rel}(t-\tau)\frac{d\varepsilon(\tau)}{d\tau}d\tau \qquad (3\text{-}1)$$

The weighting function $G_{rel}(t-\tau)$, is the value of the relaxation modulus $G_{rel}(t)$ at the elapsed time $(t-\tau)$ for each applied strain. The Fourier transform can be applied

to the convolution integral (Equation 3.1) to obtain frequency domain behaviour. For steady-state harmonic oscillations the strain rate is defined as,

$$\frac{d\varepsilon(\tau)}{d\tau} = j\omega\varepsilon(\tau) \tag{3-2}$$

where ω is the cyclic frequency and $j = \sqrt{-1}$. The Fourier transform of Equation 3-1, for the infinite time, is given as,

$$\sigma(\omega) = \int_{-\infty}^{+\infty}\left[j\omega\int_{-\infty}^{+\infty} G_{rel}(t-\tau)\varepsilon(\tau)d\tau \right]e^{-i\omega t}dt \tag{3-3}$$

Using the convolution theorem for Fourier transform,

$$\begin{aligned}\sigma(\omega) &= j\omega\int_{-\infty}^{+\infty} G_{rel}(t)e^{-i\omega t}dt\varepsilon(\omega)\\ &= j\omega G(\omega)\varepsilon(\omega)\\ &= G^*(\omega)\varepsilon(\omega)\end{aligned} \tag{3-4}$$

where $G^*(\omega)$ is the complex modulus. The complex modulus is represented as,

$$G^* = G_{real}(1+j\eta) \tag{3-5}$$

$$\eta = \frac{G_{imag}}{G_{real}} \tag{3-6}$$

where $G_{real}(\omega)$ is the real part of complex modulus and is also called the storage modulus and $\eta(\omega)$ is the loss factor.

The inverse transform can be used to find the relaxation modulus from the complex modulus,

$$G_{rel}(t) = \frac{1}{2\pi}\int_{-\infty}^{+\infty}\frac{G^*(\omega)}{j\omega}e^{iwt}d\omega \tag{3-7}$$

3.2.2 Viscoelastic models

Perfectly elastic materials do not dissipate energy during deformation so that if a load applied and then remove, all the energy is recoverable. Constitutive equation for the elastic case, is expressed as,

$$\sigma(s) = G\varepsilon(s) \tag{3-8}$$

$$\varepsilon(s) = e^{st},\ s = j\omega \tag{3-9}$$

For the viscous case (cyclic stress is proportional to the rate of strain), is expressed as,

$$\sigma(s) = \upsilon \frac{d\varepsilon(s)}{dt} \tag{3-10}$$

where υ is the dynamic viscosity.

In a viscoelastic material, viscous and elastic behaviour are combined. Therefore this kind of materials has both behaviours. The simplest combinations are shown in Figure 3.1. As it can be seen the mechanical models to predict response under different loading conditions, are Maxwell model (spring and dashpot in series), and Kelvin/Voigt model (spring and dashpot in parallel).

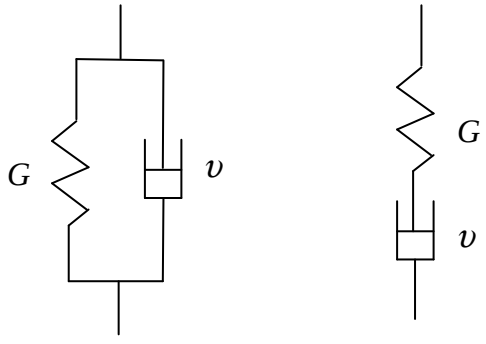

Figure 3.1: Mechanical models for viscoelastic materials, Kelvin/Voigt model (left), Maxwell model (right).

The constitutive equations for materials based on these models are,

$$\begin{aligned}\sigma(s) &= (G + \nu s)\varepsilon(s) \\ &= G(1 + \tau s)\varepsilon(s)\end{aligned} \tag{3-11}$$

for the Kelvin/Voigt model and for the Maxwell model,

$$\sigma(s) = \left(\frac{G\tau s}{1+\tau s}\right)\varepsilon(s) \tag{3-12}$$

where $\tau = \frac{\upsilon}{G}$, is a time constant.

The behaviour of real viscoelastic materials is often modelled by combinations of Voigt and Maxwell models [100]. One of the famous combinations is shown in Figure 3.2, and is known as *generalised Maxwell* model. The constitutive equation is,

$$\sigma(s) = \left(G_e + \sum_{n=1}^{N} \frac{G_n \tau_n s}{1+\tau_n s}\right)\varepsilon(s) \tag{3-13}$$

where $\tau_n = \frac{\upsilon_n}{G_n}$ is the relaxation time constant, G_n is the relaxation modulus for the n^{th} element. G_e is called as equilibrium or long-term modulus, after the viscoelastic material model having been subjected to a constant strain for a very long time, the response settles down to a constant stress. G_n and G_e are shown in Figure 3.2.

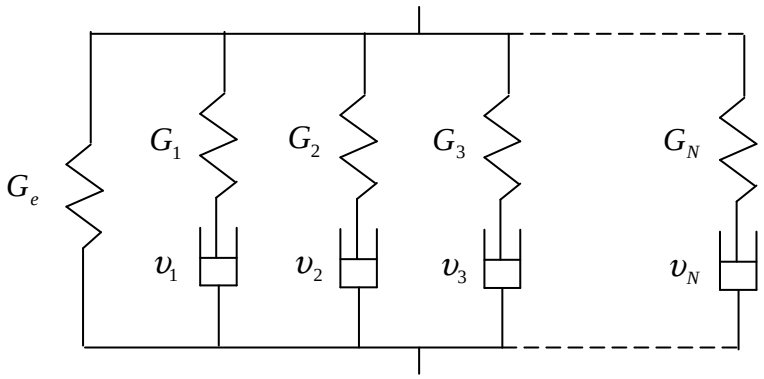

Figure 3.2: The Generalised Maxwell model

In frequency domain, the constitutive equation is given as,

$$G^*(\omega) = G_e + \sum_{n=1}^{N} \frac{G_n j\omega\tau_n}{1 + j\omega\tau_n} \tag{3-14}$$

And in time domain, the relaxation modulus is,

$$G(t) = G_e + \sum_{n=1}^{N} G_n e^{-\frac{t}{\tau_n}} \tag{3-15}$$

The constitutive equation is also known as a Prony series. The fitting of a Prony series model to experimental data is discussed later in this chapter.

3.3 Master curve derivation

Polymeric materials demonstrate viscoelastic behaviour (This can be seen in Figure 2.5). This section describes the measurement and model developed for the polymer used as a particle.

In order to present the complex modulus of a material (loss factor and Young's modulus) in a simple way, these data are presented in the form of Master Curve. For viscoelastic material a master curve can be generated from a limited number of test results that allow estimation of properties at many different combinations of temperature and frequency.

The following subsections explain the steps that are needed to obtain the master curve. For viscoelastic materials, an equivalent change in material properties can be achieved by altering the temperature or the frequency, this named as temperature-frequency superposition principle. Material properties can be transformed between the temperature and frequency domain. Measurements taken over the available frequency range at a number of different temperatures can be shifted according to the temperature-frequency superposition principle, to give frequency dependent values at all range at any reference temperature. The work carried out in this thesis involved of high loss synthetic rubber. The procedure of master curve extraction for this polymeric material is discussed in the following sub-sections. A specific chemical

description of the material was not available and the term “blue” is used to refer it in this thesis.

3.3.1 Method of reduced variables

The method of reduced variables is based on the temperature-frequency superposition principle [101]. In this method the effect of a change in temperature on viscoelastic properties is to multiply the frequency scale by a shift factor constant for a given temperature.

In reduced modulus stage, because of changing of modulus of a viscoelastic material with temperature so to generate a master curve at a reference temperature T_0 from a bunch of curves of E at different temperatures T. It should be reduced the values of E at temperature T, to the value E_0 at T_0, by means of equation,

$$E = \frac{E_0 T}{T_0} \tag{3-16}$$

This is due to dependency of stored energy upon temperature as would be predicted by the theory of rubber elasticity.

The loss factor has no reduced form because it is a ratio of reduced modulus. This step shows a vertical shift of the data at the reference temperature.

A temperature shift curve is constructed for each set of reduced modulus and loss factor. Each data curve is then shifted horizontally (parallel to the frequency axis for higher or lower frequency), to produce a single curve for modulus and a single curve for loss factor. The approach which has been used for shifting the data along the frequency axis is named WLF (William-Landel-Ferry) equation. William-Landel-Ferry have shown empirically that the shift factor for polymers is given by [91],

$$\log \alpha_T = -\frac{C_1(T - T_0)}{C_2 + (T - T_0)} \tag{3-17}$$

where $\alpha_T = \frac{f_r}{f}$ is temperature shift function. f_r is reduced frequency at temperature T_0, f is frequency at temperature T.

C_1 and C_2 are constant values, provided the reference temperature T_0 is taken to be an adjustable parameter.

As an example [102], Figure 3.3 illustrates the assembly of the master curve for the Young's modulus based on frequency-temperature superposition principle. Data obtained in a range of temperatures, T_1 to T_6 are shifted along the log-frequency axis to form a master curve over an extended frequency range at a reference temperature T_4. The shift along the log frequency axis required to superimpose data measured at temperature T on the master curve is also shown.

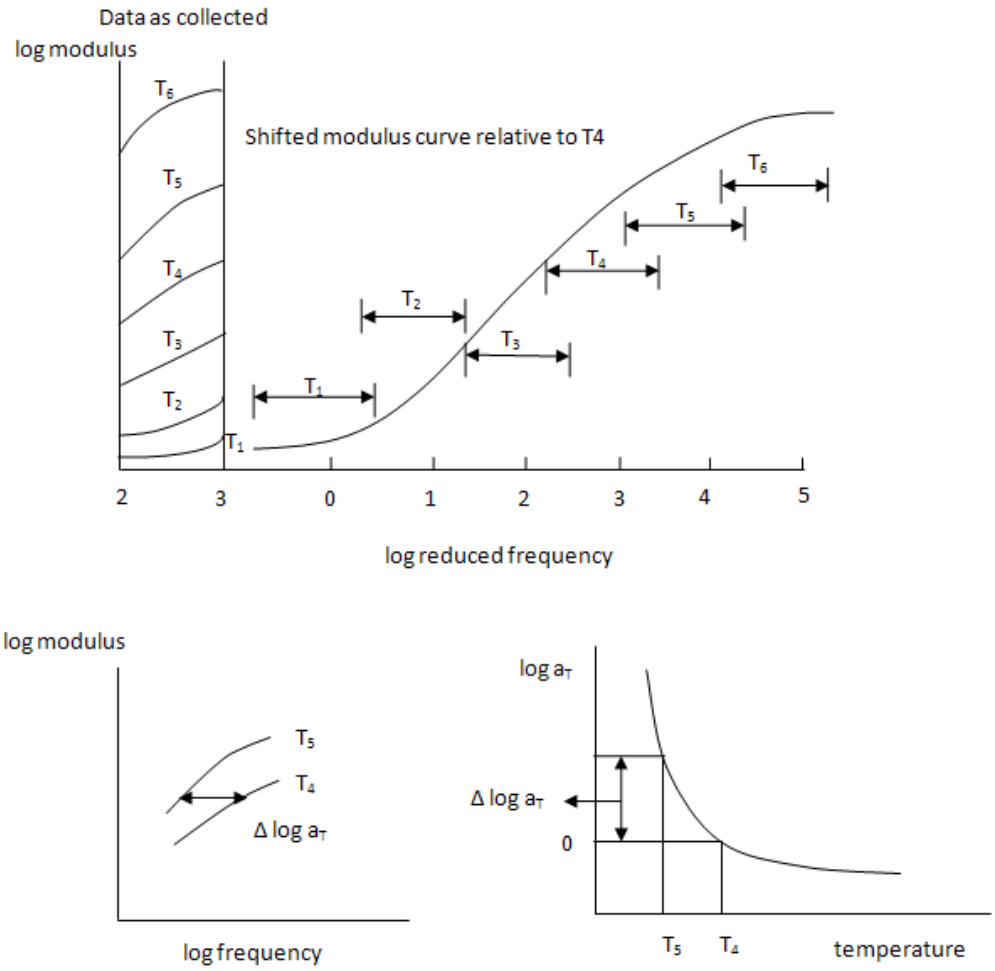

Figure 3.3: Production of the master curve for Young's modulus based on frequency-temperature superposition principle. a) Data collected at temperatures T_1 to T_6 in the frequency range of 100-1000 Hz are superimposed on the T_4 curve by applying horizontal shifts to each isothermal curve. b) The value of each shift required to construct the master curve. c) The relation of shift factor and temperature. [102]

In this work for blue rubber a reference temperature of -30°C is adjusted to be around the glass transition temperature (the highest value of loss factor) and by translating the experimental curve along the *log* frequency axis and temperature difference, the constant values are chosen when both curves merge smoothly. C_1=8.99, C_2=97.30. Figure 3.4, shows the variation of shift factor with temperature

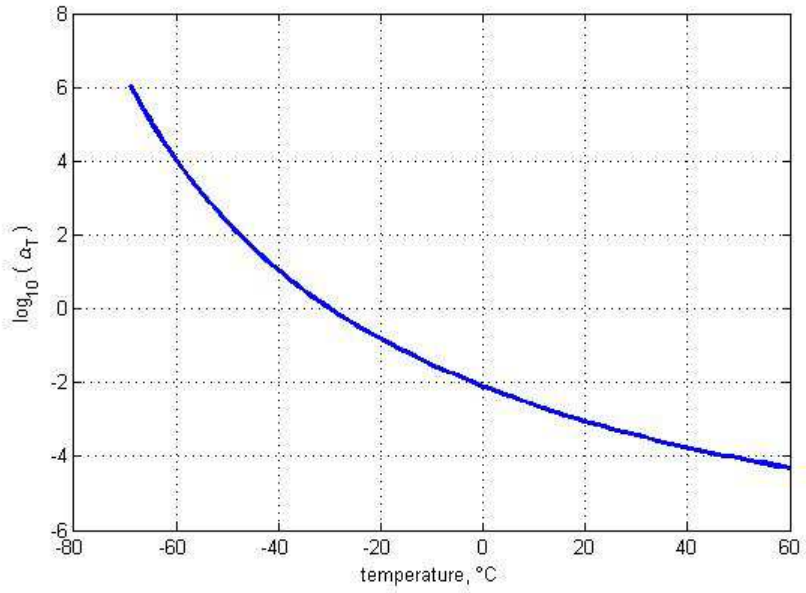

Figure 3.4: Temperature shift function versus temperature for the material of blue spherical particles

3.3.2 Data collection

This section demonstrates how the temperature frequency superimpose method was used to obtain a master curve for the polymer used in this work.

A sample of viscoelatic material was prepared. This sample was assembled in the test rig (Metravib Viscoanalyser – Figure 3.5), the test temperature were monitored. Principle parameter K^*(complex stiffness) directly is obtained. Complex stiffness is obtained from magnitude and phase difference of measured force and displacement from specimen.

The material was characterised using Dynamic Mechanical Thermal Analysis (DMTA) equipment to generate the master curves that define properties at different temperatures and frequencies. As it can be seen in Figure 3.5 and 3.6, in order to measure the material properties, a sample from sphere particle was prepared (prismatic shape) and inserted in the chamber of DMTA machine. Specimen was glued from upper and lower face to the fixture and thermocouple is used to monitor the temperature. The chamber should be closed and after that the temperature changes, for this material measurement were made at temperature in a range $\pm 70^{\circ}$C. Test was carried out at a number of frequencies between 1 and 60 Hz. In order to

justify of DMTA test data over the range of frequencies mentioned, loss factor was plotted against Young's modulus. In Appendix *G* it is shown that there is a close correspondence between the two.

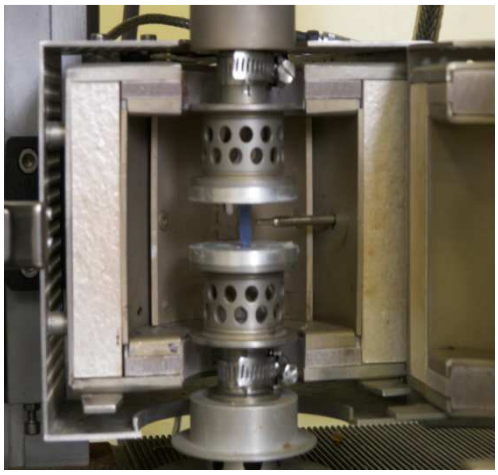

Figure 3.5: Viscoanalyser machine (DMTA) to measuring material properties

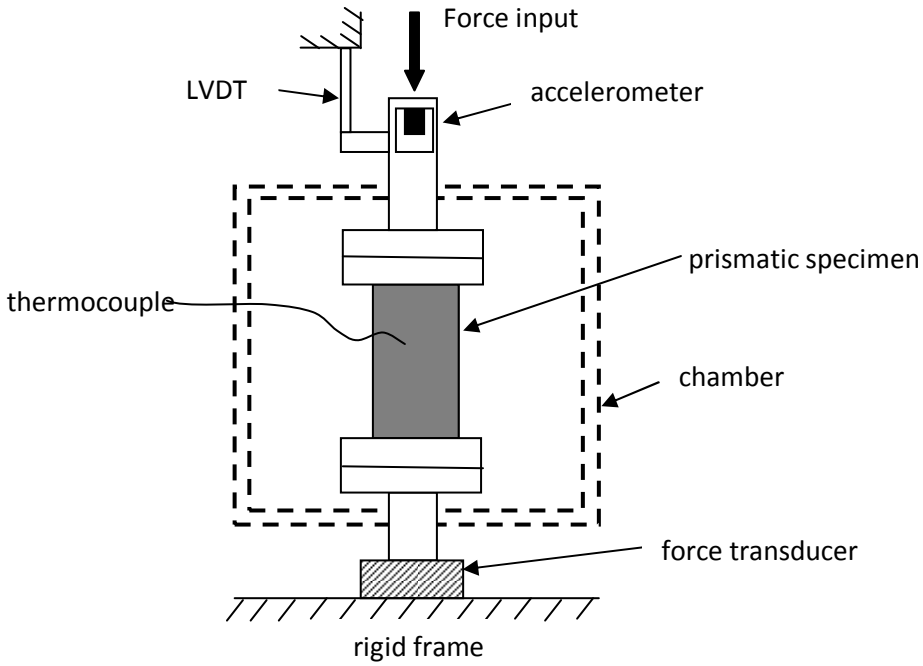

Figure 3.6: Sketch of the test rig and specimen inside it

Input sinusoidal excitation is subjected by a hydraulic actuator to the specimen. Force and displacement signals were used to estimate the complex stiffness of the specimen. From this the complex Young's modulus is obtained by using the shape factor of the geometric of specimen.

$$E = \frac{kL}{A(1+2S^2)}$$

where *A*, *L* are area of contact and length of specimen respectively. S is shape factor which is the area of one face in contact divided by the area of surrounded.

The collected test data are shown in Appendix A. As an example a few original unshifted data for loss factor and Young's modulus are given in Figure 3.7.

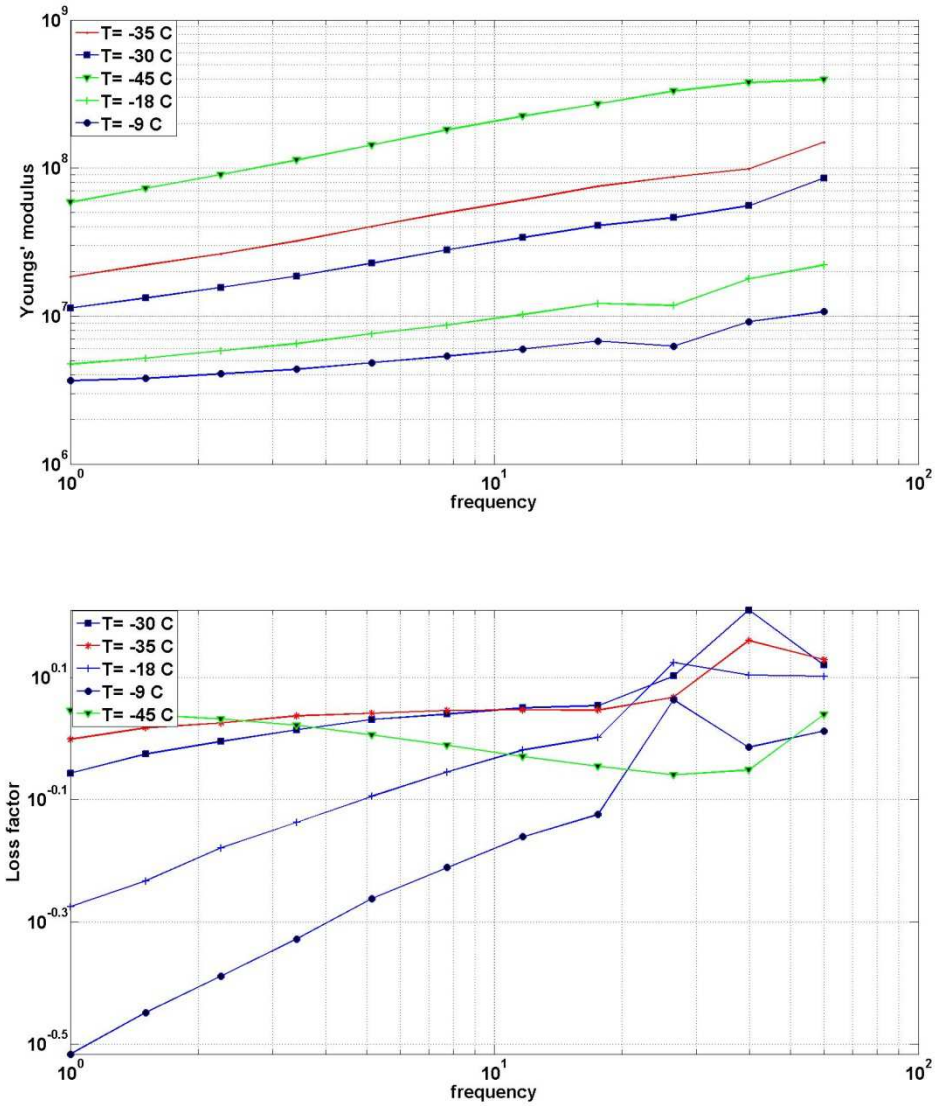

Figure 3.7: Samples of original data collected at different temperatures at DMTA

As mentioned in the previous section, each set of test data was then shifted to form a single curve for Young's modulus and a single curve for loss factor Figure 3.8.

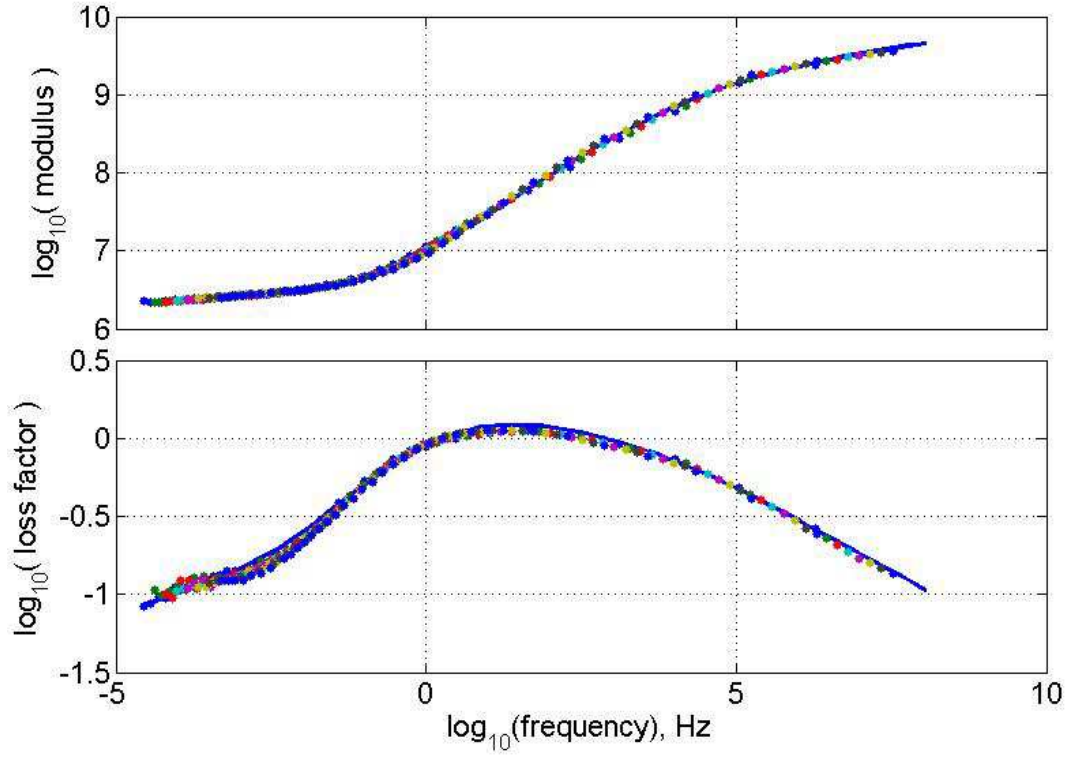

Figure 3.8: Master curve showing Young's modulus and loss factor, at reference temperature -30°C.

3.3.2 Master Curves (International plot)

A Reduced Temperature Nomogram sometimes referred as International plot or master curves. Master curves display the dynamic properties (Young's modulus and loss factor) can be read off in a same time at any combination of temperature and frequency. This method of representation has a significant advantage that all the data can be extracted quickly. Figure 3.9, shows the viscoelastic master curve for particle dampers which used in experiments. The uneven spaced diagonal lines represent constant temperature. These lines are given by the logarithmic form as,

$$\log f_r = \log f + \log \alpha_T \tag{3-18}$$

The reduced frequency axis f_r is the lower logarithmic horizontal axis. If for any value of frequency (e.g. 200Hz) and specific temperature (e.g. 10ºC) the viscoelastic properties are needed, one can draw a horizontal line from that frequency to intersect the specific temperature and then from that intersection, a vertical line which intersects the respective master carves shows the values of loss factor (0.7) and Young's modulus (7MPa). These values can read off from left vertical logarithmic axes of nomogram.

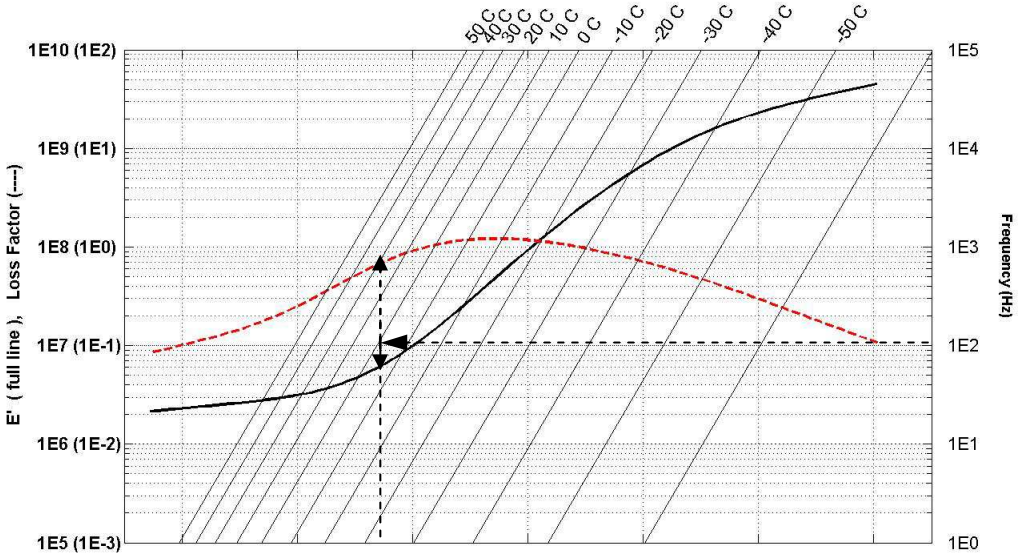

Figure 3.9: master curves for viscoelastic spherical particles

Provided that the changing of α_T respect to temperature is known, the interval between each temperature can be calculated.

3.4 Prony series calculations

In order to simulate viscoelastic materials in time-domain Finite Element analyses, viscoelasticity is implemented through the use of Prony series. Prony series representation of viscoelastic models offers a straightforward fitting approach to experimental data. As mentioned earlier the viscoelastic properties can be implemented by Equations 3-14 and 3-15 in frequency and time domain respectively, these sum of exponentials are known as Prony series. Method for fitting data using the Prony series is explained in this section.

The real and imaginary part of the Equation 3-14 can be rewritten as,

$$G_{real}(\omega) = G_e + G_0 \sum_{n=1}^{N} \left(g_n \frac{(\omega\tau_n)^2}{1+(\omega\tau_n)^2} \right)$$
$$G_{img}(\omega) = G_0 \sum_{n=1}^{N} \left(g_n \frac{\omega\tau_n}{1+(\omega\tau_n)^2} \right) \qquad (3\text{-}19)$$

where g_n and τ_n, n =1,2,…, N, are Prony series constant parameters that can be named as a Prony pairs. The loss factor can also be obtained by the ratio of imaginary to real part.

The shear relaxation modulus can be written in dimensionless form,

$$g_n(\omega) = \frac{G(\omega)}{G_0} \qquad (3\text{-}20)$$

where G_0 is the instantaneous or initial shear modulus. G_0 is given by replacing t=0 in the Equation 3-15 as,

$$G_0 = G_e + \sum_{n=1}^{N} G_n \qquad (3\text{-}21)$$

By Using Equation 3-20 and 3-21, equilibrium modulus or long term modulus is given as,

$$G_e = G_0(1 - \sum_{n=1}^{N} g_n) \tag{3-22}$$

This equation also implies that the summation of the input relative modulus, g_n must be less than or equal to 1.

In order to fit Prony series parameters to the complex modulus an optimisation routine is used. The range of frequency in the master curve is divided by even spacing. The minimum and maximum values of modulus are specified from master curve, therefore the values for g and τ could be estimated for each space/transitions. These constants then are used in the Equation 3.19 to calculate new values of modulus and loss factor. By applying mean squared error between the complex modulus defined by the Prony series parameters and defined values from master curve, is calculated. This is repeated to minimise the error. If one approximated the master-curves by e.g. three Prony terms the fitting is not accurate (see – Figure 3.10) by increasing the number of Prony series, better fitting can be obtained.

In this thesis, Prony series parameters (Prony pairs) are approximated for twenty terms. This provides good fitting of viscoelastic properties curves (see – Figure 3.11). The Prony parameters/pairs for twenty pairs are shown in the Table 3-1.

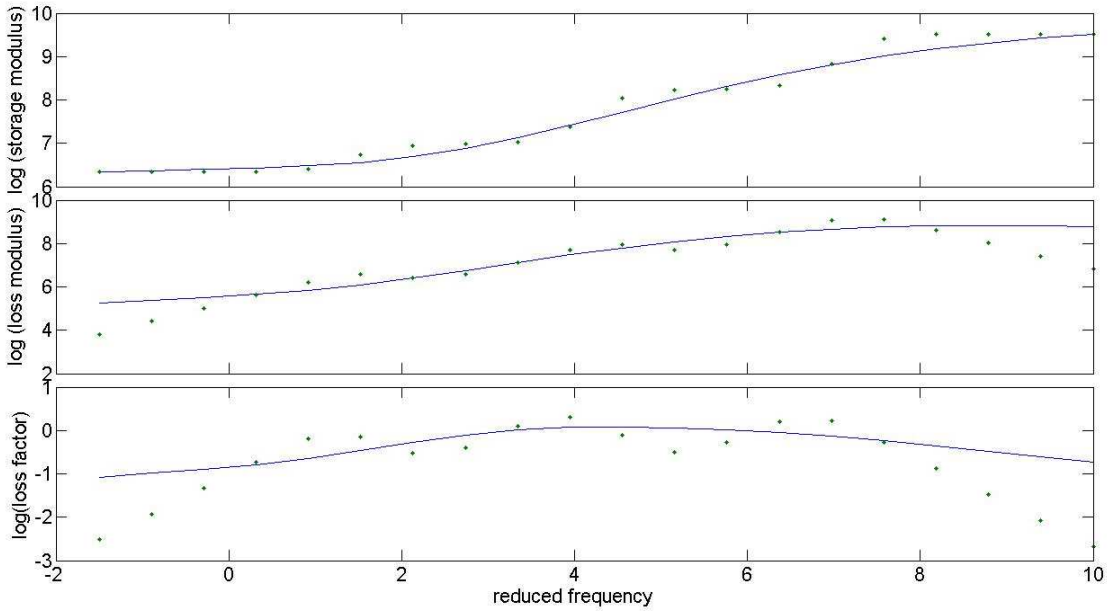

Figure 3.10: Three Prony terms fitted to viscoelastic properties (complex modulus and loss factor), the poor fitting can be seen. Viscoelastic properties derived from experiment (solid curves) and from Prony series ("•").

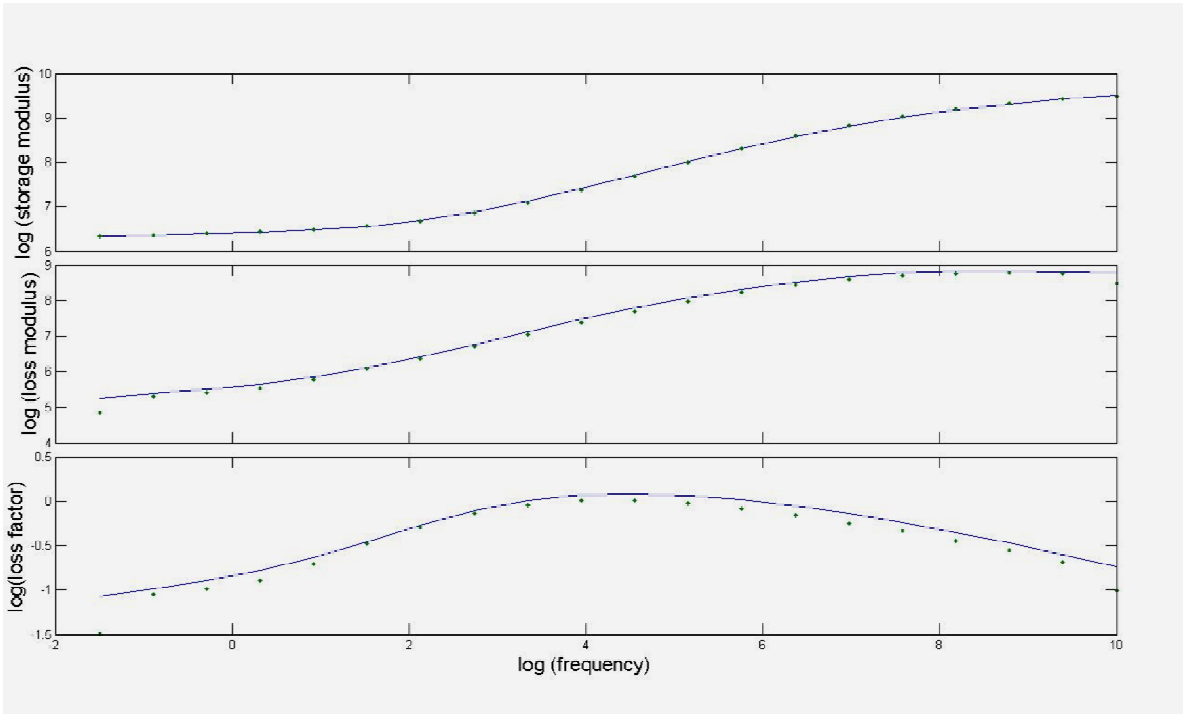

Figure 3.11: Twenty Prony terms fitted to viscoelastic properties (complex modulus and loss factor). Viscoelastic properties derived from experiment (solid curves) and from Prony series ("•").

Table 3.1: Twenty Prony terms (n=20) considered to fit to material properties at 20°C in the Figure 3.8.

n	g_i (–)	τ_i (s)
1	0.10030×10^{-3}	0.89615
2	0.39967×10^{-4}	0.25396
3	0.73353×10^{-4}	0.071969
4	0.76854×10^{-4}	0.020395
5	0.21459×10^{-3}	0.57797×10^{-2}
6	0.30055×10^{-3}	0.16379×10^{-2}
7	0.65413×10^{-3}	0.46416×10^{-3}
8	0.12727×10^{-2}	0.13154×10^{-3}
9	0.25167×10^{-2}	0.37276×10^{-4}
10	0.55635×10^{-2}	0.10564×10^{-4}
11	0.010475	0.29936×10^{-5}
12	0.023394	0.84834×10^{-6}
13	0.036909	0.24041×10^{-6}
14	0.068200	0.68129×10^{-7}
15	0.091604	0.19307×10^{-7}
16	0.11987	0.54714×10^{-8}
17	0.15757	0.15505×10^{-8}
18	0.13724	0.43940×10^{-9}
19	0.16450	0.12452×10^{-9}
20	0.17875	0.35287×10^{-10}

3.5 Damping calculation methods and energy dissipated

There are different methods to estimate damping in a vibrated system. In this work two methods have been used; one involves calculating the dissipation to the whole structure containing the granular medium while the other is based on measurement of the hysteresis loop for each individual particle. In this section those methods are explained.

3.5.1 Power dissipated Method

In this method, the damping of particles are measured in terms of power dissipated (rate of energy dissipation) in the system. In classical methods the damping is commonly measured by analysing the frequency response of the structure around its resonance frequencies and therefore the damping measurements are limited to the natural frequencies of the system.

Power dissipation measurements can be made at any frequency and amplitude and can be applied to any structure. This method was first used for particle dampers by Yang [40] and has subsequently been taken up by others [10].

The work done in a cycle to excite a mass is given as,

$$\begin{aligned} W &= F.dx \\ W &= F.\frac{dx}{dt}dt \\ W_{cycle} &= \int_0^T F\dot{x}dt \end{aligned} \tag{3-23}$$

$$P_{av} = \frac{W_{cycle}}{T} \tag{3-24}$$

where $F(t)$, $\dot{x}(t)$ and T are the force, velocity and time period of one cycle. P_{av} is the average power transmitted. The average power dissipated is given,

$$P_{av} = \frac{1}{2}\sum_{n=1}^{N} F_n.\dot{x}_n \cos(\alpha_n - \beta_n) \tag{3-25}$$

α_n and β_n are the phase of the force and velocity. Experimentally this is achieved by measuring the force applied to the system and the resulting acceleration. The measured force and acceleration are used in frequency domain and then from the Fourier transform of acceleration data, the velocity is calculated. The phase difference between the velocity and force data, are calculated and the summation of

all data are represented by the Equation 3-24. This method is based on the phase difference and is used later in Chapters 4 and 7 and used by other researchers [10, 40].

3.5.2 Hysteresis Loop Method

Energy dissipation is usually calculated under conditions of cyclic vibration. The force-displacement relationship is depending of the type of damping. In all cases force-displacement plot shows an area referred to as the hysteresis loop which is proportional to the energy lost per cycle. Figure 3.12 shows typical hysteresis loop for a viscously damped system.

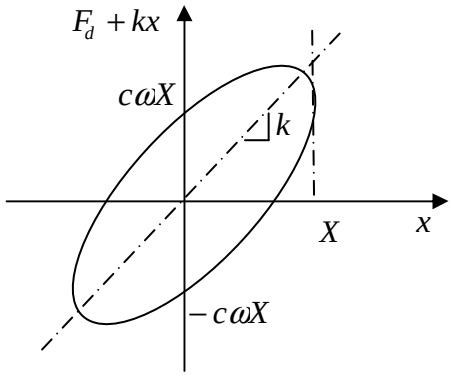

Figure 3.12: Typical hysteresis loops

The energy dissipated per cycle due to a damping force in a viscous model, is given as,

$$W = \int F_d \, dx \tag{3-26}$$

The damping force is,

$$F_d = c\dot{x} \tag{3-27}$$

where *c*, is the damping constant. With the harmonic sinusoidal displacement,

$$\begin{aligned} x &= X\sin(\omega.t-\phi) \\ \dot{x} &= \omega X\cos(\omega.t-\phi) \end{aligned} \tag{3-28}$$

By replacing the above equations the final equation for energy dissipated is given by,

$$W = \pi.c.\omega.X^2 \tag{3-29}$$

By substituting the equation for velocity in the Equation 3-27 and elliptic shape from relation between force and displacement is appeared, which the equation is,

$$\left(\frac{F_d}{c\omega X}\right)^2+\left(\frac{x}{X}\right)^2=1 \tag{3-30}$$

In this case, the spring force which is kx not taking account because it does not dissipate energy and it is only the elastic portion. By adding the force kx of the spring the hysteresis loop is rotated from horizontal shape to the new position (Figure 3.12) it is obvious that the loop area which is energy dissipated by viscous does not change.

An alternative definition of loss factor is the ratio of energy dissipated per radian to the peak strain energy U,

$$\eta = \frac{W}{2\pi U_{\max}} \tag{3-31}$$

$$U_{\max} = \frac{1}{2}kX^2 \tag{3-32}$$

To allow comparisons to be made, it is sometimes convenient to use an equivalent viscous damping c_{eq} which is by any system to that dissipated by a viscous damper.

$$\pi c_{eq}\omega X^2 = W_t \tag{3-33}$$

$$W_t = \frac{P}{f} \tag{3-34}$$

where W_t is the total energy dissipated valuated from other types of damping force, f is excitation frequency which is defined as, $f = \omega / 2\pi$ and P is the power dissipated. By combination of Equations 3-32 and 3-33 equivalent damping can be given as,

$$C_{eq} = \frac{P}{2\pi^2 (Xf)^2} \tag{3-35}$$

3.6 Chapter Summary

In this chapter, different models for viscoelastic materials were introduced. Also two methods for damping measurement which used in the net chapters were discussed. The viscoelastic properties of the material of blue spherical particles are extracted by using master curve. The procedure to derive master curve was explained by details. For this purpose an experiment with viscoanalyser machine was performed to obtain the properties. This master curve/nomogram expands the limited number of test results in a graph at any given combination of temperature and frequency. In order to fit the master curves by the viscoelastic model (generalised Maxwell equation), the parameters which named Prony parameters are calculated. These Prony series are used to define the material properties of the blue spherical particles in the FE analysis in the Chapter 5.

4 Granular Material in Low Amplitude Vibration

4.1 Introduction

In order to predict energy dissipated in a granular medium, one approach which many researchers have used is modelling each particle in the granular medium individually. In this method properties of particles in contact conditions at each contact point (such as radial and shear stiffness), and impact conditions between particles should be considered as a part of a time-marching analysis. Although this method gives considerable insight into the dynamics of granular materials, it is not always desirable; for example, large hollow structures might be filled with hundreds of thousands of particles leading to a high computational cost.

When the granular medium is subjected to low amplitude vibration (the particles do not collide and move with each other and they are in contact permanently), the medium is said to be in the solid phase/region. It is possible to approximate the granular medium as a solid and predict energy dissipation accordingly. In this work theoretical/numerical method is explained and is approximated for many complex structures. This suitability for making predictions is demonstrated by comparison with experimental results.

The study was conducted for an open topped rectangular box with rigid walls and cavity area 190×120 mm that was filled to a nominal depth of 35 mm. The granular medium consisted of 15.1 mm diameter spheres made from a blue synthetic elastomer with assumed 0.45 in Poisson's ratio. The density of polymeric spheres which used in this study is 1170 kg/m^3. The effectiveness of this system in dissipating vibration energy was studied for dynamic forcing applied horizontally.

4.2 Model for low amplitude vibration of granular medium

It has been shown that the damping of structural resonances can be increased significantly if standing waves are induced in an attached medium with high energy dissipation capacity [1]. The approach taken involves representing the granular medium as an equivalent solid using Finite Element analysis.

4.2.1 Effective material properties on equivalent homogenous solid

A granular medium subjected to a confining pressure and vibrating at low amplitude, such that particles remain in contact, can be approximated as a homogeneous solid, with equivalent spherical properties and effective bulk modulus.

For uniform and identical spheres with random packing and rough contacts, Walton [94] derived expressions for bulk modulus and effective Poisson's ratio. Assuming the spheres are made from homogeneous and isotropic viscoelastic material. In a hydrostatic pressure environment the effective (equivalent) bulk modulus is given by,

$$K = \frac{1}{6}\left(\frac{3E^2\phi^2 n^2 p}{\pi^2 (1-\nu^2_{eff})^2} \right)^{1/3} \tag{4-1}$$

where,

E = the dynamic Young's modulus of the polymer

ϕ = packing fraction of spheres

n = the number of contact points

p = the hydrostatic confining pressure

ν_{eff} = the effective Poisson's ratio

For rough spheres (i.e. coefficient of friction =1) the effective Poisson's ratio is given by [94],

$$\nu_{eff} = \frac{\nu}{2(5-3\nu)} \tag{4-2}$$

where ν is the Poisson's ratio for the sphere.

The effective Young's modulus and effective density of equivalent homogeneous medium are,

$$E_{eff} = 3(1-2\nu)K \tag{4-3}$$

$$\rho_{eff} = \rho\phi \tag{4-4}$$

The longitudinal wave speed can be obtained as,

$$C_{eff} = \sqrt{\frac{E_{eff}}{\rho_{eff}}} \tag{4-5}$$

As an example from wave speed equation, and using same polymer as used in experiment, a wave velocity about 11 m/s is obtained for an effective density of 702 kg/m^3 at 100 Hz, therefore the wavelength should be 110 mm.

4.2.2 Sphere Packing

The packing arrangement affects the packing fraction of spheres ϕ and also the number of contact points (geometric coordination number) for each sphere n. In geometry, a sphere packing is an arrangement of non-overlapping spheres within a containing space. A typical sphere packing problem is to find an arrangement in which the spheres fill as large a proportion of the space as possible. The proportion of space filled by the spheres is called the density of the arrangement.

A lattice arrangement (commonly called a regular arrangement) is one in which the centres of the spheres form a very symmetric pattern. For one sphere per lattice point, in a cubic lattice with cube side length a, the sphere radius would be $a/2$ and the atomic packing factor turns out to be about 0.524. In geometry the face-centred cubic (FCC) structure (also called cubic close packed) has a packing factor of 0.74. This can be, the highest average density – that is the greatest fraction of space occupied by spheres.

Arrangements in which the spheres do not form a lattice (often referred to as irregular) Experiments have shown that the most compact way to pack spheres randomly gives a maximum density of about 0.64 [32].

For the work presented here the spherical particles are randomly dropped into the box and shaken, they form an amorphous arrangement with a packing fraction of 0.64 (random packing) and coordination number of 6 [32].

4.2.3 Confining pressure

In a cavity filled with particles, even under static conditions, the pressure (and hence the deflection) varies with depth because of gravity loading. One way to estimate the relationship between pressure p and depth h in a granular fill subject to gravitational acceleration g is to use Janssen's model [14]. The German engineer Janssen was one of the first researchers who found the maximum pressure with depth in a grain silo. He derived an experimental equation which assumed that the walls sustain part of the weight in a granular medium. For granular materials (particles) in a container, according to Janssen's model the normal pressure p is,

$$p = \frac{\rho_{eff}\, g}{K_r S}(1 - e^{-K_r \cdot S \cdot h}) \tag{4-6}$$

where ρ_{eff} is the effective density, S the shape factor is the ratio of the container perimeter to its area. In a vertical cylinder with radius r this is given as [12],

$$S = \frac{2}{r} \tag{4-7}$$

And in a horizontal box section beam of length b and width w ,

$$S = \frac{2(b+w)}{bw} \tag{4-8}$$

K_r is the redirection factor (vertical stresses are re-directed horizontally) and often assumed using 0.7 based on experimental work [14].

The pressure value from Janssen's model has been shown to be less than would be with the hydrostatic assumption (pressure caused by gravity g in a fluid) and it reaches to a saturation pressure and more depth does not affect by pressure increasing [12]. The pressure p caused by gravity g in a fluid at depth h which is given by,

$$p = \rho_{eff}\, gh \tag{4-9}$$

Figure 4.1 shows the effect of depth on pressure calculated using the Equation 4-9 and Janssen models. The calculations are based on box section cavity with dimensions that used in this work.

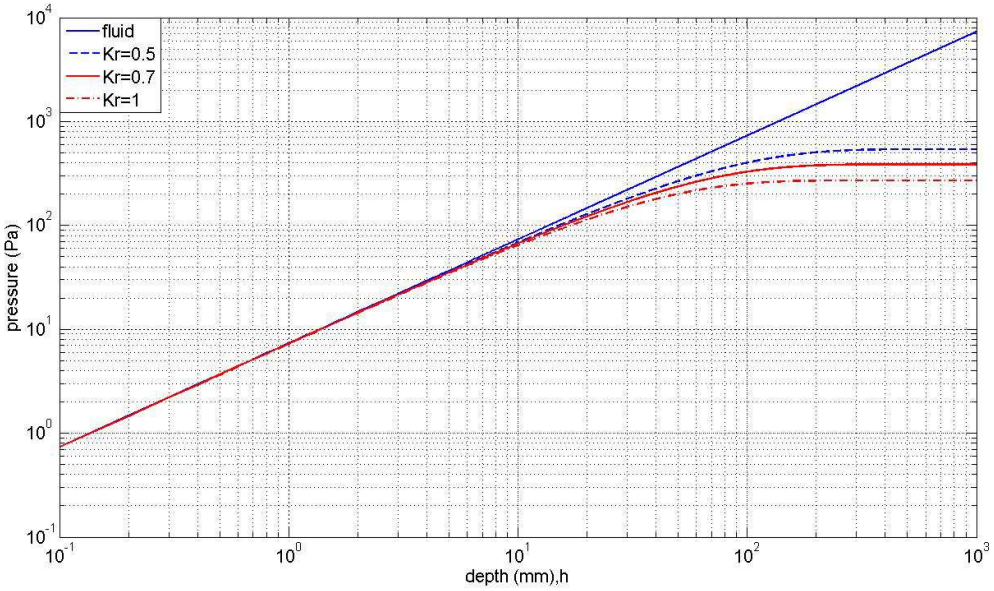

Figure 4.1: Effect of depth and redirection factor on pressure for a cavity with same cross-section of the one used.

4.3 Standing waves

For this work, standing waves are considered for calculating the energy dissipation from the system. The reason for this is that standing waves produce the highest displacement on the viscoelastic material and therefore this is where the maximum energy dissipation occurs. This is also considered in other research work [47,96].

Standing wave information (i.e. natural frequency, mode shape and effective mass for horizontal motion) was obtained for the internal cavity (granular medium) using a standard elastic eigenvalue extraction routine assuming an effective Young's modulus based on properties at 100 Hz.

4.3.1 Modal analysis of homogenous material

ANSYS v12.1 (workbench) was used as finite elements software. Solid elements (Solid 186 - quadratic brick 20 nodes) were used to model the fill medium and the material was assumed to be fixed rigidly at all five contacting walls.

To match conditions in experiments (See section 4-4) the average height of particles in the container was set as 35mm. Being viscoelastic, the Young's modulus of the polymeric particles change with exciting frequency. It is a factor not accommodated in standard FE routines. In this work, frequency dependence was approximated instead by scaling natural frequency according to,

$$\omega_n = \omega_{n,100\,Hz}\sqrt{\frac{E_{actual}}{E_{100\,Hz}}} \tag{4-10}$$

Where the final value of ω_n was attained by iteration. The relative change in frequency for the material considered is shown in Figure 4.2.

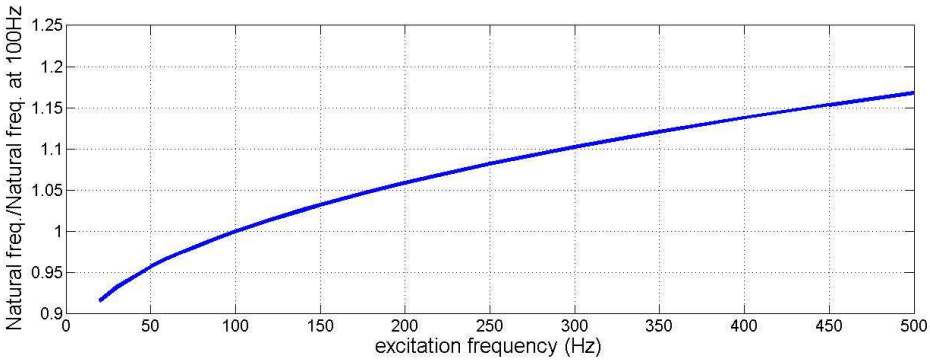

Figure 4.2: Ratio of natural frequencies over natural frequency at 100Hz, versus excitation frequencies.

As part of the approximation, mode shape and effective mass were assumed not to change with material Young's modulus. Typical modes having high effective mass and their properties are shown in Figure 4.3. The full set of properties of these mode shapes are provided in Appendix B.

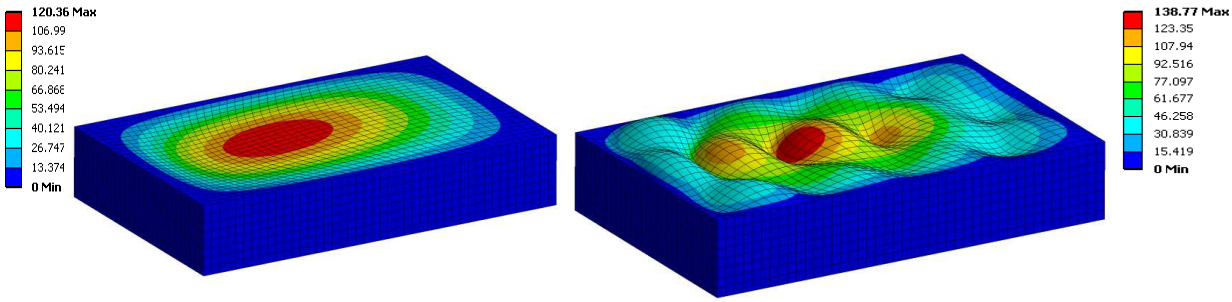

Mode 1: 67Hz, 0.302kg Mode 71: 165.1Hz, 0.032kg

Figure 4.3: Typical mode shapes with significant horizontal contribution (Mode 1 and Mode 71 from left to right respectively).Young's modulus 88.26 kPa, at 100Hz

4.3.2 Base excitation

In this work, a rigid container was filled with spherical particles and subjected to sinusoidal vibration in the horizontal direction. This is equivalent to applying base excitation to the contents of the container. The use of an equivalent solid approximation and modal analysis allowed representation of the granular system as many decoupled SDOF units. In SDOF units $m_{i\,eff}$ and $k_{i\,eff}$ are the effective mass and stiffness of each mode ($i = 1,2,...$) as shown in Figure 4.4.

The dampers of each mode can be approximated as,

$$c_{ieff} = 2\zeta\sqrt{k_{i\,eff}\,m_{i\,eff}} \tag{4-11}$$

$$\eta = 2\zeta \tag{4-12}$$

where $c_{i\,eff}$ and ζ are damping constant and damping ratio respectively, η is the loss factor of the viscoelastic material at that particular frequency. As the granular system subjected to base motion, each mode moves by a different amount, expressed as a relative displacement, where $z_i = x_i - y$ as,

$$z_i = \frac{m_{ieff}\, y\omega^2}{k_{ieff} - \omega^2 m_{ieff} + j\omega c_{ieff}} \tag{4-13}$$

where ω and ω_n are the excitation and natural frequency respectively.

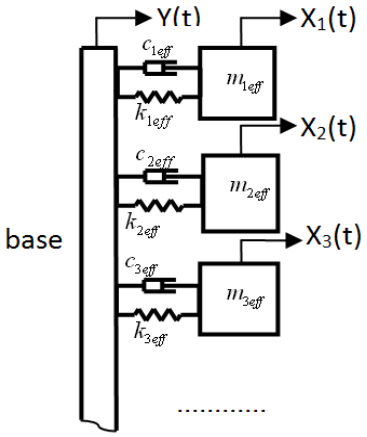

Figure 4.4: Base excitation for decoupled system

The total power dissipated is obtained from the real part of the total complex power [10, 40] from all SDOF units and is calculated using [103],

$$\text{Total power dissipated} = \sum_{i=1}^{N} \frac{1}{2} c_i . \omega^2 \Re(z_i)^2 \tag{4-14}$$

where i = 1,..., N, N is number of modes. The summation of all power dissipated in each individual SDOF system provides the total power dissipated in the system.

4.3.3 Analysis method

In this subsection the process of how the FE model is populated with data is explained. For the FE model, effective Young's modulus, effective density and effective Poisson's ratio are needed. These values are calculated by following steps:

- Effective Poisson's ratio from the Equation 4-2.
- ϕ and n, are constant values and defined from section 4.2.2 (sphere packing).

- Effective density from the Equation 4-4.
- The average confining pressure of filling particles is calculated by the Equation 4-6 or Equation 4-9 (with the hydrostatic assumption).
- Young's modulus (E) of particle material is derived from master curve (Chapter 3). It is obvious that this value should be updated each time by changing the excitation frequency.
- Bulk modulus from the Equation 4-1.
- Effective Young's modulus from the Equation 4-3.

4.4 Experimental validation

In this section, the test rig for damping measurement of granular medium in horizontal vibration and low amplitude is explained and experimental results will compared by theory approach and also simulation.

4.4.1 Granular medium test rig for horizontal vibration

For the physical experiments the container was constructed using blocks of Perspex 30 mm in thickness. This provided high rigidity and good visibility as shown in Figure 4.5. The container was suspended using nylon line and light metal springs to simulate free boundary conditions. Excitation was provided via an electrodynamic exciter attached to base. It is assumed the container is completely rigid. The experiment was repeated for the case with the container empty in order to find the phase error due to the boundary conditions and electronics. This error, although relatively small (5% at 350 Hz), was subtracted from measurement to provide true contribution of the granular medium.

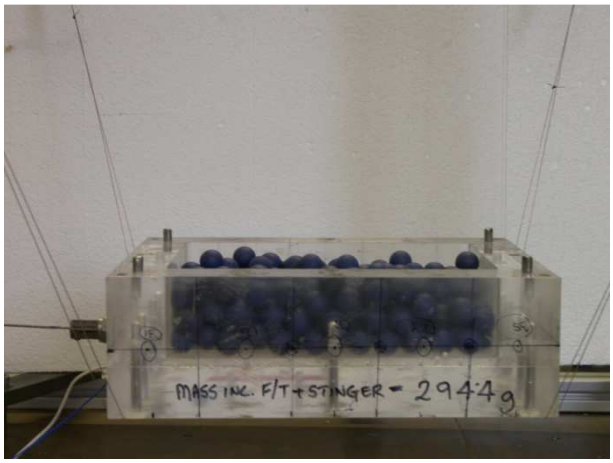

Figure 4.5: Experimental set-up showing container and particles, the transparent container suspended by nylon line and electrodynamic exciter attached horizontally to the base.

Initial tests showed that flexible modes of the container were above 500 Hz while the rigid body modes were below 5 Hz. The container was then filled with 260 randomly placed particles and testing carried out at various frequencies and amplitudes. The force and acceleration are measured and as explained in Chapter 3, the power dissipated is calculated.

The raw data at 350 Hz for acceleration and force are shown in Figure 4.6. Also the power dissipated calculated versus frequency excitation (for all measured data) are shown in Figure 4.7. It should be noted that at some frequencies the experiment were repeated in order to investigate the effect of amplitude dependency of medium.

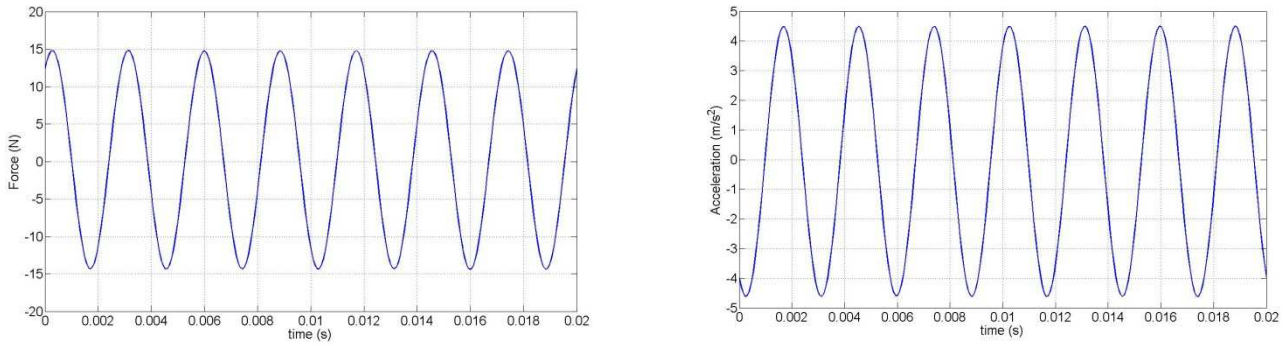

Figure 4.6: Typical measured values for force and acceleration at 350 Hz.

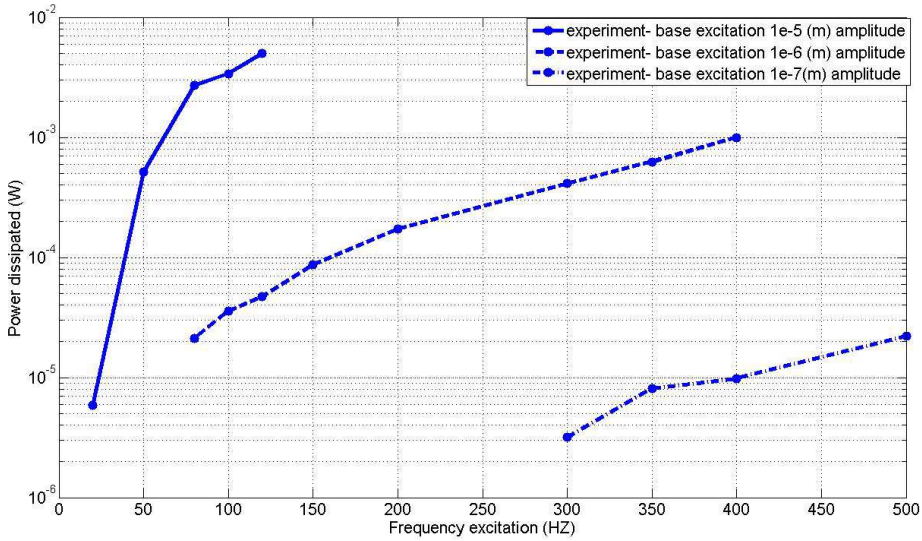

Figure 4.7: Power dissipation measured at three different excitation levels, in a range of excitation frequencies.

4.4.2 Validation of theory approach by experiment

In this section, a comparison is made between the damping predicted by theory/numerical method and experiments at very low amplitudes. As a large frequency range was of interest, results are compared for displacement amplitudes of 10^{-7}, 10^{-6} and 10^{-5} metres depending on the frequency. These values were selected to ensure maximum accelerations remained less than $\Gamma = 0.3$. ($\Gamma = \frac{X\omega^2}{g}$)

In Figure 4.8, the equivalent damping is calculated as,

$$C_{eq} = \frac{P_{total}}{2(\pi X f)^2} \tag{4-15}$$

where X, f are amplitude and frequency of excitation in Hz. As it can be seen, the results show that prediction method performs well in the frequency range 80 to 400 Hz. At higher frequencies increased damping in the experiment is thought to arise from the presence of container wall resonances. Below 80 Hz, the wave approach does not match the experiment as it only considers standing waves – the lowest of which is near this figure.

As an investigation into how much the prediction changes if the material properties were assumed not to change with frequency, was conducted by assuming constant properties at 100 Hz. The results show that as the material properties do not change by frequency, therefore the equivalent damping shows smaller values than the other curve with real properties (See – Figure 4.8).

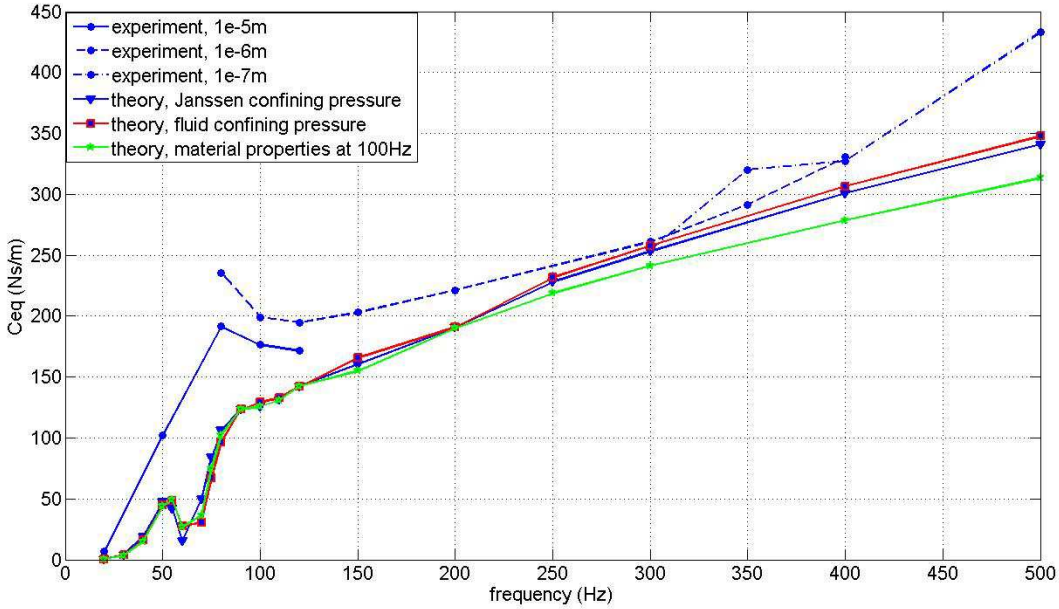

Figure 4.8: Comparison of equivalent damping for three different displacements amplitude levels.

The effects of amplitude on the effective damping excitation is summarised in Table 4.1. In each case, although the amplitude of excitation is increased by factor of 10, the equivalent damping does not change dramatically and the ratio is around 1. This shows (as was expected) that the damping of the granular system at low amplitude is amplitude independent [12].

Table 4.1: Experimental results of damping ratio at different frequencies and excitation amplitudes.

Excitation frequency *Hz*	Lower displacement X_{low}, *m*	Higher displacement X_{high}, *m*	Damping ratio $C_{eq\ (high)}/C_{eq\ (low)}$
120	10^{-6}	10^{-5}	0.88
300	10^{-7}	10^{-6}	1.03
350	10^{-7}	10^{-6}	0.91
400	10^{-7}	10^{-6}	1.01

.

4.5 Chapter summary

This chapter has considered the damping from polymeric granular materials under low amplitude excitation. In this case it has been shown that the medium can be approximated as solid homogenous material attached to the host structure. Energy is dissipated by the generation of internal standing waves within the granular medium.

A theoretical/numerical approach, in which the equivalent elastic properties of the medium were estimated using equations developed by Walton were then used in conjunction with a finite element analysis. Comparison of the method with experiment shows fairly good agreement. Little effect of amplitude at $\Gamma < 0.3$ excitation has been observed which is in agreement with other research [12]. The method could therefore be easily applied for more complex structures.

5 Properties of Individual Spherical Particles

5.1 Introduction

The properties of individual particles have a considerable influence on the behaviour of a granular system. These include dynamic properties which, for viscoelastic particles depend on excitation frequency and temperature and contact properties at the interface which are also affected by the geometrical shape. This work involves a numerical study using Finite Element (FE) method to investigate the contact stiffness of each particle and a comparison of those with existing theories and experiment. In addition to FE method, in order to obtain the dynamic properties of individual spheres a test rig was designed and used to measure the properties (stiffness and energy dissipated) at different frequencies. The performance of test rig was validated using two specific cylindrical specimens. The results of this work are used in simulation of the granular medium using the Discrete Element Method in Chapter 6.

5.2 Hertz contact theory

Contact mechanics is the study of the deformation of solids that touch each other at one or more points. The original work in the contact behaviour of spheres dates back to work published in 1880 by Heinrich Hertz [104].

Hertz developed a theory to calculate the contact area and pressure between the two surfaces and predict the resulting compression and stress induced in the objects. This theory relates the circular contact area between two spheres to the elastic deformation properties of the materials. For curved surfaces in contact the Hertzian model through its equations allows calculation of contact area, maximum and average compressive stress and maximum deflection.

There are some assumptions in Hertzian theory that should be noted.

- The strains are small and within the elastic limit,
- The area of contact is much smaller than the radius of the body.
- The surfaces are continuous and initial contact is a point or a line.
- The surfaces are frictionless.

The first two assumption these assumptions imply that $a << R$ where a is the contact radius and R is the effective radius of curvature of the two solids.

A non-conforming contact is that under zero loads, they only touch at a point (or possibly along a line). In the non-conforming case, the contact area is small compared to the sizes of the objects and the stresses are highly concentrated in this area. Such a contact is called concentrated. In Figure 5-1 two spheres in normal contact are shown which the radius of contact area is recognised.

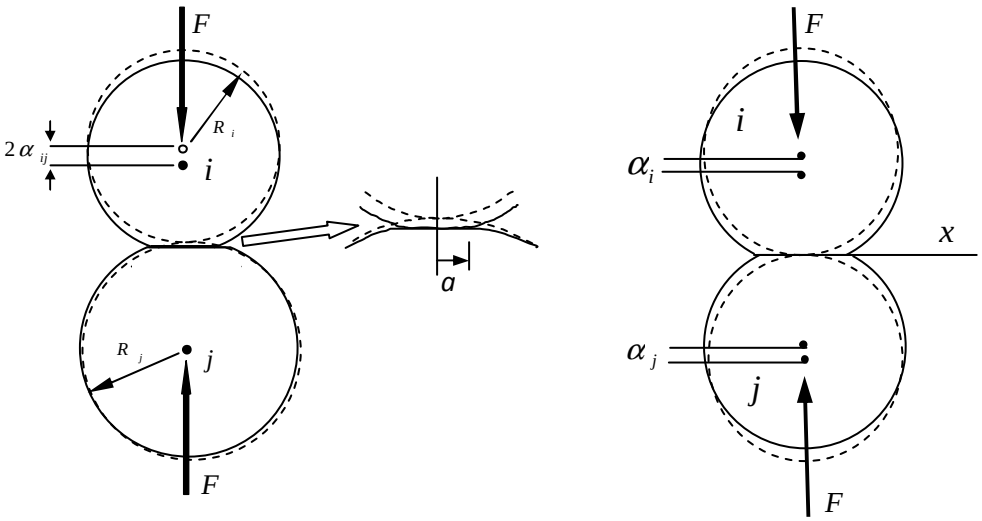

Figure 5.1: Two spheres (i, j) in normal contact where *a* is radius of the contact area and α is displacement of each sphere after loading, dashed lines show positions before loading.

The contact surface between the spheres is circular with radius *a* and according to Hertz equation [104,105] the pressure at a point such as *A* in the contact area, at a distance *r* from centre *o* is given as, (see Figure 5.2)

$$p(r) = p_m \sqrt{1-(\frac{r}{a})^2} \qquad (5\text{-}1)$$

where p_m is the maximum normal pressure accruing at $r = 0$, by integrating p over whole contact area and rearranging for p_m, (this is related to normal force contact)

$$p_m = \frac{3F_z}{2\pi.a^2} \qquad (5\text{-}2)$$

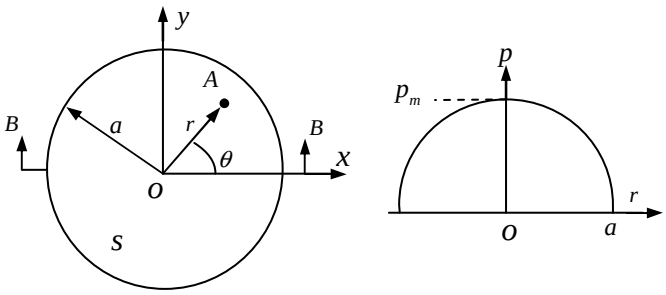

Figure 5.2: The circular contact area in left side and normal pressure distribution with maximum value p_m in the right hand side.

The normal force contact (F_z) as a function of normal displacement approach (δ) was defined by Hertz's equation according to,

$$\delta = \alpha_i + \alpha_j \tag{5-3}$$

$$F_z = \frac{4}{3} E^* R^{*0.5} \delta^{3/2} \tag{5-4}$$

where E^* and R^* are effective Young's modulus and radius and δ is the approach between two bodies. For contact between Bodies 1 (i) and 2 (j), these are given by,

$$\frac{1}{E^*} = \frac{1-\nu_1^{\,2}}{E_1} + \frac{1-\nu_2^{\,2}}{E_2} \tag{5-5}$$

$$\frac{1}{R^*} = \frac{1}{R_1} + \frac{1}{R_2} \tag{5-6}$$

The radius of contact a is defined as,

$$a = (R^* \delta)^{0.5} \tag{5-7}$$

The maximum contact pressure can be also calculated from Equation 5-2 as a function of normal displacement and radius of spherical particle by replacing Equations 5-4, 5-7. This could be used as an initial point when yield and plasticity of material is noticed.

For defining the radial stiffness of each sphere where two identical spheres are in contact, one can differentiate from Equation (5-4), F_z respect to $\delta/2$, the radial stiffness for each sphere is given by,

$$k_n = 4E^* a \tag{5-8}$$

For calculation efficiency, it is sometimes desirable to obtain a linear spring to represent the nonlinear force-deflection behaviour. Practical experimentation has shown that force deflection curves often deviate from Hertz theory because of roughness and contamination of the surface layer. For metal particles, some authors have used an equivalent linear spring that stores the same amount of energy as a Hertzian one up to the yield force of the contact [10,106]. For flexible polymers, this approach is unsuitable as material failure occurs at much larger strains than those experienced. The approach taken here in this work is to use the average stiffness k_n up to a defined deflection δ_0. The stiffness from Hertz theory is obtained by taking the gradient of the force-deflection curve to get,

$$\begin{aligned} k_n &= \frac{1}{\delta_0}\int_0^{\delta_0} 4E^*\sqrt{R^*\,\delta_n}\,\mathrm{d}\delta_n \\ &= \frac{2}{3}k_{n0} \end{aligned} \tag{5-9}$$

where k_{n0} is the stiffness at the maximum deflection. This approach allows a linear stiffness value to be estimated from the stiffness measured during an experiment.

5.2.1 FE analysis for normal stiffness of spherical particle

The most common element shapes used in three dimensional are tetrahedral and hexahedral. If the geometry of model is complex and changing, the tetrahedral are better suited although it needs more elements to fill the volume in comparison with hexahedral with same edge length. Element types could be low or high order. For low- order elements, nodes are sited on vertices and the interpolation functions between those are linear. For high-order elements there are additional nodes between vertices and interpolations for three nodes on each length are quadratic. These high-order elements usually have better results than the others.

In this work, the element used was a higher order 3-D, 10-node tetrahedral shape (Solid 187 in ANSYS) [107]. This element has quadratic displacement behaviour and is well suited to modelling irregular meshes. It consists of ten nodes having three degrees of freedom at each node. A sketch of this element is shown in Figure 5.3.

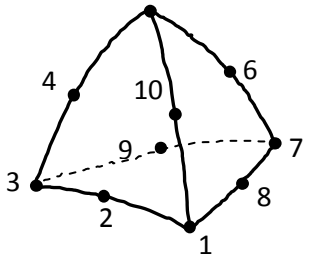

Figure 5.3: Tetrahedral solid element with ten nodes

The material was represented in FE using a hyperelastic model. As unfilled polymers are generally linear to large strain, the Neo-Hookean option was used – this has a potential applicable strain range of 0-30%. In the Neo-Hookean model, the form of strain energy is given by,

$$U = \frac{G}{2}(\bar{I} - 3) + \frac{1}{d_i}(J - 1)^2 \qquad (5\text{-}10)$$

where

U = strain energy per unit reference volume

$\bar{I}$ = first deviatoric strain invariant

G = initial shear modulus of the material

d_i = material incompressibility parameter

J = determinant of the elastic deformation gradient

The material incompressibility is defined by,

$$d_i = \frac{2}{K} \tag{5-11}$$

where,

$$K = \frac{E}{3(1-2\nu)} \tag{5-12}$$

If the initial Young's modulus and Poisson's ratio of the material is known, one can obtain the initial shear modulus using:

$$G = \frac{E}{2(1+\nu)} \tag{5-13}$$

A comparison between FE and Hertz's equation was conducted for a sphere with 15 mm diameter and Poisson's ratio of 0.4 located between two steel plates for compressing up to 1.4mm. Recalling Equation 5-6, this equation relates to two spheres in contact. However in this comparison, R_2 is infinite and therefore this term is equal to zero and can be remove making Equation 5-6 valid for plate/sphere contact. In the FE model symmetrical boundaries were chosen and the two middle nodes in contact between plates and sphere were constructed to move only vertically to prevent sliding. The element size in the contact zone was reduced to 0.08R (R is the radius of particle). The convergence of the FE model was checked by increasing the number of nodes from 10455 to 35350 – in this case the normal force changed from 10.00 to 10.26N. Considering the complexities of this FE model (e.g. contact and geometric nonlinearities), this difference in normal force is insignificant.

Figure 5.4, shows the model in ANSYS v.12.1 – workbench.

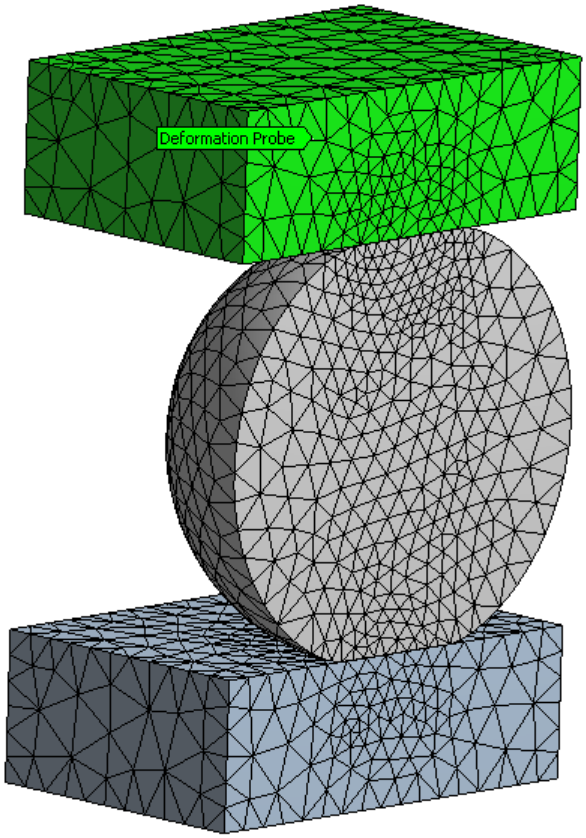

Figure 5.4: Half model of sphere compressed to 1.4 mm, showing increased mesh density around contact points.

5.2.2 Comparison with Hertz theory

The force-compression result from the FE model in Figure 5.4 is shown in Figure 5.5. Note that the result is for one contact side, i.e. half of the total compression, in order to compare convergence with Hertz contact theory. It can be seen that at low pressure, when the contact area is still small, the two curves match fairly well however at higher force levels the curves diverge. The reason for this is that at higher force levels, the contact area increases and therefore does not meet the Hertz theory assumption of small contact area.

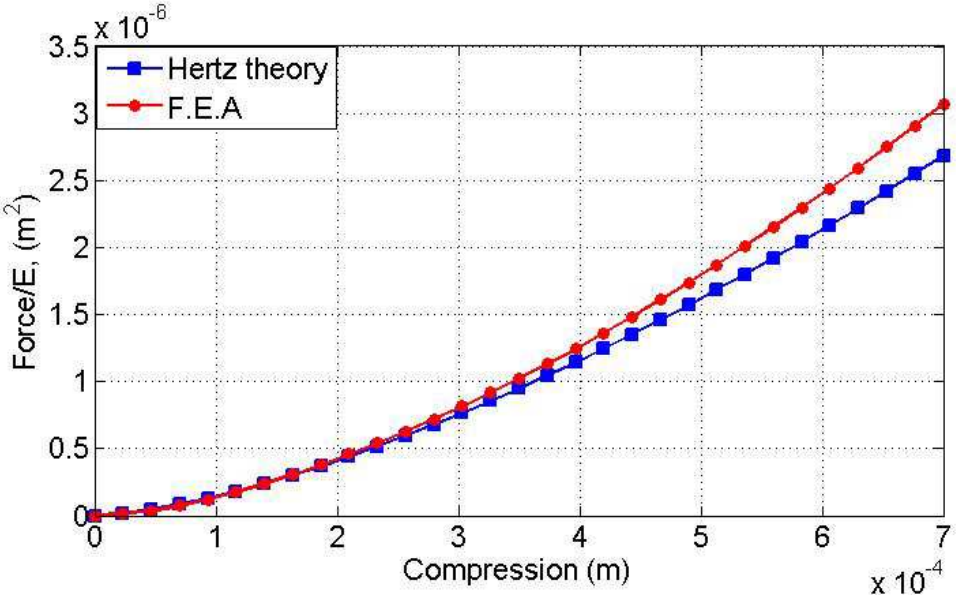

Figure 5.5: Comparison of ratio of reaction force over Young's modulus in FE analysis with Hertz theory approach.

5.3 Mindlin-Deresiewicz shear contact theory

For particle dampers not only do the particles have compressive loads but they also have shear loads from adjacent particles. With Hertz theory only the compressive loads are considered. Therefore the introduction of shear contact theory is necessary.

Theory concerning the shear displacement of spheres relative to the contact area was developed by Mindlin [108] and was used by others [109, 110]. The shear force for a sphere is given by,

$$F_x = \mu F_z \left(1 - (1 - \frac{16Gax}{3(2-\nu)\mu F_z})^{3/2} \right) \tag{5-14}$$

where $G, a, \nu, \mu,$ are shear modulus, area of contact, Poisson's ratio and friction coefficient respectively.

F_x and F_z are the forces applied in horizontal and vertical directions respectively and x represents tangential displacement. Shear stiffness k_s is calculated by differentiating Equation (5-14), respect to x, it is given by,

$$k_s = \frac{8Ga}{2-\nu}(1-\frac{F_x}{\mu F_z})^{1/3} \tag{5-15}$$

At zero shear force, the initial shear stiffness k_{s0} is given by

$$k_{s0} = \frac{8Ga}{2-\nu} \tag{5-16}$$

By replacing shear modulus from Equation 5-13, the ratio between initial shear stiffness and normal stiffness (Equation 5-8) is become,

$$\frac{k_{s0}}{k_n} = \frac{2(1-\nu)}{2-\nu} \tag{5-17}$$

5.3.1 FE analysis for shear stiffness of spherical particle

Much like Hertz's equation, Mindlin's equation is limited to small displacements for linear materials. To validate that Mindlin's equation holds for the material and displacements used in this work, a comparison is made using an FE model.

Since the FE model considers contact nonlinearities, the computational time is large. This can however be reduced by using symmetric boundary conditions in which two quarter spheres are in contact as shown in Figure 5.6. The symmetric boundary conditions are applied along the flat surfaces normal to the z- axis. It is obvious that another line of symmetry exists; however, since a load is applied in the tangential direction, the symmetric portion will possess an equal but opposite force making the system to be in equilibrium. The properties used for the spheres are the same as those listed in section 5.2 while the coefficient of friction between the spheres is assumed to be 1 (discussed further in Chapter 7).

The lower sphere is constrained in all degrees of freedom (DOF) at its mid-plane that is parallel to the x-z plane. The simulation is split into three loadsteps to provide the

full compression displacement before applying the tangential displacement. For, the first loadstep, a linearly ramped displacement from 0mm to 0.1mm is applied to the x-z mid-plane of the upper sphere in the negative y-axis. This displacement is held for loadsteps 2 and 3. Loadstep 2 is a rest step that is used to provide time between the ending point of loadstep 1 and the beginning of additional loading in loadstep 3. In loadstep 3 a linearly ramped tangential displacement from 0 mm to 0.01mm is applied to the x-z mid-plane of the upper sphere in the x-axis. Since the simulation is nonlinear, each loadstep is split into multiple substeps of 50, 5 and 60 for loadsteps 1, 2 and 3, respectively. The loadstep history is shown in Figure 5.7.

When two spheres come into contact, this is initialised as a point. The stresses/strains therefore quickly dissipate throughout the sphere. The contact area is highly sensitive to be able to accurately capture the behaviour. A mesh refinement is used in this area with an element size equal to $0.03R$ while the remaining mesh is $0.25R$, where R is the radius of the sphere. A similar method has been used by Quoc [111] which indicated a good correlation between analytical and numerical methods.

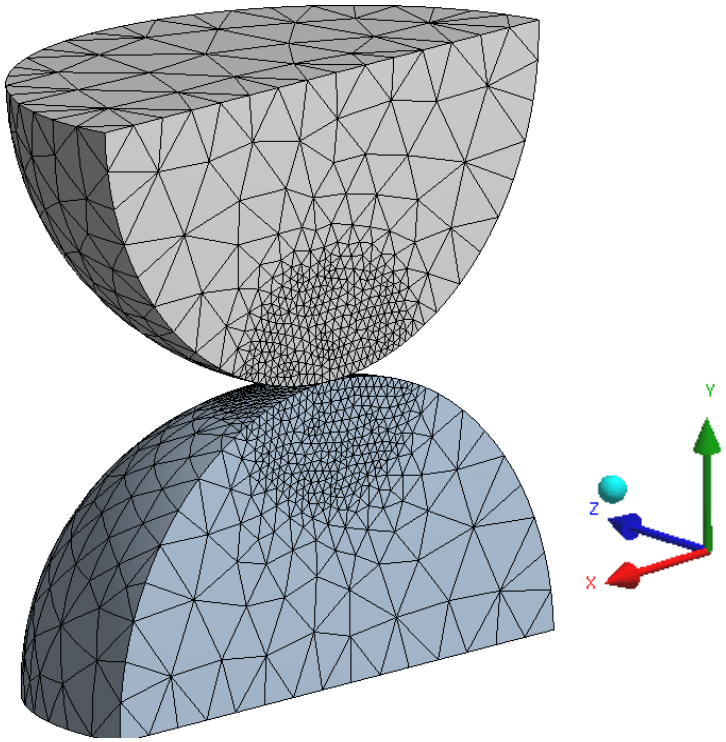

Figure 5.6: View of semi polymeric hemisphere in contact

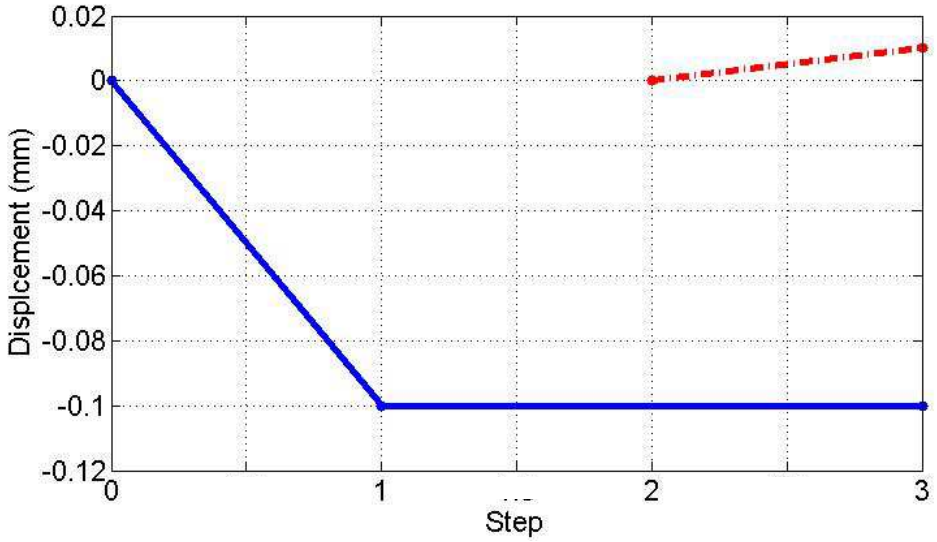

Figure 5.7: Displacement applied to the quarter of spheres versus different steps, solid line represents normal compression while dashed line represents shear displacement which was applied during last step (step 2 to 3).

The normal pressure zone in contact area can be seen in Figure 5.8. This shows symmetric pressure distribution. The pressure increases in the first step (under compression) and then keeps constant during shear motion.

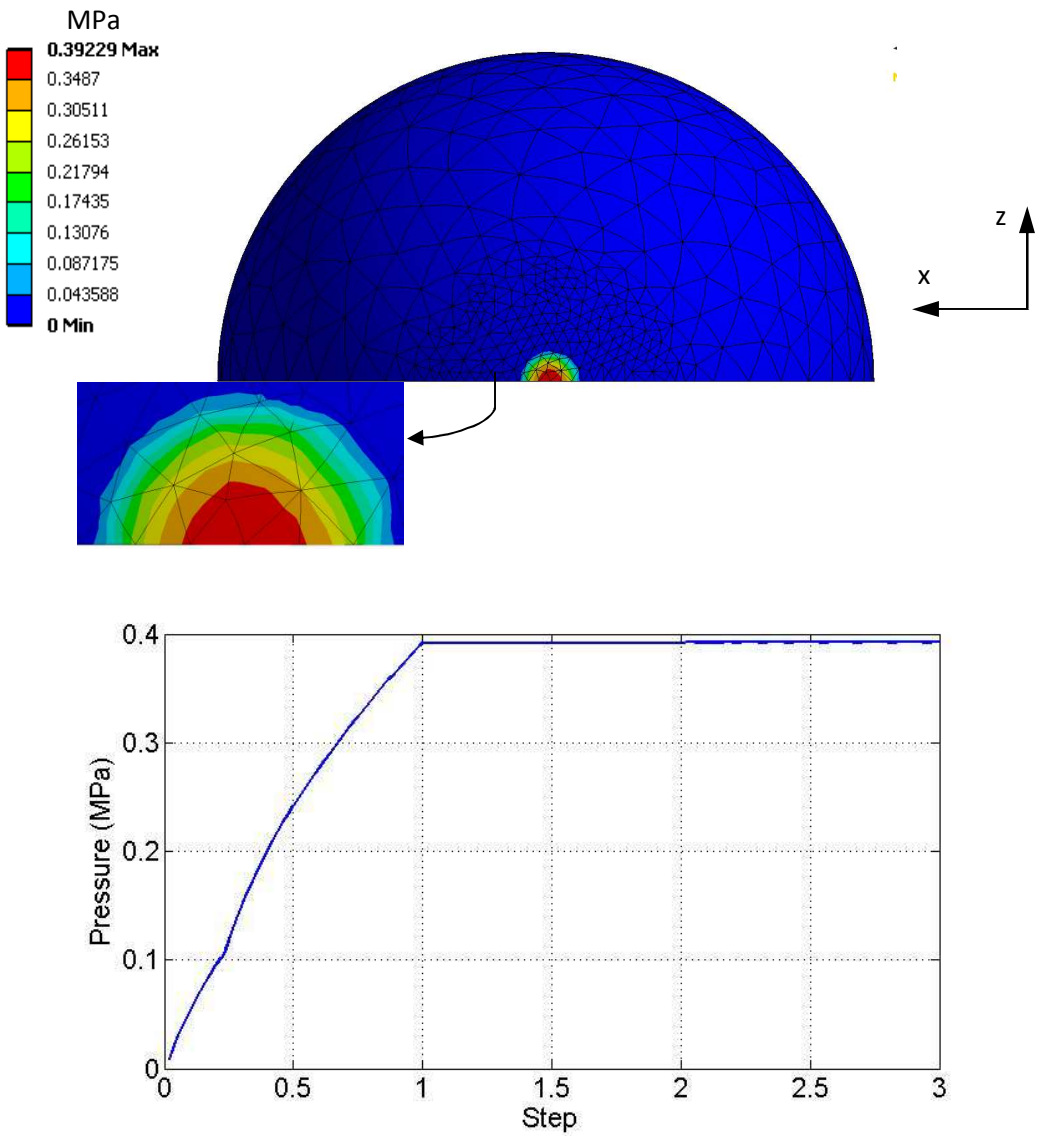

Figure 5.8: Normal pressures versus time steps (top view of lower sphere in Figure 5.6)

5.3.2 FE model comparison with Mindlin theory

The force-compression result of FE model in Figure 5.6 has been shown in Figures 5.9 and 5.10. In Figure 5.9 the comparison with Hertz with very small compression is presented for the compression stage (step 1). Both theoretical and numerical methods are in good agreement. In Figure 5.10 the comparison between Mindlin theory and FE is shown.

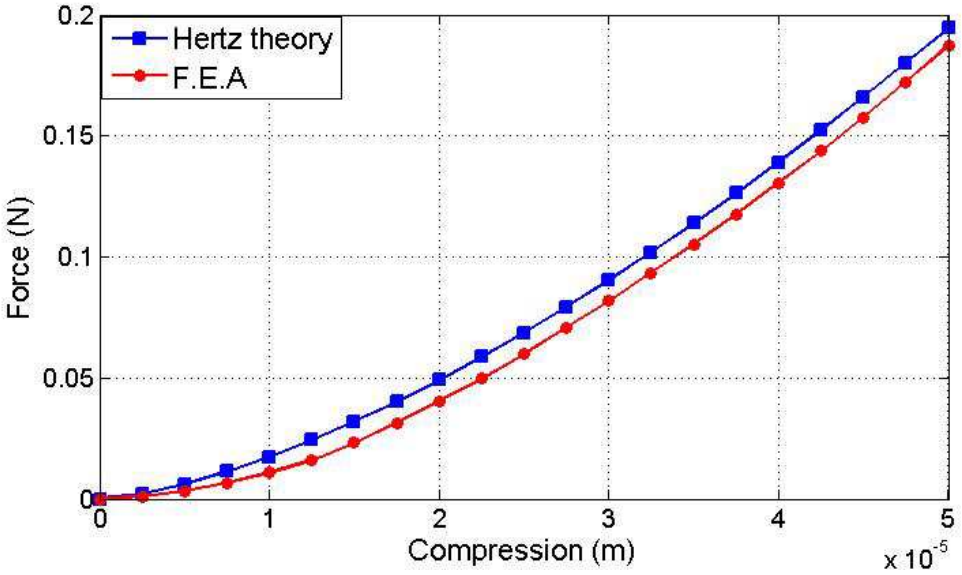

Figure 5.9: Vertical forces versus compression for two spheres in contact as shown in Figure 5.6, comparison between hertz theory and F.E model

Figure 5.10 represents the third step when the shear displacement is applied. As it can be seen, the theory is matched reasonably well at low amplitude indicating that Equation 5-15 holds. Since the shear stiffness is dependent on the mesh, two different mesh densities have been used to show the sensitivity. Although the FE result with 32029 elements varies from Mindlin's theory, it does however represent the same trend. When the elements are reduced to 9188, bilinearity occurs where the initial stiffness is higher than Mindlin theory, while the secant stiffness is the same as the FE results with 32029 elements. This indicates an insignificant discretisation. The difference between FE and Mindlin's theory is expected since Mindlin's theory does not account for all of the complexities such as changes in the contact area. However, these are considered be in good agreement still.

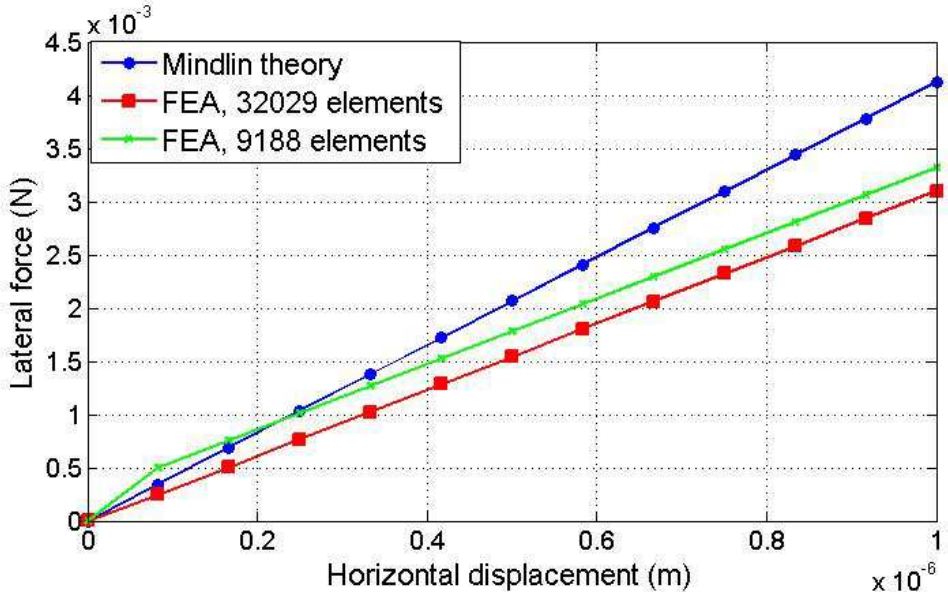

Figure 5.10: Lateral force applied spheres versus horizontally displacement, comparison between theory approach and FE.

5.4 Drop test of spherical particle

A study of the impact response of viscoelastic particles was carried out to investigates the ability of the Prony series model to replicate real behaviour. This simulation was performed as another validation of viscoelastic particle at very short times interval. Using the Prony series fitted to the real properties of viscoelastic material in Chapter 3, is applied and the transient response behaviour is compared with drop experiment. The parameters for Prony series at 15°C is shown is Appendix C.

5.4.1 Experiment using high speed camera

A high speed video camera was used to capture progress as particles were dropped onto a rigid heavy table. The camera was set to record at 1000 fps in a 512×128 pixel area. Two halogen flood-lights were used to provide enough light to capture the image. The velocities before and after impact were calculated by tracking the positions at the extreme diameter of the sphere by counting the pixels and by knowing the camera sampling rate. The pixel size was calibrated by knowing the diameter of the sphere and the number of pixel along the diameter. These results are given in the next section where they are compared with results from the FE analysis.

5.4.2 FE analysis and comparison with experiment

The FE model used for transient analysis is shown in Figure 5.11. In order to prevent any deviation of the sphere during impact, from the normal direction (perpendicular to the upper face of plate), the displacements of the two nodes at the top and bottom of the sphere were constrained to move only in the normal direction. The lower face of the steel plate was fixed rigidly.

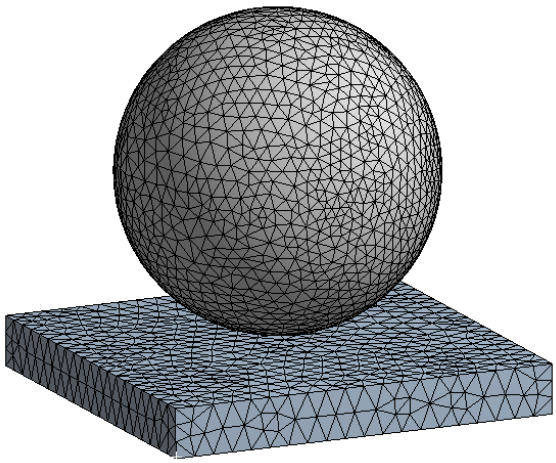

Figure 5.11: Spherical particle in impact with steel plate

Figure 5.12 shows the material behaviour of the particles, the relaxation of the Young's modulus versus time.

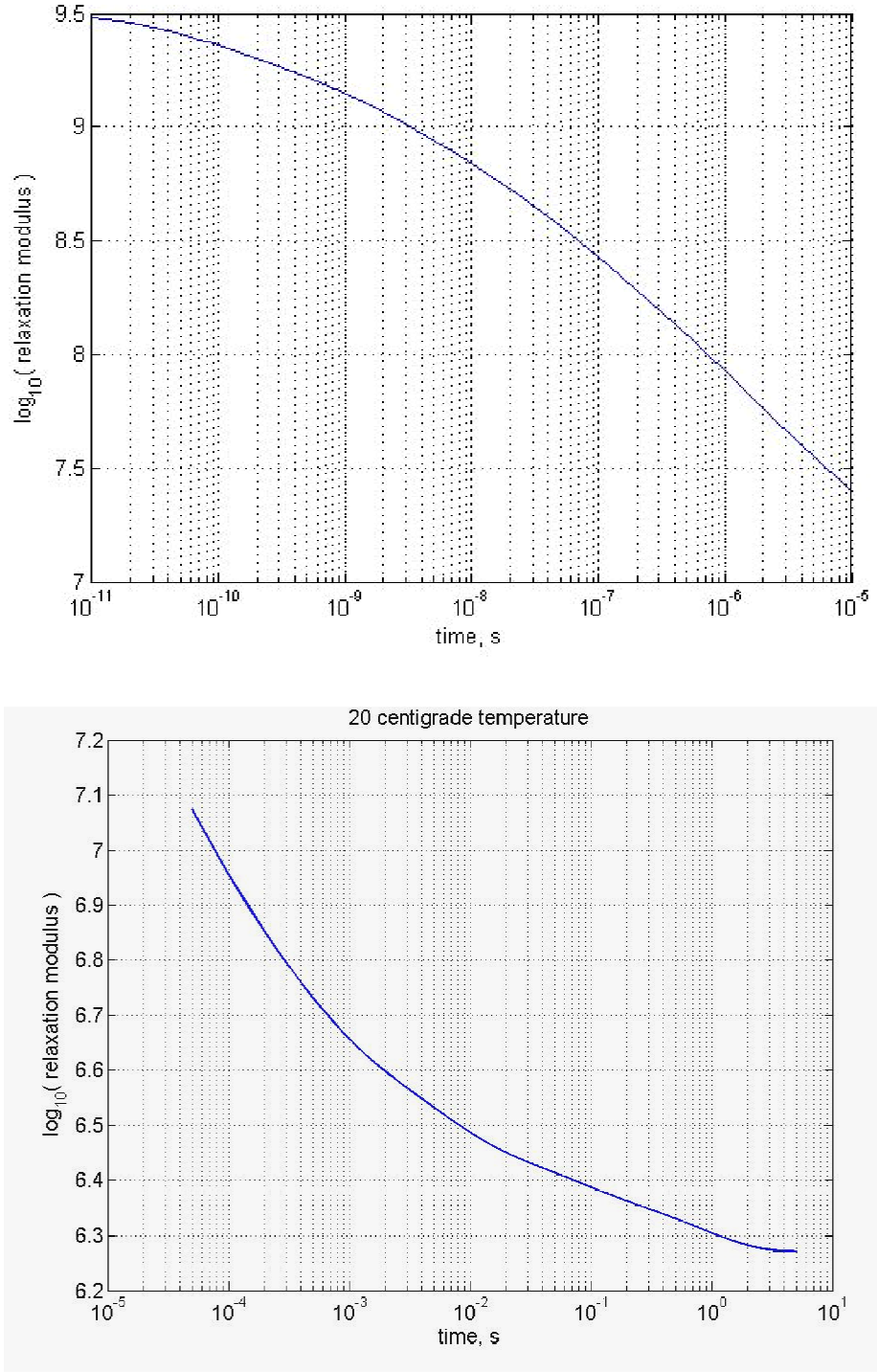

Figure 5.12: Changing in Young's modulus vs. time at 20°C

All velocities are taken from the selected node which was positioned at the extreme diameter, of the sphere, that lies in the plane parallel to the impact surface. The

velocity around the time of impact for two different initial velocities is shown in Figure 5.13.

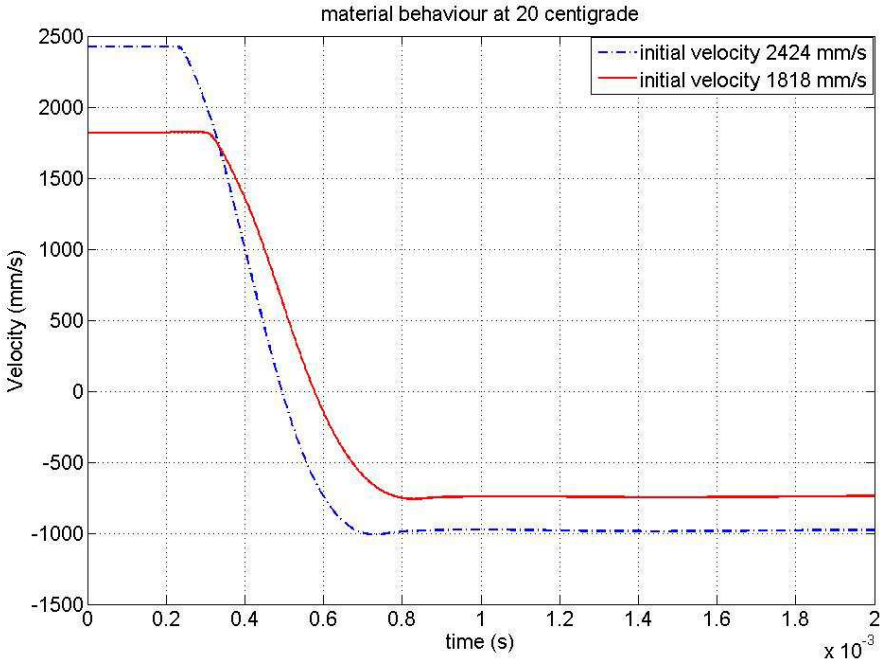

Figure 5.13: Velocity tracking at different initial conditions at 20ºC, positive velocity values represent velocity toward the plate and negative values represent velocity away from the plate.

The sensitivity of the model was also investigated by decreasing the step size and evaluating the velocity after impact. These results are shown in Table 5.1 for an initial velocity of 2424mm/s. Achieving perfect convergence was found to be very difficult and time consuming. In the Table 5.2, the rebound velocity for two different temperatures and different initial conditions are compared.

Table 5.1: Comparison of velocity after impact for different step sizes from an initial velocity of 2424 mm/s.

Step size	Velocity after impact mm/s
200	1000
1000	935
2000	922

Table 5.2: Comparison between experiment (with high speed camera, HS) and FE in different temperature, and different initial velocities.

Initial velocity (mm/s)	Velocity after impact (mm/s)		
	Experiment (HS)	FE (15ºC)	FE (20ºC)
1818	655	707	761
2036	668	790	848
2160	800	837	897
2251	825	871	932
2424	855	936	999

The viscoelastic property of the particle shows the changing in Young's modulus in time domain, Figure 5.12. It can be seen that whenever the time step is too large, because of the steep gradient of the graph in the beginning, this part is missed. As the steep gradient is associated with the zone of maximum damping in the material, the simulation shows less damping in comparison with experiment therefore the rebound velocity is fairly higher than experiment, as it can be seen in Table 5.2.

The deformation history at the contact with the smallest initial velocity, used 1818 mm/s, is shown in Figure 5.14. It can be seen that the peak deformation in this particular case is 0.4 mm. At this deformation, Figure 5.5 indicates that the FE model is stiffer than the Hertzian model and might be another reason for the higher value of rebound velocity obtained form FE.

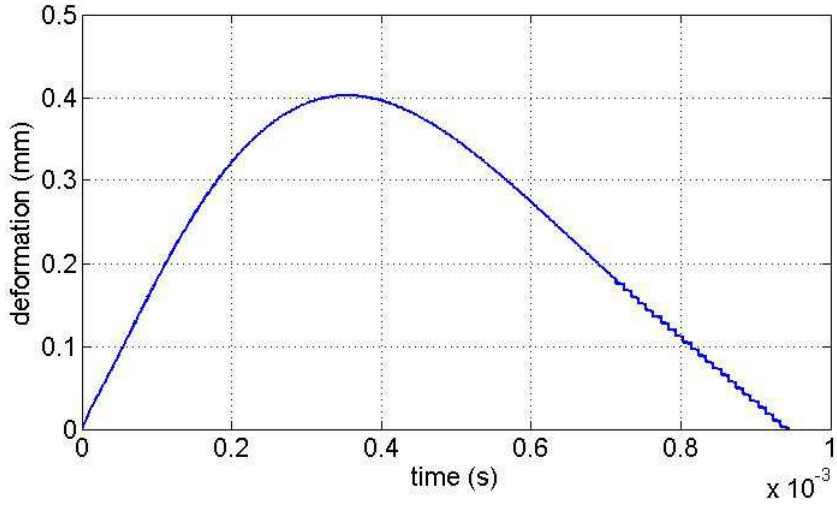

Figure 5.14: Deformation history during impact for initial velocity at 1818mm/s.

For reference, it was considered useful to compare the deformation seen in this text with those typically experienced in a practical granular damper – experiments of the kind reported in Chapter 7 and an equivalent simulation carried out. From that simulation the typical velocity of particle is shown in Figure 5.15. As it can be seen the highest velocity of the particle is around 200 mm/s which is lower than for the impact test and the largest deformation is attained 0.06 mm (Figure 5.16). This suggests that the modelling approach used is valid for the conditions studied later.

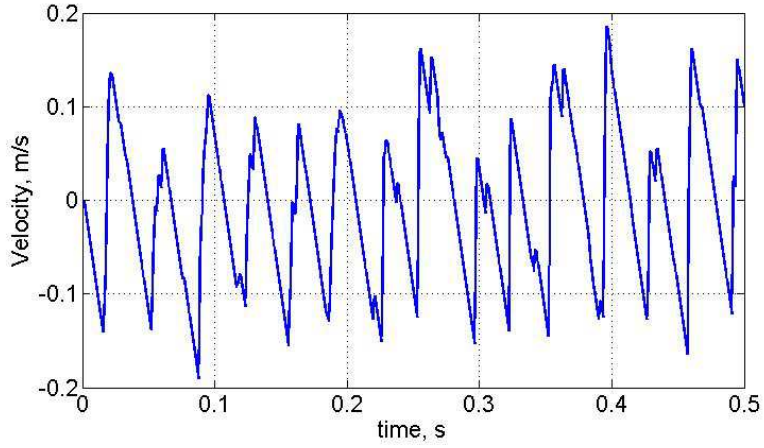

Figure 5.15: Typical velocity history of a spherical particle within granular medium

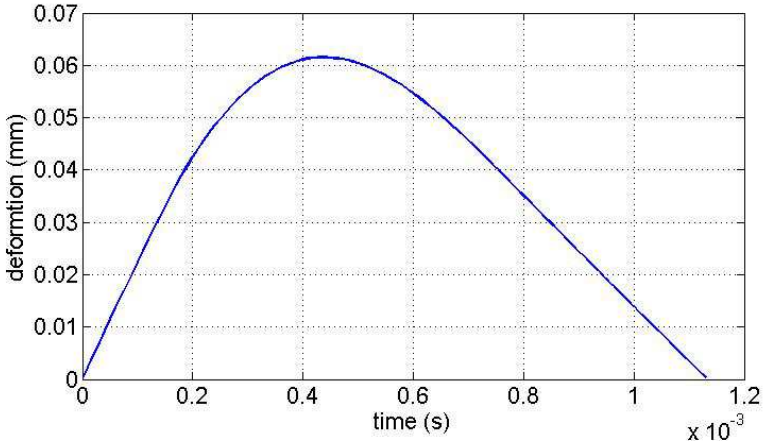

Figure 5.16: Deformation history during impact for initial velocity at 200 mm/s.

5.5 Dynamic properties of individual polymeric spheres

Experiments were carried out in order to obtain the dynamic properties of the polymeric spheres used in this work. These are explained here.

5.5.1 Test rig for measuring stiffness and energy dissipated of individual particles

The polymeric particles used in this work are shown in Figure 5.17.

Figure 5.17: Polymeric spherical particles used in experiment

A test rig was constructed to measure the dynamic stiffness and loss factor of the particles over an approximate frequency range of 2–500 Hz with varying amounts of static preload. A schematic drawing and photograph are provided in Figure 5.18. Three particles were tested simultaneously, compressed to preset amounts between the upper and lower plates. The lower plate was recessed slightly (three depressions each 3 mm depth and 12.5 mm radius) to locate particles equally in radial and circumferential positions. Detailed drawings of the upper and lower plates are produced in Appendix D. The static deflection of the particles was adjusted by altering the compression of the helical bias spring using the threaded bolt. The bias spring was made of stainless steel, with mass 2.7 g, stiffness 19.77 N/mm, and longitudinal resonance much greater than the frequencies of excitation. Sinusoidal excitation was provided to the upper plate by an electrodynamic exciter via a 2 mm

diameter stinger rod. The dynamic force applied by the shaker was measured using a piezoelectric force transducer while the displacement and acceleration of the upper plate were measured using, respectively, a laser displacement probe and an accelerometer. Initial calibration tests that were carried out included the use of a miniature load cell in line with the bias spring. This helped establish the spring stiffness. Additionally, comparisons were made between the accelerometer and laser signals to ensure that they were recording results accurately [112].

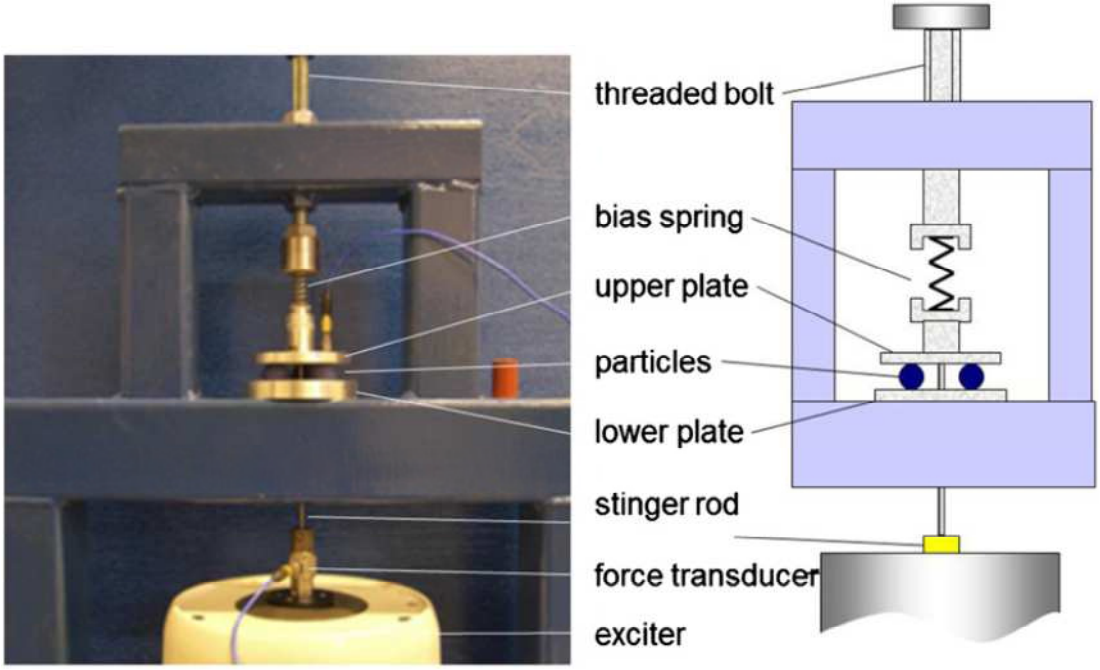

Figure 5.18: Test rig for measuring complex dynamic stiffness of viscoelastic particles.

The signal flow diagram for the experiment is shown in Figure 5.19. Data acquisition was carried out using a four channel digital oscilloscope (Picoscope) linked to a laptop PC. A sampling rate of 5 kHz was used.

From the measured time histories, the stiffness and loss factor were obtained in the following way. The force F applied to the particles was calculated using,

$$F = F_{ft} - k_{bs}\ x - m_p \ddot{x} \tag{5-18}$$

where k_{bs} is the stiffness of the bias spring, F_{ft} is the reading from force transducer and m_p is the combined moving mass (including the plate, stinger rod and

accelerometer) which was found to be 70±2 grams. The quoted variability originated from the uncertain effects of the accelerometer wire. Variables x and $\ddot{x}$ are displacement and acceleration of the mass while the force F_{ft} is the measurement from force transducer. For sinusoidal excitation, the force-displacement curve for a damped system forms a hysteresis loop. The dynamic stiffness and loss factor were estimated from the loop.

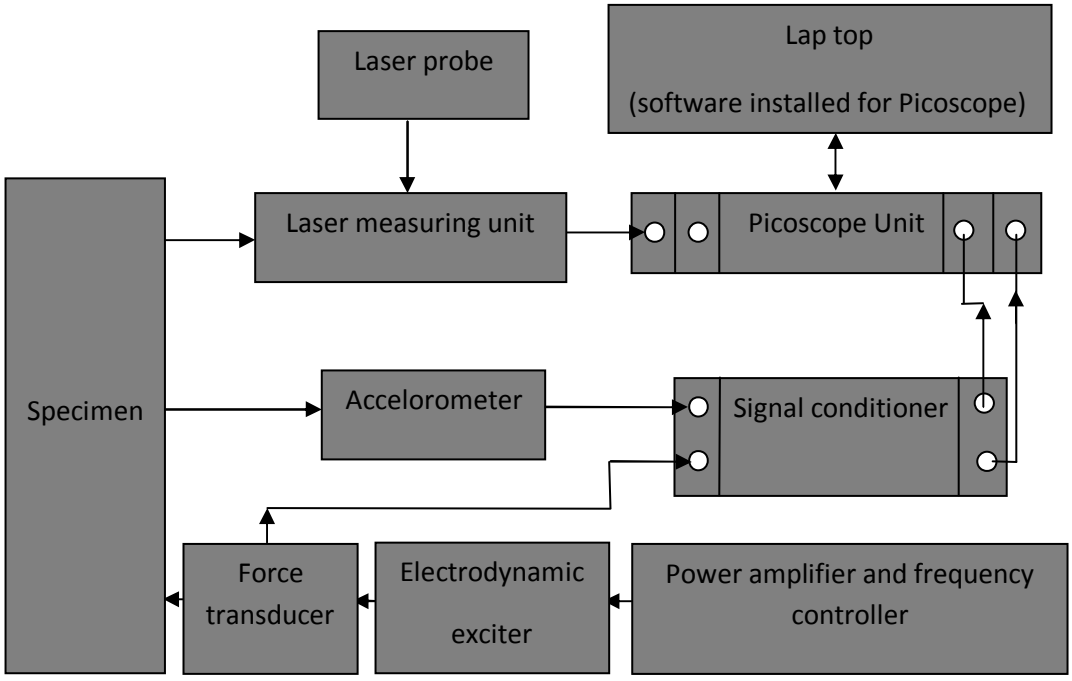

Figure 5.19: Experimental for properties of spherical particles, signal flow diagram

In this work, average properties over the loop were required for use in the DEM model. The dynamic stiffness was therefore obtained by fitting a straight line through the hysteresis loop, the stiffness being the gradient of this line. The loss factor as explained by detail in Chapter 3, is defined as the ratio of average energy dissipated from the system per radian to the maximum dynamic strain energy in the cycle U_m.

In order to validate the performance of the test rig, the elastic modulus and loss factor for two different viscoelastic materials (Dow Corning DC3120 and Sorbothane 60) were obtained using a Metravib Viscoanalyser VA2000 test

machine, the data are presented in Appendix E. The dynamic stiffness and loss factor for cylindrical specimens of each material was predicted using,

$$k = \frac{EA}{L}(1 + 2S^2) \tag{5-19}$$

S is the shape factor (area of one face in contact divided by the area of surrounded) for the specimen [113]. E, A and L are Young's modulus, area and length of specimen, respectively.

Specimens were also manufactured (Figure 5.20) and tested on the test rig. Results are presented in Table 5.3.

Figure 5.20: Test specimens (surface damage caused during removal from test rig)

Table 5.3: Test rig validation results (all measurements at 20°C and 10 Hz)

Material	**Specimen dimensions,** mm			**Material properties** from Viscoanalyser		**Loss factor**, η	**Dynamic stiffness** k_n N/mm	
	length	inner dia.	outer dia.	Young's modulus, MPa	loss factor	measured in test rig	predicted using Equation 5.19	measured in test rig
DC 3120	22.3	7.0	14.2	3.6 ± 0.18	0.075±0.007	0.102±0.008	25 ± 2	24 ± 1.9 (4% error)
Sorbothane 60	9.0	3.0	21.0	0.73± 0.04	0.438±0.004	0.479 ± 0.05	43.1 ± 1	46.8 ± 0.8

It can be seen that there is good agreement between the results. Careful observation on the measurements, suggests that there is an average overestimation of around 0.034 in the test rig results. This is assumed to arise from friction in the test rig and this value was subtracted from every subsequent measurement. The hysteresis loops for the two materials are presented in Figure 5.21.

5.5.2 Measurement of particle properties

Using the validated rig, tests were then carried out on spherical particles. These particles were 15.1 mm diameter spheres make from blue elastomer tested in Chapter 3. For testing carried out at 44 Hz, the force traces showing the three components in Equation 5-18, are presented in Figure 5.22. The contribution of the inertia of the moving mass is evident. The resulting hysteresis loop and the linear fit applied are presented in Figure 5.23. These indicate an average value of approximately 29 N/mm for the dynamic stiffness for three particles (in parallel).

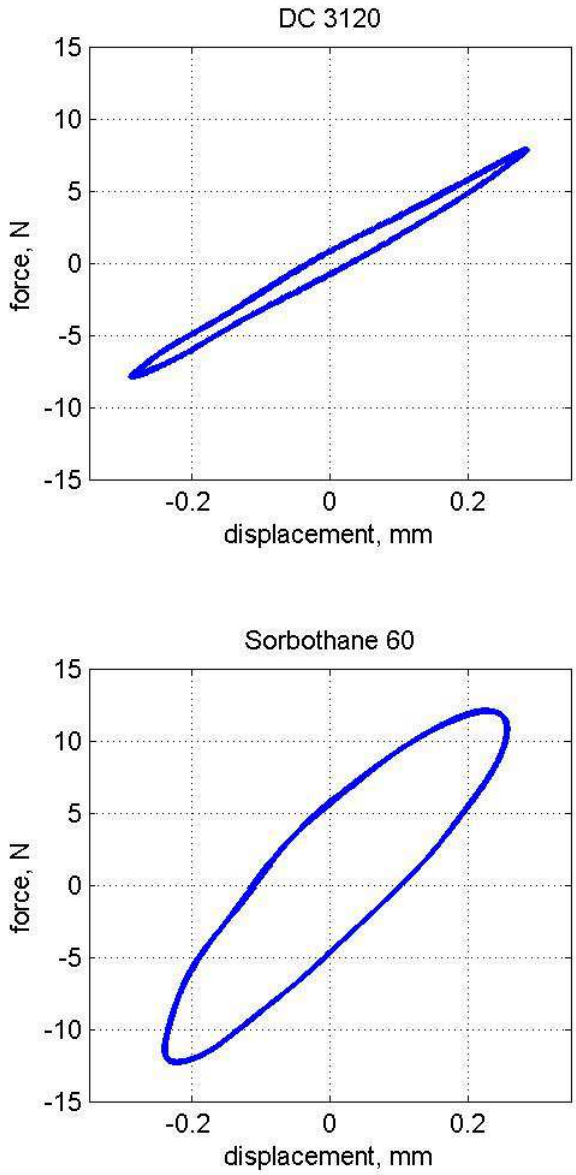

Figure 5.21: Hysteresis loops from test rig for DC3120 and Sorbothane 60 cylindrical specimens at 10 Hz

This gives an approximate normal stiffness of 9.7 N/mm for each sphere at this compression level. Using Equation 5-9, the average sphere stiffness was therefore estimated to be 6.5 N/mm.

Properties of the spheres were measured at different frequency and pre-compression levels. Results are summarised in Table 5.4. Note that variability in the loss factor measurements between individual cycles is around 5%. A range in stiffness values is

quoted to give an indication of the level of uncertainty from cycle to cycle variability and underlying nonlinearity due to the shape of the particles.

The effect of changing static pre-compression on the stiffness of particles is presented in Figure 5-24. It can be seen that the stiffness increases considerably with pre-compression while the change in loss factor is relatively small. This is reasonable as viscoelastic materials are expected to be linear with strain and the stiffness is affected by the change in geometry. The effect of changing excitation frequency can be seen in Figure 5-25.

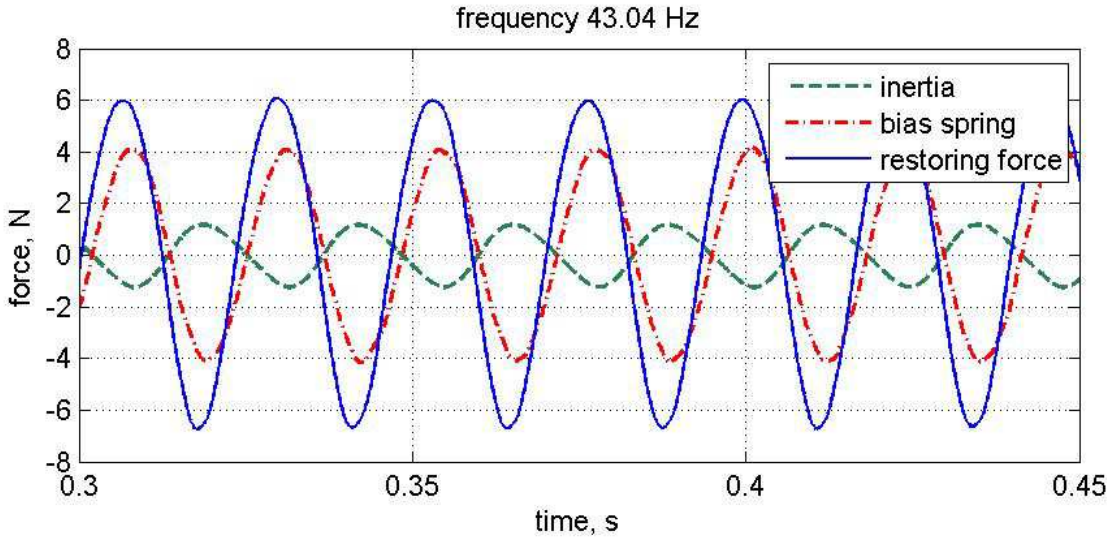

Figure 5.22: Time history of force terms (Equation 5-18) for 3 spheres under 0.64 mm pre-compression

Note that at higher frequencies, the displacement amplitude was reduced to keep the power output of the shaker at a nominally similar level. The results (Table 5-4) show that the stiffness varies only slightly over the frequency range considered while the increase in damping is more significant.

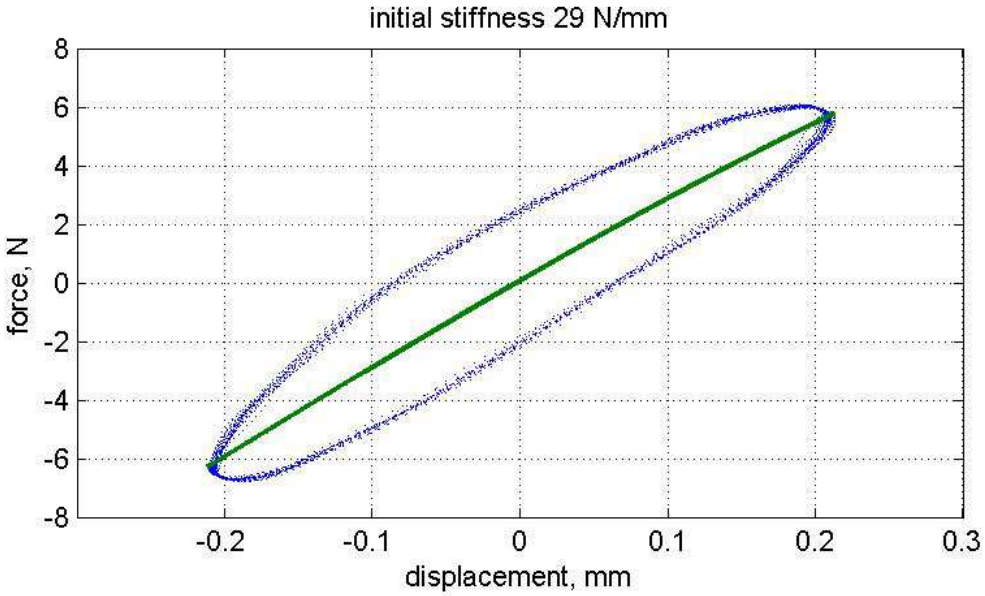

Figure 5.23: Hysteresis loop for three viscoelastic particles at 44Hz and 0.64 mm pre-compression

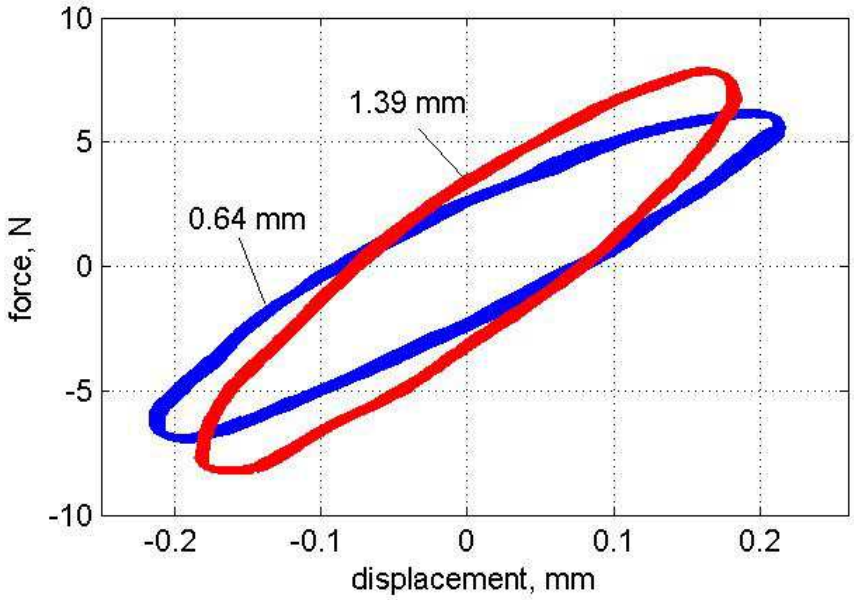

Figure 5.24: Measured hysteresis loops at 44 Hz with two different levels of static pre-compression

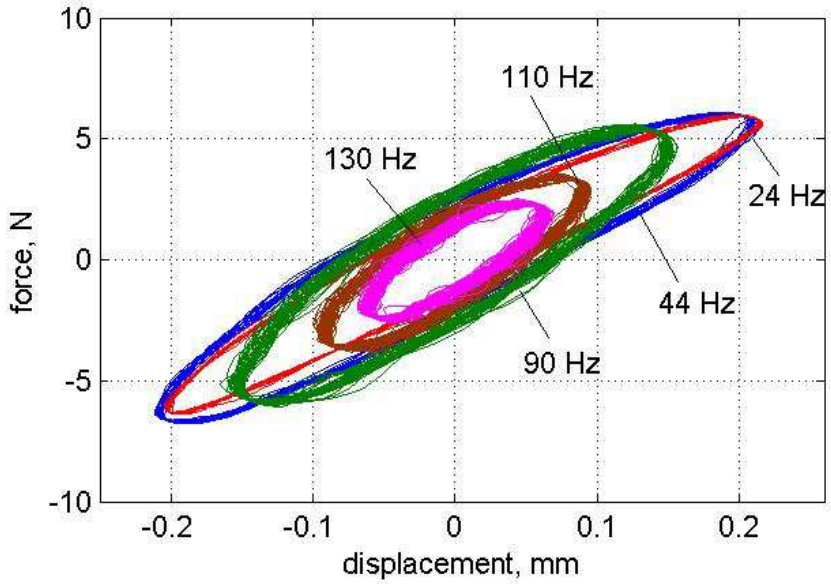

Figure 5.25: Measured hysteresis loops at five different frequencies with static pre-compression 0.64mm

Table 5.4: Measured dynamic stiffness for blue spheres under different conditions.

Pre-compression (mm)	**Frequency (Hz)**	**Loss factor**	**Stiffness (N/m)**		
			Min	**Average**	**Max**
0.64	24	0.21	23.4	29.2	30.6
0.64	44	0.36	24.1	29.0	30.8
0.64	90	0.45	28.7	33.9	34.2
0.64	110	0.55	29.4	33.1	33.2
0.64	130	0.53	28.4	34.4	40.3
1.39	44	0.43	38.9	39.5	44.9

5.6 Chapter summary

In this chapter, It was shown that the FE model of the spherical particle with hyperelastic property was in good agreement with Hertz contact theory also shear stiffness and relation with normal stiffness, the FE model shows fairly well with Mindlin theory.

A study of the impact response of viscoelastic particles was carried out to test the ability of the Prony series in conjunction with the FE model to replicate real behaviour. The velocities before and after impact were tracked and recorded. Also the drop test was performed and the velocities just before and after contact were measured using a high speed camera. The comparison between velocities in model and experiment shows a fairly good agreement, although the FE model has less damping than experiment. This discrepancy arises from the steep gradient of the Young's modulus relaxation curve, as the time step misses.

The properties (dynamic stiffness and loss factor) of each individual sphere particle were measured via a calibrated designed test rig. These measured values are used in DEM simulations in next chapter.

6 The discrete element method for modelling the vibration of a granular medium

6.1 Introduction

The discrete element method (DEM) also called a distinct element method was introduced by Cundall [66] for the analysis of rock mechanics problems. DEM is a numerical method for computing the motion of a large number of particles of micrometre-scale size and above. Today, DEM is widely accepted as an effective method of addressing engineering problems in granular and discontinuous materials, especially in granular flows, powder mechanics, and rock mechanics.

The discrete element method can be computationally intensive, which limits either the length of a simulation or the number of particles. The dynamic behaviour is represented numerically by a time stepping algorithm in which it is assumed that the velocities and accelerations are constant within each time step. The method is the same as a finite-difference algorithm.

The calculations performed in the DEM alternate between the application of Newton's second law to the particles and a force-displacement law at the contacts. Newton's second law is used to determine the motion of each particle arising from the contact and gravity, and the force-displacement law at the contact defines the forces cause by the relative motion at each contact.

Particle flow code (PFC) is commercial software which is based on DEM [114]. PFC in three-dimensional mode has been used in this work to simulate the granular medium.

Use of two force-displacement law and law of motion along with time step determination is explained in this chapter. The contact model and the approach used to define each parameter such as stiffness and damping are also discussed. The procedure used for polymeric particles is also explained. At the end, to better understand of the behaviour of granular medium over a wide range of amplitude of excitation, a parametric study is performed.

6.2 DEM calculation procedure

The DEM software employed uses a time stepping algorithm involving the equations of motion for particles and the contact force arising from interaction between particles and walls. These contacts between are formed and broken automatically. The force-displacement law is then used in each contact to update the contact forces based on the relative motion between the two interacting bodies. The law of motion is applied to each particle to update its velocity and position arising from the contact force and any other body forces (e.g. from gravity). Container positions that define the walls are updated for input velocities to the walls.

6.2.1 Contact force

The contact force (force-displacement) law arises in the contact area between particles and between particles and walls. The contact force is projected to two components; one in the normal direction along n_i vector (unit normal vector to the contact plane) and the other component is in the tangential direction which lies on the contact plane.

The contact force is therefore expressed by two components,

$$F = F_n + F_s \tag{6-1}$$

where F_n and F_s are normal and shear component vectors of the contact force.

The normal contact force vector is given by,

$$F_n = k_n d_o n_i \tag{6-2}$$

where k_n is the normal stiffness at the contact and d_o is the overlap of two entities (particle-particle or particle-wall). For nonlinear contact the Hertz equation is considered and the modulus and Poisson ratio should be defined.

The contact velocity v, of the two entities *a* and *b*, is the relative velocity of each entity to the other, at the contact point.

$$v = (\dot{x}_c)_b - (\dot{x}_c)_a \tag{6-3}$$

$$v = \left(\dot{x}_i + e_{ijk}\omega_j(x_{k,c} - x_k)\right)_b - \left(\dot{x}_i + e_{ijk}\omega_j(x_{k,c} - x_k)\right)_a \tag{6-4}$$

which consists of translational and rotational velocity. The subscript *c* stand for contact point, ω is angular velocity of the particle and e_{ijk} is permutation symbol is defined as,

$$e_{ijk} = \begin{cases} +1, \text{if } , (i,\ j, k) \text{ is} (1,2,3), (3,1,2) \text{or } (2,3,1) \\ -1, \text{if } , (i,\ j, k) \text{is } (1,3,2), (3,2,1) \text{or } (2,1,3) \\ 0, \text{if } , i = j, \text{or } j = k, \text{or } k = i \end{cases} \tag{6-5}$$

$$v = v_n + v_s \tag{6-6}$$

where v_n and v_s are normal and shear component vectors of the contact velocity respectively.

During each time step Δt the increment of shear displacement component is calculated using the shear velocity component as,

$$\Delta d_s = v_s \Delta t \tag{6-7}$$

This is used to calculate the shear force increment vector as,

$$\Delta F_s = k_s \Delta d_s \tag{6-8}$$

where k_s is the shear stiffness at the contact.

6.2.2 Application of Newton's second law

The motion of each particle in a granular medium is calculated from the summation of forces and moment vectors applied to it. The motion of particle is described as translational and rotational motion. The equation of motion for translational vector can be expressed as,

$$F_i = m(\ddot{x}_i - g_i) \tag{6-9}$$

where F_i, m, g are the resultant force, mass of particle and gravity respectively. $\ddot{x}$ is acceleration of centre of mass.

The equation of rotational motion for a spherical particle is given by,

$$M_i = I\,\dot{\omega}_i \tag{6-10}$$

where $M, I, \dot{\omega}$ are the resultant moments, moment of inertia and angular acceleration respectively. The moment of inertia for a spherical particle with radius R is given as,

$$I = \frac{2}{3} mR^2 \tag{6-11}$$

The equations of motion are integrated using centred finite difference method in time step Δt. The accelerations at time t is calculated based on velocities at mid - intervals. The accelerations are,

$$\ddot{x}_i(t) = \frac{1}{\Delta t}(\dot{x}_i(t + \Delta t/2) - \dot{x}_i(t - \Delta t/2)) \tag{6-12}$$

$$\dot{\omega}_i(t) = \frac{1}{\Delta t}(\omega_i(t + \Delta t/2) - \omega_i(t - \Delta t/2)) \tag{6-13}$$

By substituting Equations (6-12), (6-13) in equations of motions (6-9), (6-10) and calculating velocities at time $t + \Delta t/2$ one can obtain,

$$\dot{x}_i(t + \Delta t/2) = \dot{x}_i(t - \Delta t/2) + (\frac{F_i(t)}{m} + g_i)\Delta t \tag{6-14}$$

$$\omega_i(t + \Delta t/2) = \omega_i(t - \Delta t/2) + (\frac{M_i(t)}{I})\Delta t \tag{6-15}$$

These velocities are used to update the position of the particle centre by,

$$x_i(t + \Delta t) = x_i(t) + \dot{x}_i(t + \Delta t/2).\Delta t \tag{6-16}$$

In PFC3D when analysing a system with many particles a critical time step is determined automatically. This value is chosen at each iteration step. The critical time step is proportional to the highest natural frequency in the system, so to perform a global eigenvalue analysis of the system is expensive. Therefore a simplified approach is taken to estimate the critical time step. A simple analysis of a decoupled multi degree of freedom system of linear springs and masses lead to a critical time step which is defined by,

$$t_{crit} = \begin{cases} \sqrt{m_{\min} / k_{translatioal}} \\ \sqrt{I_{\min} / k_{rotational}} \end{cases} \tag{6-17}$$

where $m_{\min}$ and $I_{\min}$ are the smallest mass and moment of inertia in the system respectively while $k_{translational}$ and $k_{rotational}$ are highest effective stiffness in translational and rotational directions from every degree of freedom. The final critical time step is taken to be the minimum of all critical time steps computed for all degrees of all bodies.

The actual time step is taken as a multiplication of this estimated value by a safety factor. In this work the safety factor, is set to by default as 0.8.

6.2.3 Contact model

Contact conditions are defined in the normal and shear directions as shown in Figure. 6.1. The symbols m, k and c stand for mass, stiffness and damping, respectively, and the subscripts n and s refer to normal and shear directions. The following subsections explain the simplifications employed and the resulting nature of each element used in this study. In general particle-wall interactions have a similar form although the effective mass is replaced by particle mass and the stiffness, friction and viscous damping elements have different values that describe particle-wall contact.

6.2.3.1 Viscoelasticity

The particles considered in this work are made of polymers that exhibit viscoelasticity. Representation of realistic viscoelastic behaviour in the time domain analyses is always challenging as simple models such as the standard linear viscoelastic model do not match the properties of real materials particularly well while more complex multi-element models such as the Generalised Maxwell (represented as a Prony series) significantly increase the calculation cost.

The approach taken here is to use the Kelvin-Voigt model that comprises a spring and dashpot in parallel. The advantage of this approach is that the model is standard for most commercial DEM software – see Figure 6.1 for normal and shear contact models between particles. However, use of just one spring and dashpot is a

considerable simplification and some consideration needs to be given as to its suitability for granular viscoelastics.

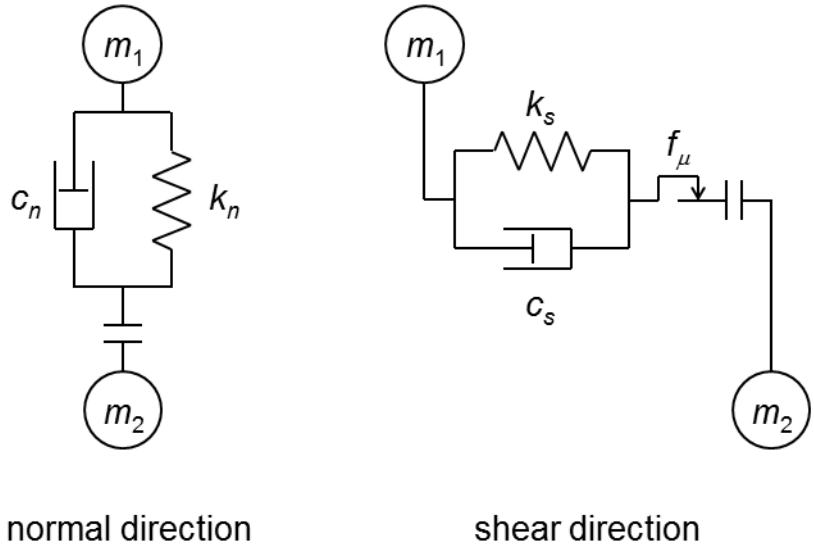

Figure 6.1: Contacts elements in DEM

In a viscoelastic material, the Young's modulus *E* and the loss factor η are frequency dependent. Use of a Kelvin-Voigt model requires the selection of a spring and a dashpot whose properties do not depend on frequency. The model is therefore completely accurate at only one frequency. Clearly the selection of this frequency is an important part of obtaining the most representative model. One approach is to assume that inter-particle interactions are dominated by the impulse response of the bodies momentarily in contact. In this case, properties are those at the natural frequency of the touching particles. An alternative approach, when considering mono-frequency, harmonic excitation is to use the excitation frequency. In either case, it is important to note that for the Kelvin-Voigt model, the equivalent loss factor is given by,

$$\eta = \frac{c\omega}{k} \tag{6-18}$$

where η, k, c and ω are loss factor, stiffness, damping constant and frequency respectively. Hence it can be seen that the equivalent loss factor increases with frequency. Figure 6.2 shows typical shapes of the modulus and loss factor curves obtained using multi-element Prony series and the Kelvin-Voigt model. It is

interesting to note that while the Kelvin-Voigt model is only exact at one frequency, it provides a reasonable estimate to the curve at lower frequencies i.e. if the effective temperature is some way above the glass transition.

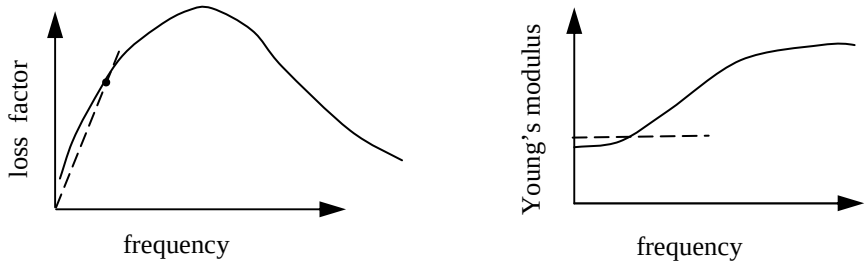

Figure 6.2: Comparison Kelvin-Voigt model (dash line) with Prony series (solid line)

As it was shown in Chapter 5, the maximum deformation of particles in the operating zone (experiment) is very small therefore normal and shear behaviour were assumed linear, this also could lead to reduced computational costs in PFC3D. The zone in which the viscoelastic material operates can also affect the Poisson's ratio [115] and the coefficient of friction [116]. Rather than attempt complicated experimental activities to measure these properties, they are assumed constant in this work. Poisson's ratio equal 0.45 and coefficient of friction equal to 1 are assumed.

6.2.3.2 Stiffness normal and tangential to the contact surface

The contact stiffness is defined by normal stiffness (k_n) and shear stiffness (k_s). For a linear system the stiffness of the two contacting particles or particle and wall act in series, the contact normal stiffness is given by,

$$k_n = \frac{(k_n)_a (k_n)_b}{(k_n)_a + (k_n)_b} \tag{6-19}$$

where notations a, b indicate each entity. Similar equation for the contact shear stiffness is given by,

$$k_s = \frac{(k_s)_a (k_s)_b}{(k_s)_a + (k_s)_b} \tag{6-20}$$

6.2.3.3 Viscous damping

In the contact model employed, the normal and shear dashpots are parallel to the associated springs. Damping force is added to contact force, both shear and normal components create force which is given by,

$$F_i = c_i v_i \tag{6-21}$$

c_i is damping constant which for normal case is c_n and for shear case is c_s and v_i is the relative velocity at contact and as explained for damping constant, it depends on which direction it is, it could be v_n or v_s.

In PFC3D, the damping constant is not defined directly and instead of that the damping ratio is used. It is given as,

$$\zeta_i = \frac{c_i}{2\sqrt{k_i m_{eff}}} \tag{6-22}$$

where k_i is the contact stiffness $(i = n, \text{normal}; s, \text{shear})$ and m is effective mass. For particle-wall contact it is taken as particle mass and in the case of particle-particle interaction it is defined as,

$$m_{eff} = \frac{m_1 . m_2}{m_1 + m_2} \tag{6-23}$$

where m_1 and m_2 are mass of particle 1 and 2 respectively.

The damping for a viscoelastic material is usually characterised in terms of loss factor. The coefficient c of an equivalent viscous damper at a given frequency ω is,

$$c_n = \frac{k_n . \eta}{\omega} \tag{6-24}$$

If instead, it is assumed that the behaviour is dominated by the contact resonance, this becomes,

$$c_n = \eta\sqrt{m_{eff}k_n} \tag{6-25}$$

Note that stiffness and damper terms are in general, assumed to be different in normal and shear directions. In the shear direction, there is no consensus on the correct expression for damping. Some have ignored this term completely [38], others have assumed that the viscous damping coefficient in the tangential direction is the same as the one in the normal direction [108]. For viscoelastic particles, the energy dissipated is directly proportional to the loss factor multiplied by the stiffness. Thus the shear damping coefficient can be written as,

$$c_s = c_n\frac{k_s}{k_n} \tag{6-26}$$

As already mentioned in PFC3D, damper coefficients are input as a fraction of critical damping. Hence,

$$\zeta_n = \frac{\eta}{2} \tag{6-27}$$

And hence the shear damping ratio is given by,

$$\zeta_s = \zeta_n\sqrt{\frac{k_s}{k_n}} \tag{6-28}$$

The viscous force is applied after sliding check; also if the contact is sliding so that the shear contact-model force has reached the Coulomb limit, then the viscous shear force is reduced to zero.

6.2.3.4 Friction force

Friction is estimated using the Coulomb equation which is a relation between normal and shear force, such that two bodies in contact may slip on each other. In the model, slipping is always active. The slip is explained by the friction coefficient at the contact which is taken as minimum friction coefficient of the two particles or particle and wall.

The contact is checked for sliding conditions by checking the maximum allowable shear contact force which is given by,

$$F_s\big|_{\max} = \mu . F_{n,i} \tag{6-29}$$

where μ is friction coefficient. If the applied shear force is greater than maximum shear force calculated by above mentioned equation, then slip is allowed to occur during next cycle. So the condition for slipping is given by,

$$F_{s,i} > F_s\big|_{\max} \tag{6-30}$$

And the magnitude of $F_{s,i}$ is substituted by $F_s\big|_{\max}$.

So as it mentioned in the models used, Coulomb friction is assumed to govern the slip between particles (and between particles and walls). In the work reported here, the coefficient of friction μ was considered to be uniform for all contacts.

6.3 PFC simulation for container with polymeric particle dampers

In order to make the appropriate model in PFC3d, first of all the appropriate properties of materials are required. In this work a box filled with the blue elastomeric spheres was considered. Stiffness and damping of particles can be obtained by theoretical and experimental methods described in Chapter 5.

Another required parameter was the density of particles. The weight and also the diameter of ten particles were measured and the average taken. For each particle the diameter was 15.1±0.01 mm and mass 2.11±0.01 grams indicates a density of 1170 kg/m^3. The density and diameter of each particle were input to the code.

The next step was to generate the container and define the stiffness of all walls. The internal dimensions of the container were 180×120×40 mm and it had walls 30mm thickness. The container material was assumed to be Perspex – a material that is much stiffer than polymeric particles. For the container, the normal and shear stiffness were assumed to be 100 MN/m and 70 MN/m respectively.

After defining the appropriate material and physical properties of each individual particle in PFC3D code, then the specific numbers of particles were generated. This involved two main steps.

First, a specific number of were randomly generated and located within the specified volume. In this work, 200 particles were used for vertical vibrations and 260 for horizontal vibrations studies. For relatively high-density packing, random settling of locations can create a medium that does not fit within the generated volume. To solve this problem two steps were taken. First, the radius of particles was temporarily reduced to a set amount – a suitable value of 66% were found by trial and error – then an automatic procedure attempted to fit these particles into the available space without overlapping. In total 2×10^6 attempts were used in this work – see Figure 6.3.

After generating and fitting particles into the model, they were allowed to fall under gravity and settle over a period of 60,000 time steps. This was to encourage the medium to its equilibrium state – see Figure 6.4. It was considered that the model was in equilibrium when the maximum or average unbalanced force was small compared to the maximum or average contact force. Typical average unbalance forces were found to be 5.36×10^{-9} N while the maximum unbalanced force was 1.28×10^{-7} N (see Appendix F) – the small values show that steady state conditions were effectively reached. Assuming only forces applied due to the mass of particles, the mean contact force was found to be 2.78×10^{-2} N, many times larger than the unbalanced forces (see – Figure 6.5). Note that during this step, the radius of the

particle was also increased back to the original value by multiplying the factor of 1/0.66. The output data file can be seen in the Appendix F.

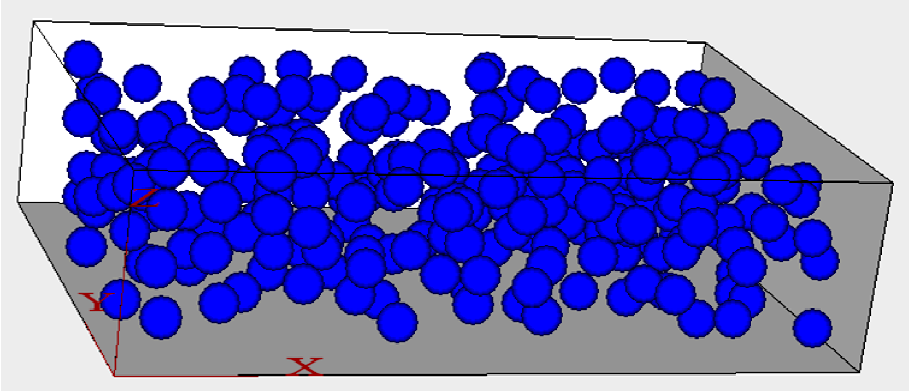

Figure 6.3: Random generation of particles, In the first step generating particles with smaller size.

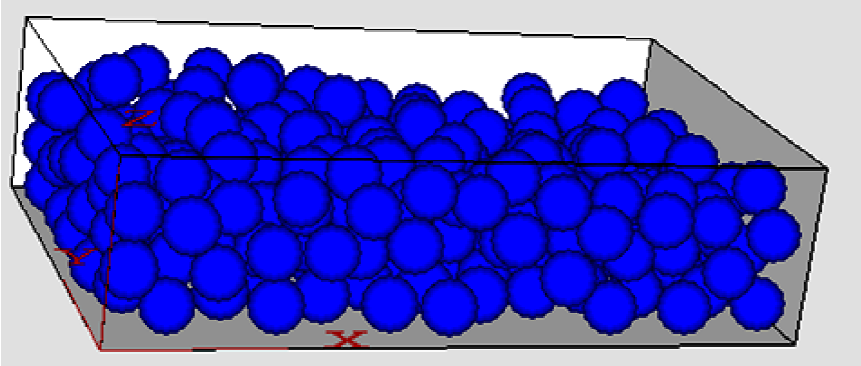

Figure 6.4: Container and particles in equilibrium

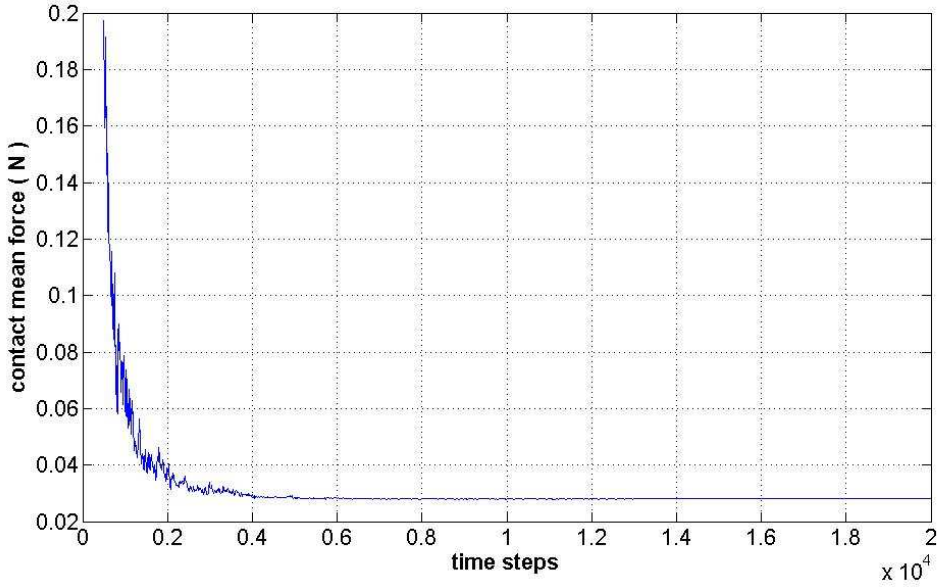

Figure 6.5: Average contact force versus time steps, after particles reach equilibrium in the end of step two.

The next step was to apply boundary conditions. Here, the boundary condition was a translational sinusoidal velocity applied to all the walls. In general 50,000 time steps, approximated equivalent to 0.5 s, of shaking were recorded.

For the purposes of model validation, simulations were carried out at acceleration amplitude of around 1.6 g and frequencies 30, 50, 90 and 130 Hz. (the comparisons with experiments are shown in the next chapter). Here, plots showing energy dissipation over time for 200 particles in vertical vibration and are shown in Figures 6.6 to 6.10. The power dissipation is the gradient of the energy dissipation curve. In each case the total dissipation is shown by fitting a polynomial line through the total energy dissipated graph, these values for power dissipated are compared with experiment in the next chapter. Also in each case the energy dissipated which is made up from friction (at contacts) and viscous (material loss) terms can be seen. The intercept value for polynomial line is thought to be transition time for the vibrating damper to break up the clumps of particles which by increasing excitation frequency it decreases.

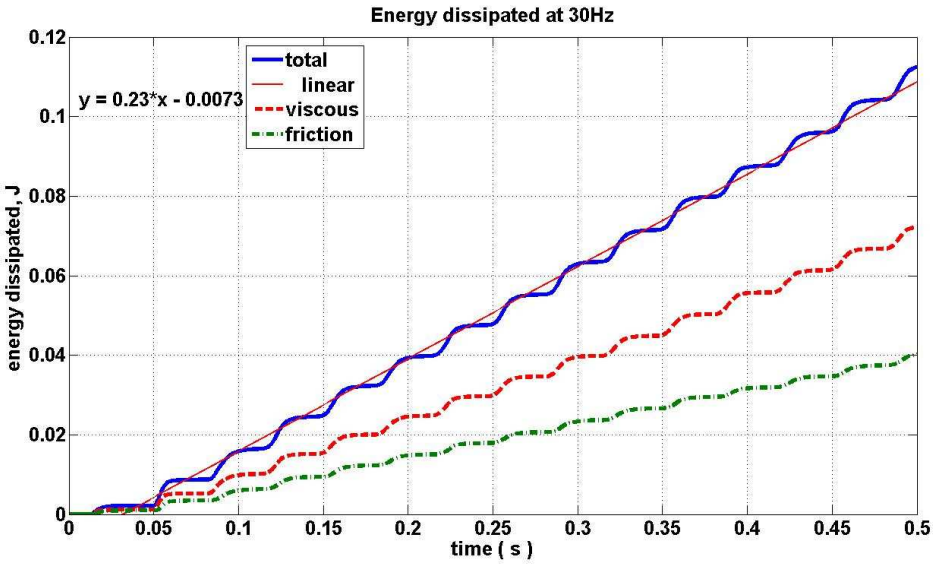

Figure 6.6: Energy dissipation at 30 Hz, 200 particles in vertical excitation.

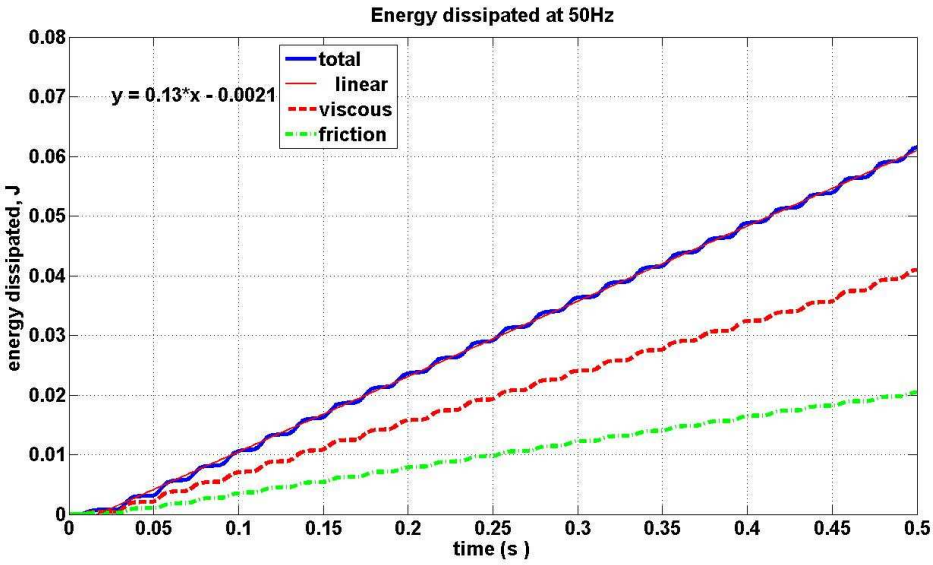

Figure 6.7: Energy dissipation at 50 Hz, 200 particles in vertical excitation.

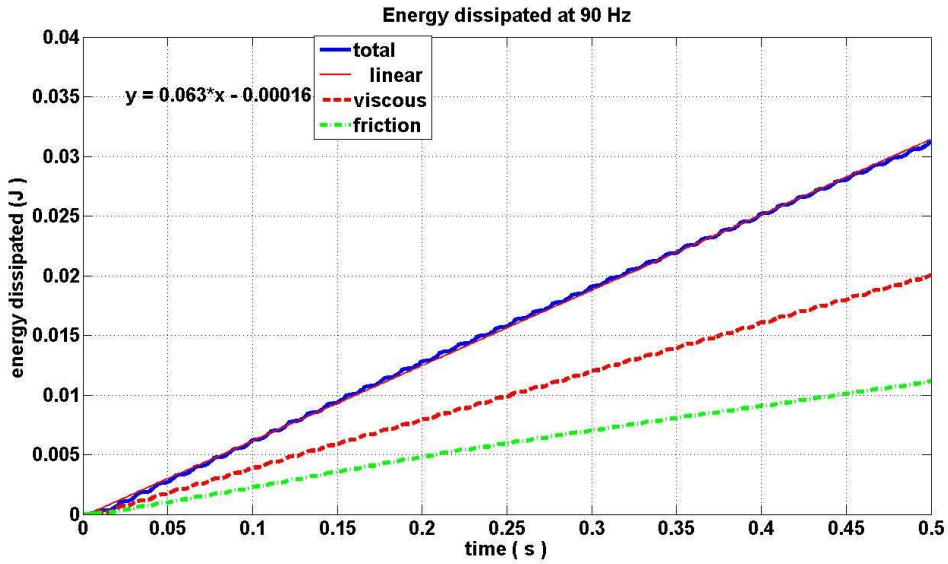

Figure 6.8: Energy dissipation at 90 Hz, 200 particles in vertical excitation.

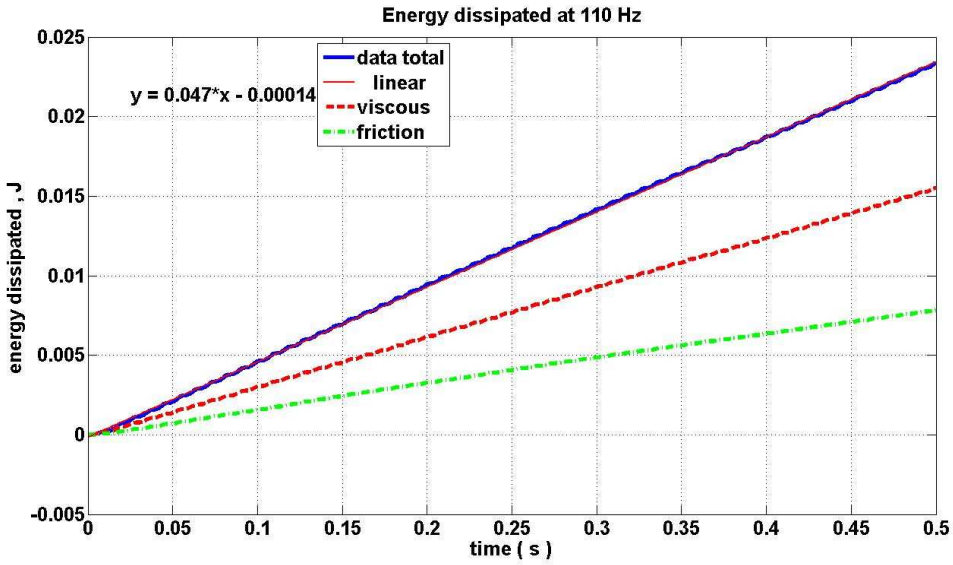

Figure 6.9: Energy dissipation at 110 Hz, 200 particles in vertical excitation.

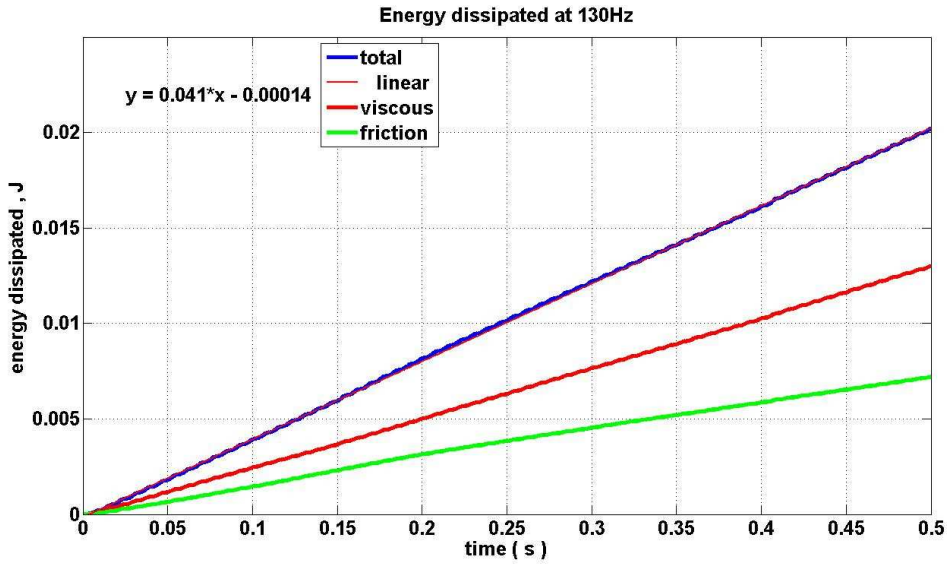

Figure 6.10: Energy dissipation at 130 Hz, 200 particles in vertical excitation.

As an another validation of the DEM model, the comparisons between the experiment represented in Chapter 4, for low amplitude vibration, and simulations by PFC3D are shown in Figure 6.11. The results show good agreement, although at 500 Hz frequency they are far from each other which it is thought because of the first natural frequency of container. (Initial tests showed that flexible modes of the container were above 500 Hz while the rigid body modes were below 5 Hz).

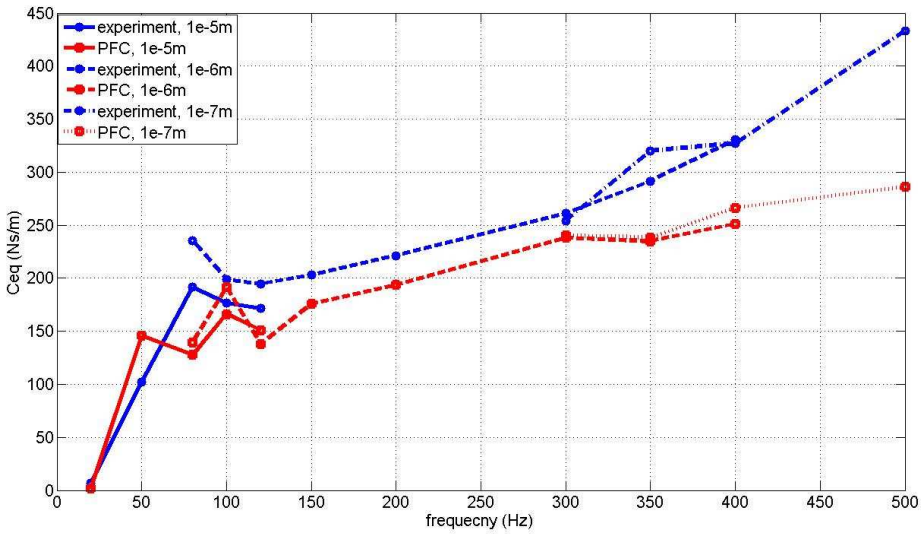

Figure 6.11: Comparison between experiment (which were performed in chapter 4-horizontal vibration) and DEM modelling

In Figures 6.12 and 6.13 and also in Table 6.1, the power dissipated from horizontal vibration for 260 particles at different amplitudes are shown. As it can be seen in Figure 6.13, when the vibration level is very low most of energy dissipated is due to viscous effect.

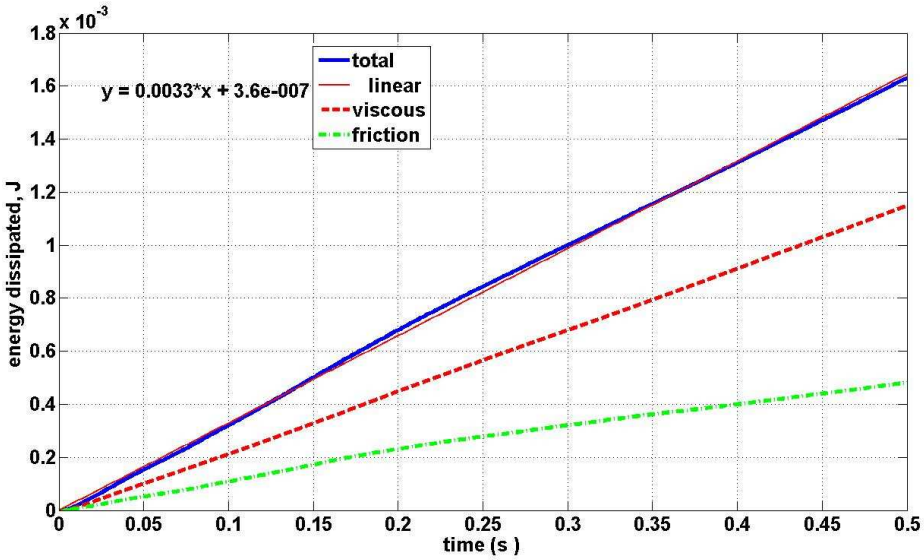

Figure 6-12: Energy dissipated at 100Hz, amplitude 10^{-5} m, 260 particles in horizontal vibration.

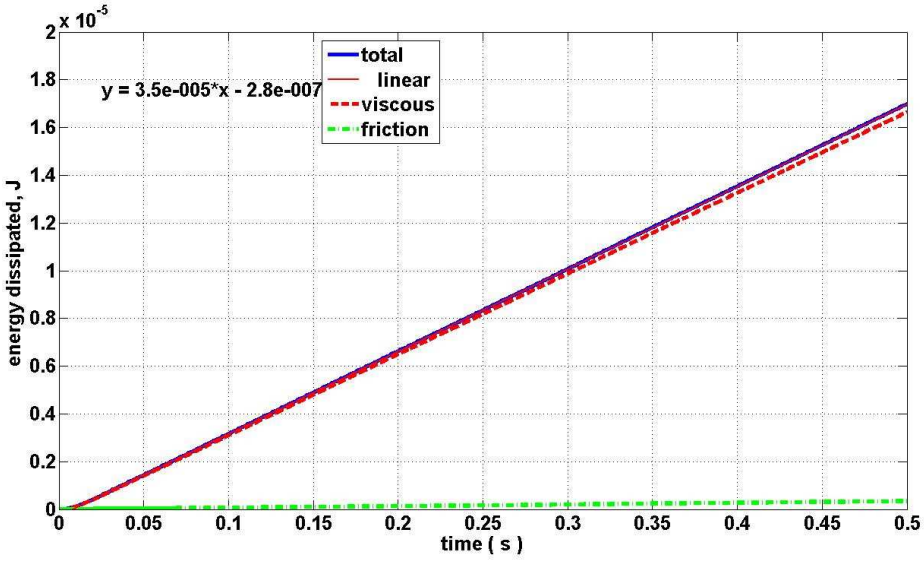

Figure 6.13: Energy dissipated at 100Hz, amplitude 10^{-6} m, 260 particles in horizontal vibration.

Table 6.1: shows the total energy dissipated and fraction of the energy dissipated by friction for the PFC model in Figure 6.11.

Frequency excitation (Hz)	Amplitude (m)	Total power dissipated (W)	Fraction of energy dissipated by friction
80	10^{-5}	1.8×10^{-3}	0.44
120	10^{-5}	4.9×10^{-3}	0.24
120	10^{-6}	3.4×10^{-5}	≈0
150	10^{-6}	7.5×10^{-5}	≈0
200	10^{-6}	8.3×10^{-5}	≈0
300	10^{-6}	3.8×10^{-4}	≈0
300	10^{-7}	3×10^{-6}	≈0
350	10^{-6}	5×10^{-4}	≈0
400	10^{-6}	7.7×10^{-4}	≈0
400	10^{-7}	8×10^{-6}	≈0
500	10^{-7}	1.5×10^{-7}	≈0

6.3.1 Parametric study

The sensitivity of damping to horizontal excitation amplitude was studied using DEM – see Figure 6.14. The trend of behaviour of granular medium at different zones (*a, b, c, d*) also can be seen in the work by Saluena *et.al* [13].

It can be seen that in the very low amplitude (solid) region (zone *a*) where the particles are in contact permanently performance is close to that predicted using the low amplitude theory. The equivalent damping at this zone is almost independent to vibration amplitudes (solid region) and is higher than the convection and gas regions (zones *c* and *d*) where the particles collides and moving to each other. Because of permanent contact between particles, in this zone (zone *a*) the energy dissipation by friction is almost zero. However for very low damping ratio (0.025) it can be seen that a small rise in energy loss occurs with amplitude. More investigation in this zone shows that little friction dissipation is present (see – Figure 6.15).

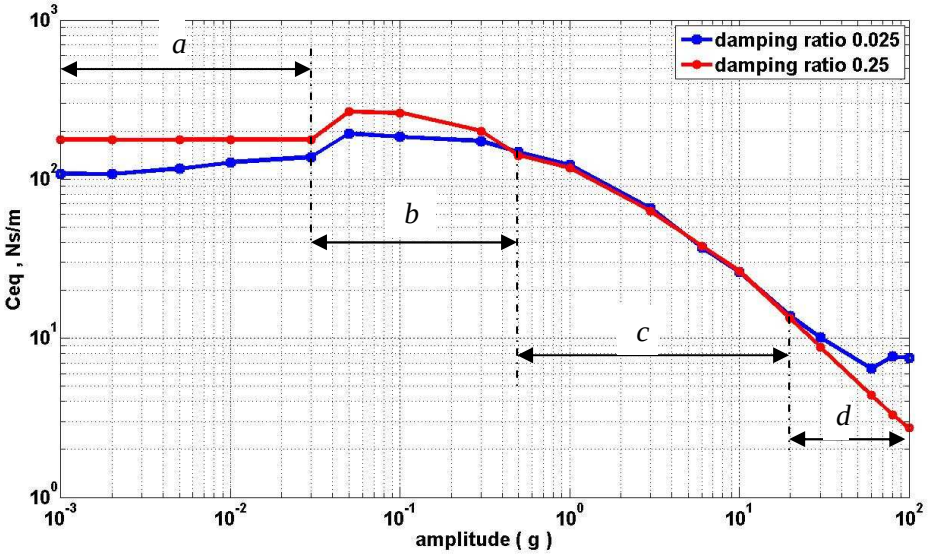

Figure 6.14: Equivalent damping versus excitation amplitude, at 100Hz excitation

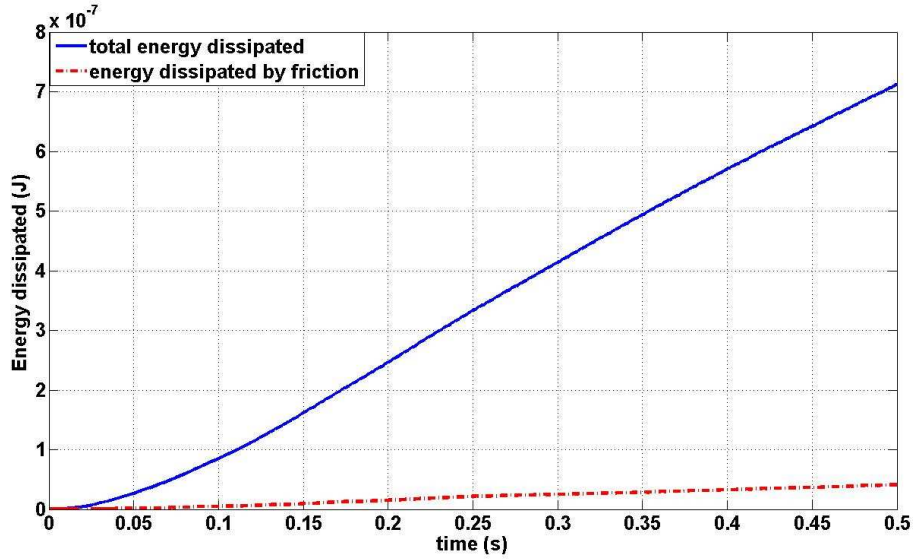

Figure 6.15: Energy dissipated at 100Hz, 0.01g amplitude, damping ratio 0.025 (zone *a*)

In zone *b*, in Figure 6.16, a clearer increase in damping can be seen between 0.03g and 0.05g.This increasin might be because of spinning of particles which can be physically seen in the container during the experiment, so that the friction increases and the total damping increases. This raising of friction can be seen in Figure 6.16.

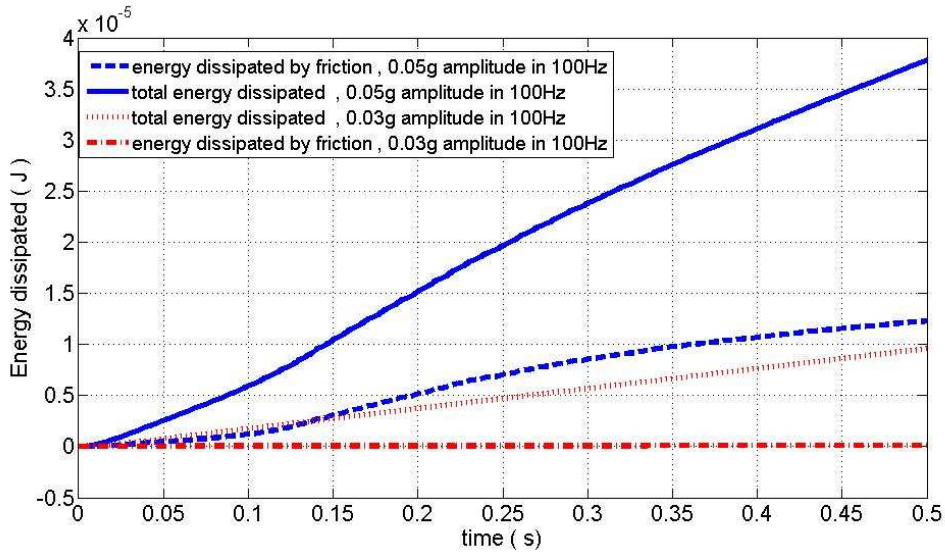

Figure 6.16: In the transition region from 0.03g (solid region) to 0.05g (transition region) exciting amplitude, the energy dissipation by friction increases considerably.

At higher amplitudes in the zone *c* which is called convection, the particles slide and roll more freely over each other. In this case there is a trade off between damping due to friction and viscous effects as resulting in the similar damping levels irrespective of the material loss factor [13].

Increasing the amplitude to extremely high levels (zone d), the particles separate from each other (gas region). It can be seen the particles with lower damping reach the gas region earlier because are less sticky that the other type and more collisions can happen so although the damping for each individual particle is less but the total damping increases [13].

6.4 Chapter summary

In this chapter the application of Discrete Element method to energy dissipation from a granular medium was described. The procedure used and the detailed steps employed were explained.

The model was run at several different frequencies under vertical vibration in order to generate data for comparison with experiment in the next chapter.

Horizontal vibration of the granular medium (identical to those experiments in the Chapter 4) was also studied. Different displacement amplitudes and a wide range of frequencies were applied to the model and power dissipated from total energy dissipated trace was extracted by linear interpolation (gradient of energy trace). The results were compared with experiments performed in Chapter 4, and are in good agreement.

A parametric study was also performed in this chapter to observe the different behaviours of granular medium with a wide range of amplitude excitations. It was shown that there are different zones in the vibrated granular medium depends on the amplitude of vibrations. At low amplitude most of the cases the energy dissipated due to friction is nearly zero, although by increasing the amplitude, the total damping

is increased, this might be because of spinning of particle which can be physically seen in the container that causes friction phenomenon. By further increasing in amplitude the particles start sliding and rolling on each other which named convection zone and there is a trade off between two different types of particles (low and high damping ratio). At very high amplitude where the particles separate totally from each other, the total damping of particles with smaller damping ratio, is higher than the other type that could be because of more number of impact between them in compared with particles with high loss factor. This phenomenon was also observed in previous literature [13].

The models which made in this chapter showed good agreement with experiments performed in Chapters 4 and 7.

7 Spherical Particle Dampers as Granular Materials at Higher Amplitude Vibration

7.1 Introduction

Damping strategies that use granular materials to attenuate structural vibrations generally rely on one of the two very different mechanisms for dissipating energy. For low vibration amplitudes, where particles always remain in contact and do not slip relative to one another, success depends on the ability to maximise energy dissipation within individual particles. If however, excitation is such that separation and slip between particles does occur (inelastic collision and friction), optimisation of the energy loss at the contact points becomes important and even particles with low internal loss, for example steel ball bearings, can give excellent vibration suppression. In practice, it is often desirable to have good damping performance over a wide range of amplitudes. While amplitude dependence has been widely studied for traditional particle dampers involving low-loss hard particles, very little information is currently available for systems based on larger particles made from materials with significant internal energy dissipation capacity.

7.2 Simulation of damper effectiveness

Measured properties of individual particles were used with DEM simulations to predict the performance of a polymeric particle damper subjected to a range of different amplitudes and frequencies. The model was validated under a number of different conditions by making comparisons with experimental results. The damper used in this study involved a rigid box with internal dimensions 180×120×40 mm containing 200 spherical particles, each 15.1 mm in diameter, made from an elastomer whose characteristics was described in Chapter 3. Values of key parameters used in the simulations are presented in Table 7.1. Measurement of the normal stiffness and loss factor of the spheres was described in Chapter 5. As it was noted in the previous chapter that the polymer was operating between the rubber and transition zones the Poisson's ratio was assumed to be 0.45 and a value of 1.0 was assumed for the coefficient of friction for all contacts.

The details of how to generate the model in PFC was provided in Chapter 6. The final stage in this process was to apply sinusoidal velocity to the walls as a boundary condition. In this work the time length for shaking was 0.6 s which was equivalent to 60,000 steps.

Table 7.1: Properties of the baseline granular medium used for power dissipation studies.

	Item	Unit	Value
General	Number of particles	each	200
	Particle diameter	mm	15.1
	Particle mass	gram	2.11
	All coefficients of friction	n/a	1.0
Particle-particle contacts	Normal stiffness (k_n)	N/m	6,500
	Shear stiffness (k_s)	N/m	4,613
	Normal damping ratio (ζ_n)	n/a	0.200
	Shear damping ratio (ζ_s)	n/a	0.168
Particle-Wall contacts	Normal stiffness (k_n)	N/m	13,000
	Shear stiffness (k_s)	N/m	9,226
	Normal damping ratio (ζ_n)	n/a	0.200
	Shear damping ratio((ζ_s)	n/a	0.168

A typical plot showing energy dissipation over time is presented in Figure 7.1. The power dissipation is the gradient of the energy dissipation curve. In this case the total dissipation is 0.14 W. It can be seen it that is made up from friction (at contacts) and viscous (material loss) terms. For the purposes of model validation, simulations were carried out at acceleration amplitude of 1.6 g and frequencies 10, 50, 90 and 130 Hz.

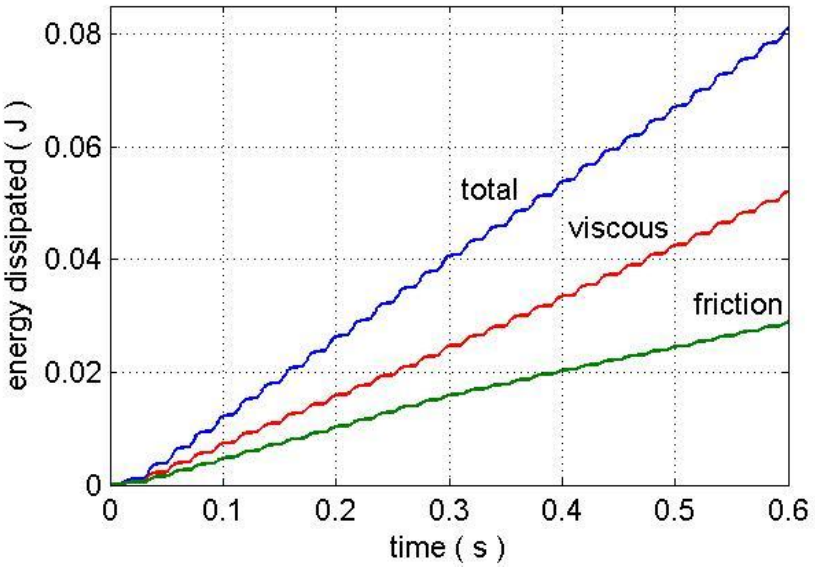

Figure 7.1: Energy dissipation at 50Hz, 1.7g amplitude

7.3 Experimental validation of model

For the physical experiments, the container was constructed using blocks of Perspex that were 30 mm in thickness to provide high rigidity but also visibility. Figure 7.2, shows the signal flow diagram for the experiment. Data acquisition and test control were carried out using a two-channel Siglab unit connected to a PC.

The container was suspended using nylon line and light metal springs to simulate free boundary conditions and an electrodynamic exciter attached to base – see Figure 7.3. Initial tests showed that flexible modes of the container were above 500 Hz while the rigid body modes were below 5 Hz.

200 particles were placed randomly in the container and the power dissipation measured at various amplitudes and frequencies. Power dissipation was measured using the Fourier-based power flow method that Yang [40] and Wong [10] used in their work. This method explained in detail in Chapter 3.

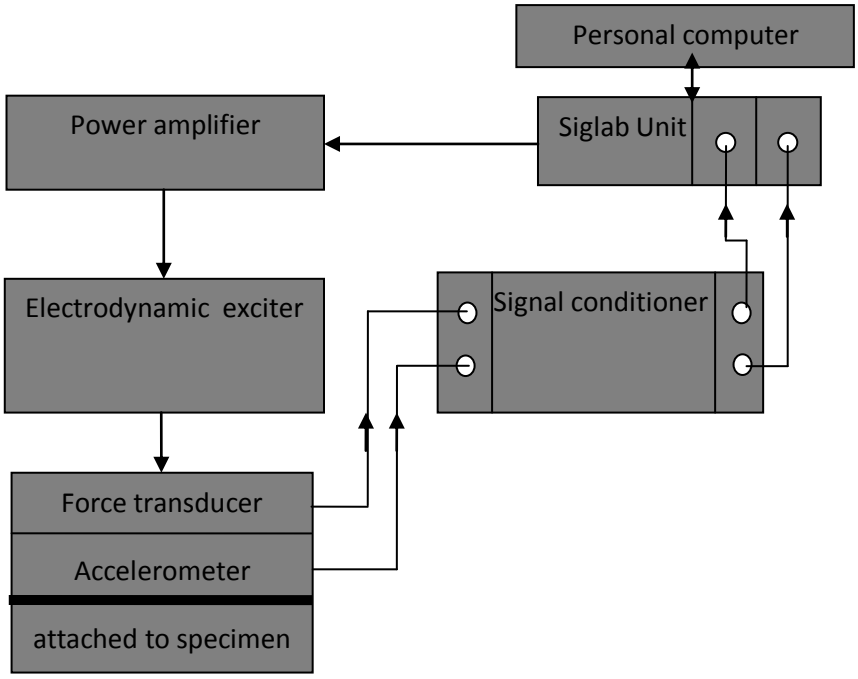

Figure 7.2: Experimental for power dissipation of granular medium, signal flow diagram.

It was assumed that the excitation was perfectly sinusoidal and the container was completely rigid. The experiment was repeated for the case with the container empty in order to find the phase error due to the boundary conditions and electronics. This error, although relatively small (being 1% at 50 Hz), was subtracted from subsequent measurements of the full system to provide true contribution of the granular medium. Power dissipation levels obtained from experiment and simulation for different frequencies and equal acceleration amplitude (1.6g) are given in Figure 7.4. Simulation results were produced in two ways: stiffness and damping were assumed fixed according to the values defined in Table 7.1 or they were allowed to vary with frequency according to the measurements described in Chapter 6. Although the simulations somewhat overestimate the dissipated energy, both approaches provide reasonable correlation with the measured results and hence it can be concluded that the simplifications made in the model are acceptable in the amplitude and frequency ranges considered.

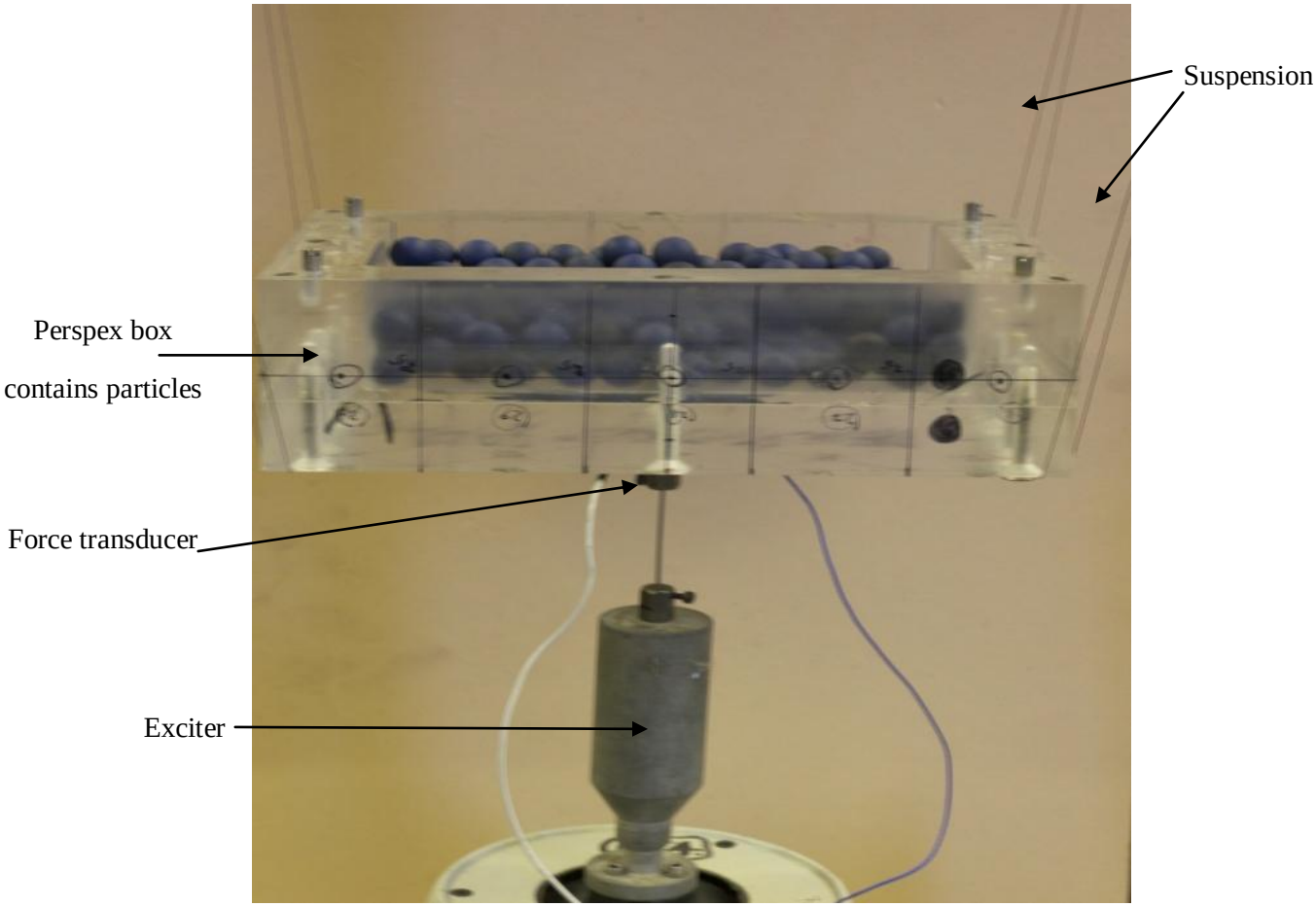

Figure 7.3: Test rig for power dissipation measurement of a granular medium.

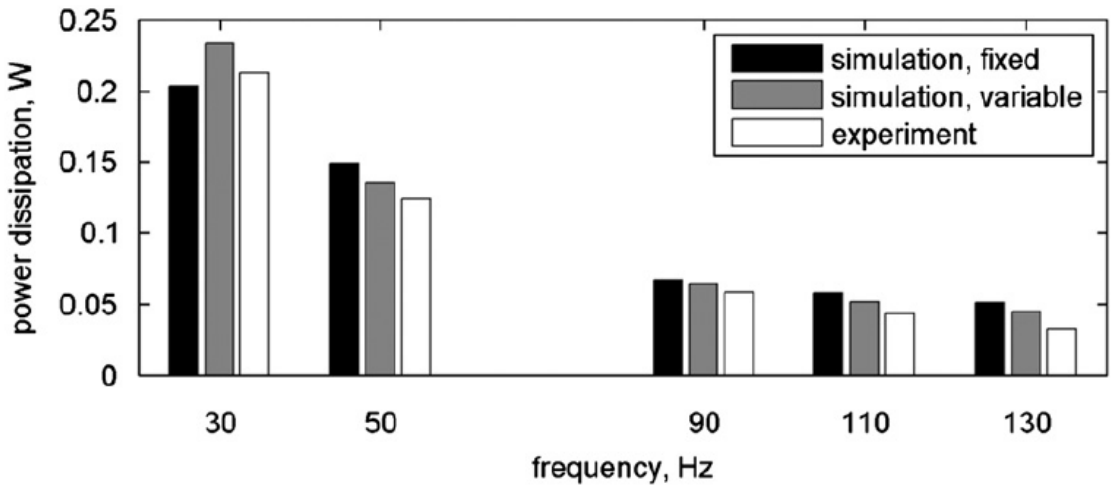

Figure 7.4: Comparison of power dissipation from experiment and simulation at acceleration amplitude 1.6 g. *Fixed* refers to the properties specified in Table 7.1 and *variable*, refers to the properties changing with frequency according to the master curve.

7.4 Observations of granular medium behaviour

Performance of granular medium subjected to pure sinusoidal vibration is studied using validated DEM model to various parameters. This was considered important not only to give understanding of the behaviour of the granular system but also to provide confidence in the model as parameters such as the friction coefficient were estimated.

It can be seen in Figure 7.5 that at a constant vibration frequency (50 Hz) the power dissipation is increased by increasing the amplitude of vibration. This would be expected from most dampers. However, the nonlinearity of the dissipation mechanism can be seen by considering instead the damping coefficient of an equivalent grounded viscous damper – this is plotted against amplitude in Figure 7.6. Here it can be observed that the damper coefficient is optimised at around 1.6 g excitation level. This nonlinear behaviour is consistent with experimental observation of metallic particle dampers in the literature [10].

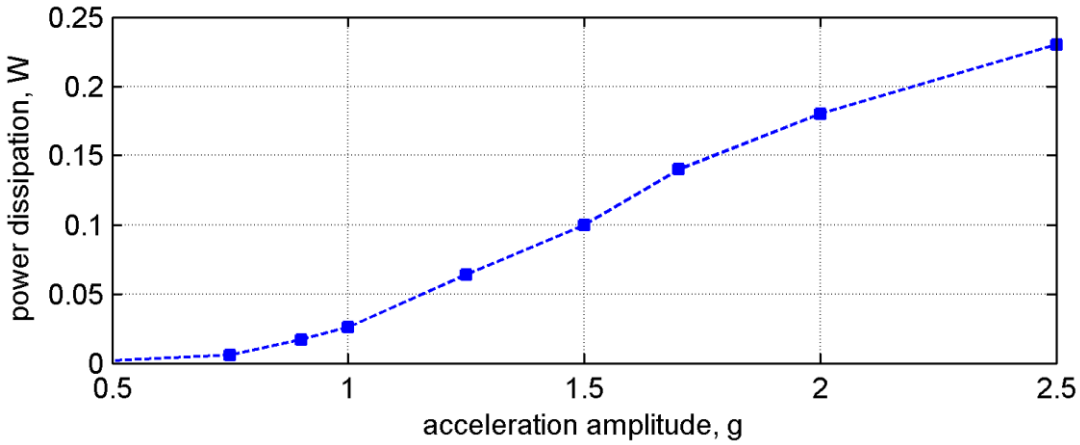

Figure 7.5: Effect of acceleration amplitude on power dissipation at 50 Hz (simulated).

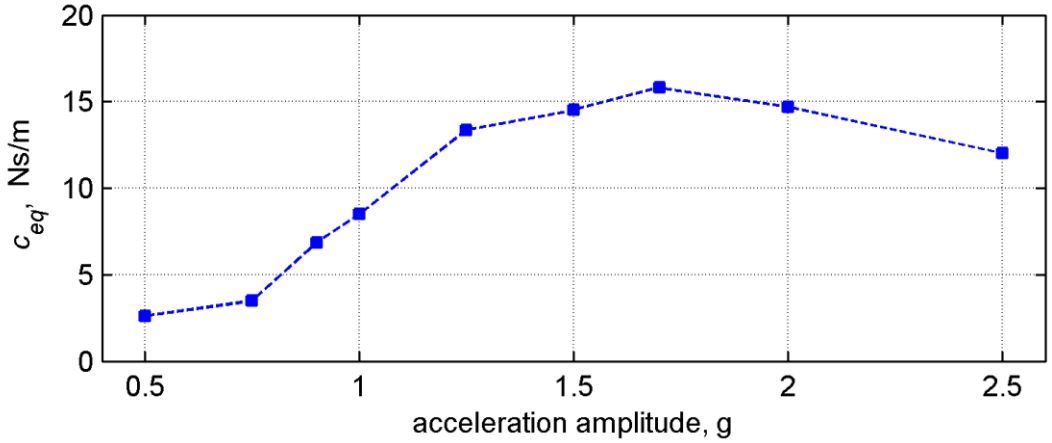

Figure 7.6: Effect of acceleration amplitude on equivalent viscous damping at 50 Hz (simulated).

The effect of excitation frequency on the power dissipation from the granular medium is presented in Figure 7.7. The drop in dissipation as the frequency rises is because acceleration amplitude is kept constant – resulting in lower deflections at higher frequencies. For comparison, results for an equivalent linear damper with performance matching that of the granular medium at 30 Hz are also given. It can be seen that the granular medium provides significantly better performance at higher frequencies than the linear system – behaviour also noted previously for metal particles [63].

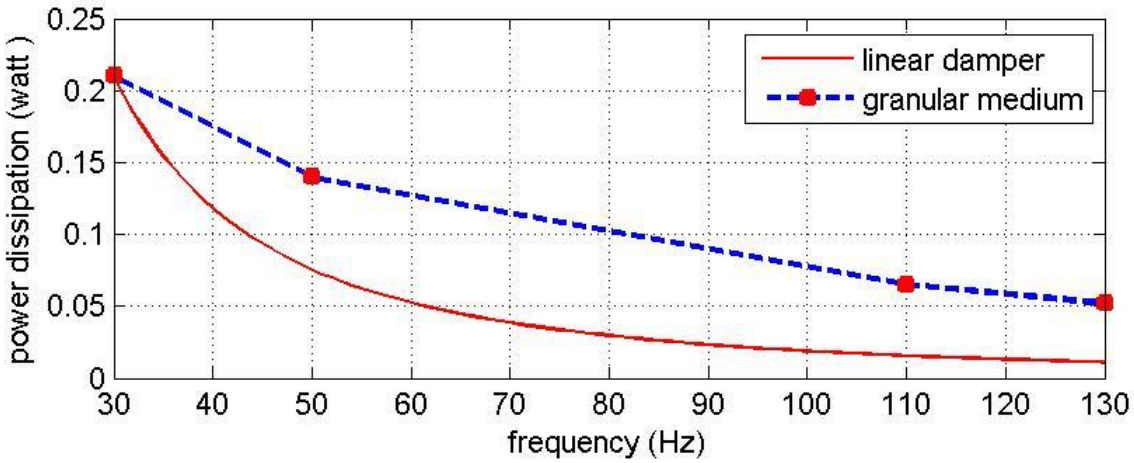

Figure 7.7: Effects of frequency on power dissipation for the granular medium and a linear damper at 1.7g acceleration amplitude (simulated).

Energy dissipation in the viscoelastic particle damper model can occur through interface friction and internal (viscous) loss. Figure 7.8 shows that power dissipation is not significantly affected by the friction coefficient. While this result appears somewhat counter-intuitive, as friction is a significant energy dissipation mechanism, this phenomenon has been noted previously for traditional particle dampers [10].

At very low amplitudes, it has been shown that system damping is directly proportional to the material damping of the spheres as shown in Chapter 4.

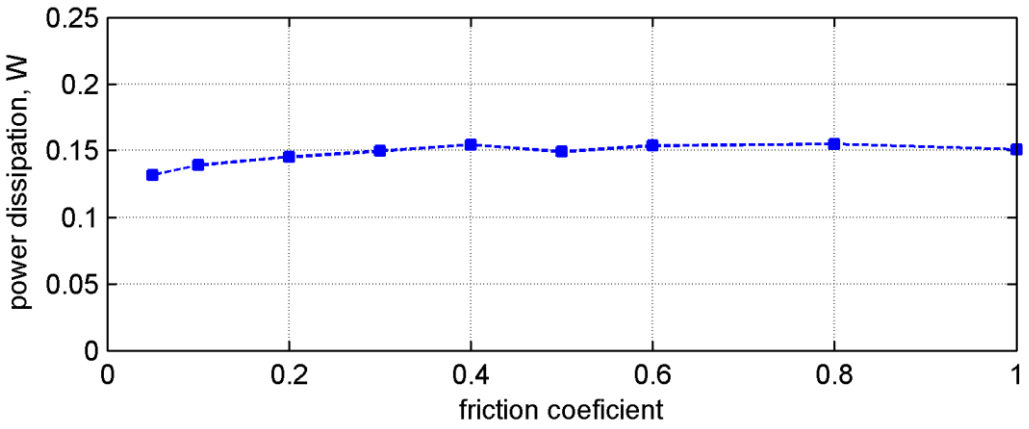

Figure 7.8: Effect of friction of coefficient on power dissipation at 50 Hz and 1.6g acceleration amplitude (simulated).

As this was thought to be unlikely at higher amplitudes simulations were carried out for different values of particle damping ratio. Results at 50 Hz and 1.6 g are presented in Figure 7.9. This plot also includes the fraction of dissipation that is attributed to viscous loss – the remainder is from friction. It can be seen that the overall power dissipation does not change significantly. When the loss in the particles is low, there is a significant amount of friction damping and as the internal damping in the sphere increases, the friction contribution drops. These results explain why it was possible to obtain good predictions of energy dissipation performance (presented in the previous section) without knowing accurately the actual friction coefficient between the particles and between particles and walls.

Sensitivity of performance to contact stiffness at different frequencies is shown in Figure 7.10. It can be seen that small changes in stiffness (e.g., factor of two) do not dramatically affect the overall behaviour. Note that the reduction in power

dissipation with frequency is because the acceleration amplitude is held constant at 1.6 g – under these conditions the velocity and displacement reduce at higher frequencies.

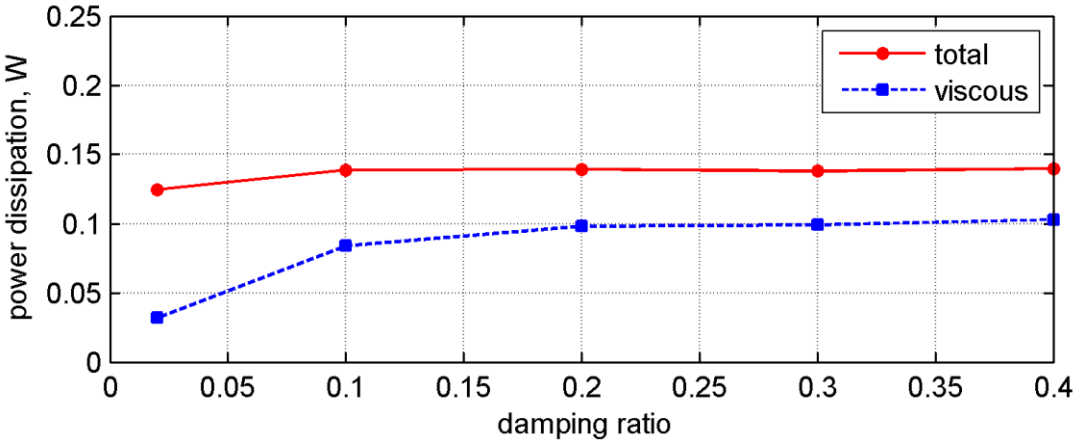

Figure 7.9: Effect of damping ratio on power dissipation at 50 Hz and 1.6 g acceleration amplitude (simulated).

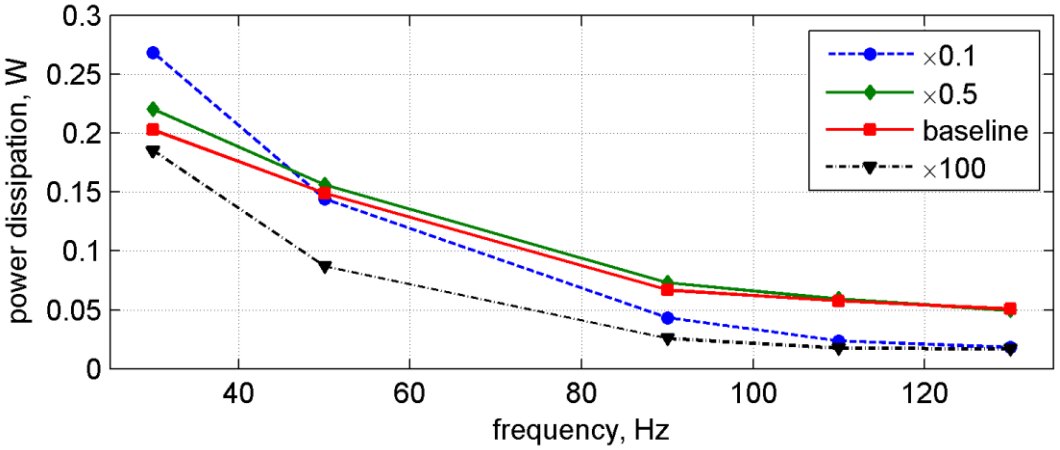

Figure 7.10: Effect of particle stiffness on power dissipation at different frequencies (simulated).

In Figure 7.10, it can be seen that for very soft particles, energy dissipation is concentrated in the lower frequencies. If the particles are much harder (typical of polymer spheres in the glassy zone), overall power dissipation is somewhat lower.
As the material loss factor was the same for each stiffness level considered, it can be seen that large variations in contact stiffness are important.

A comparison between vertical and horizontal direction has been shown in Figure 7.11 and Figure 7.12. Energy dissipation changes with direction of shaking, as it can be seen in vertical vibration more energy is dissipated. The vertical model has been already verified by experiment. In this comparison all other parameters are identical for both conditions and the excitation amplitude is 0.01g, so both cases are in the solid region and dissipation by friction is negligible.

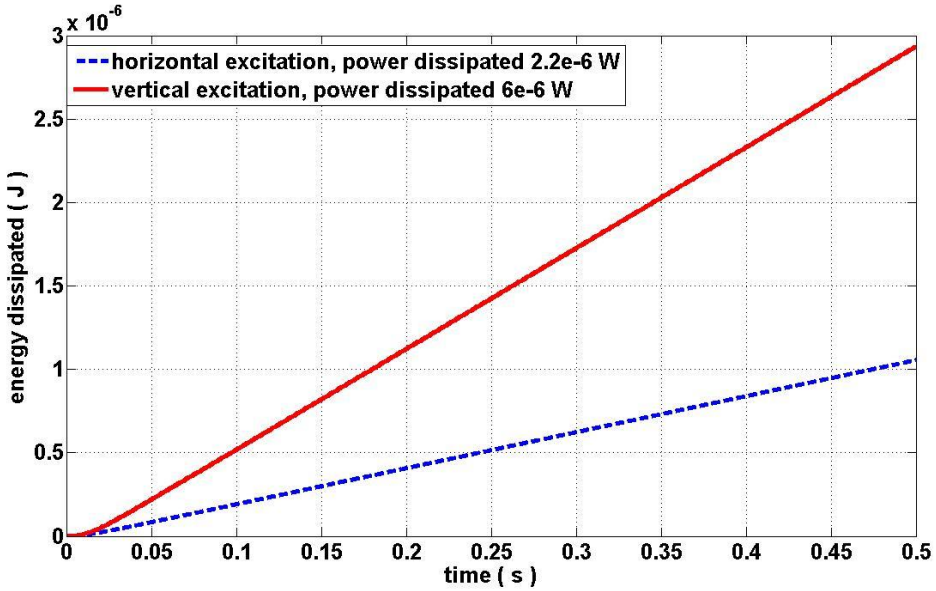

Figure 7.11: Energy dissipated in two different conditions in solid region, dash-line is in horizontal vibration and solid line for vertical vibration. Amplitude of exciting is 0.01g (simulated).

When the excitation amplitude is increased to 2*g*, particles tend to slide on each other. Energy dissipated is presented in Figure 7.12. While the total dissipation is considerably higher for vertical vibrations (around 3 times) the amount of friction induced loss is nearly the same for both directions.

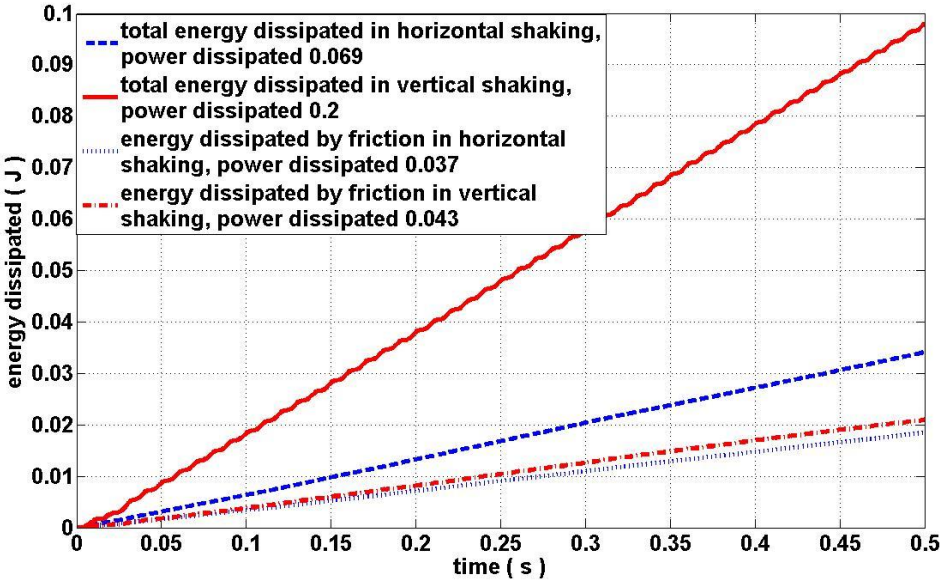

Figure 7.12: Energy dissipated by friction in horizontal vibration in comparison with vertical vibration. The exciting amplitude is 2g (simulated).

Chapter summary

In this chapter, the power dissipated in granular medium comprising spherical polymeric particles that was subjected to higher amplitude excitation vibration (sinusoidal waveform) in the direction of gravity (vertical vibration), is considered. Spherical viscoelastic particles are partially filled in a box with rectangular cross section whose walls are made of thick blocks of Perspex. Numerical and experimental studies were made of the power dissipation from the medium. Simulations of the medium were obtained using a three-dimensional Discrete Element Method (DEM) code. The measurements (stiffness and loss factor) of individual particles in chapter 5 were used as input parameters for using in the simulation studies. The power dissipation of the granular medium obtained from simulation was compared with that from a physical experiment and found to be in good agreement (Figure 7.4). The sensitivity of power dissipation to amplitude, frequency of excitation and friction coefficient was investigated. Also at the end of the Chapter, a numerical comparison between power dissipated of the medium under vertical and horizontal excitation is performed.

8 Sensitivity Analysis on Granular Medium

8.1 Introduction

Sensitivity Analysis (SA) is "the study of how the uncertainty in the output of a model (numerical or otherwise) can be apportioned to different sources of uncertainty in the model input" [117].

In this chapter, in order to gain better understanding of sensitivity of energy dissipated to the friction coefficient and damping ratio, an SDOF system was used, then after that, the sensitivity of the power dissipated in a granular medium on convection phase, with different independent variables, is investigated. The input parameters are stiffness, damping and friction coefficient of each individual particle. The method used here is based on Saltelli's approach [117]. Other method was used in chapter 7, which all other input parameters were kept constant and only one parameter changed several times to observe how does it affects to the energy output of the system. The purpose of this chapter is to make a comparison between the two methods to evaluate whether one is better than the other.

8.2 Sensitivity analysis on simulated SDOF model

In order to gain better understanding of the behaviour and effect of friction and damping on granular medium a simple sliding (SDOF) model was developed – see Figure 8.1.

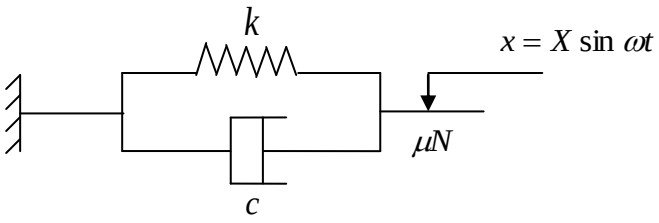

Figure 8.1: Simple sliding model

The force developed in this model when subjected to sinusoidal displacement was simulated in Matlab code. The displacement is shown in Figure 8.2. As it can be seen the displacement is given so that in the first period has smaller amplitude and gradually reaches to steady state, and has zero slope in the beginning, this is because to prevent high velocity at the start point and therefore preventing from sliding. In this calculation it was assumed that the normal force to this sliding model is constant and friction coefficient changes from 0 to 1.4 and loss factor ranging from 0 to 1.2. By running the code, the energy dissipated is calculated from the hysteresis loop for variable input. Although the displacement is sinusoidal, because of the friction element the force-history is not a completely sinusoidal response. Typical force varying with time is shown in Figure 8.3.

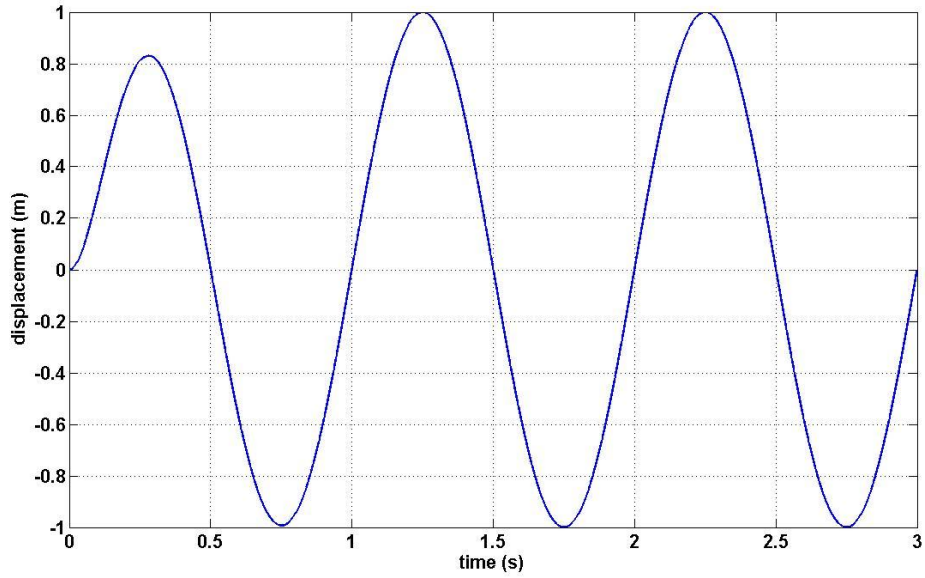

Figure 8.2: A typical input displacement history of sliding SDOF model.

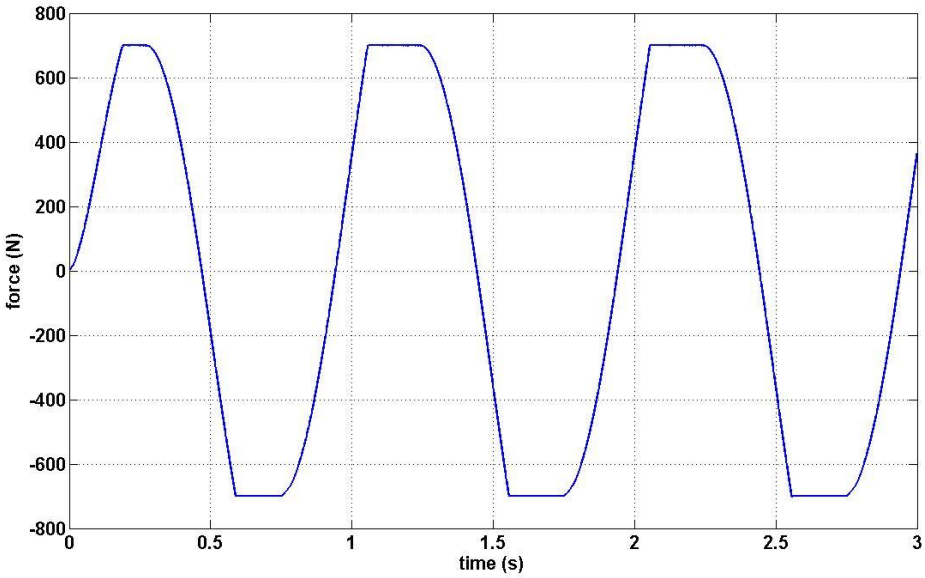

Figure 8.3: A typical force history response of sliding SDOF model.

For different values of loss factor (which is proportional to damping ratio) and friction coefficient, the force-displacement values are plotted which represent the hysteresis loop. The Matlab code runs many of times and gets the energy per cycle (the area of each loop shows the energy dissipated from simple model).

Figure 8.4, is a typical hysteresis loop (friction coefficient has a high value, 1.4 and loss factor is up to 0.6) which calculated when the friction coefficient is very high so that friction does not happen and most energy dissipated is because of viscous damping. These phenomena can also be seen in upper part of contour plot Figure 8.7.

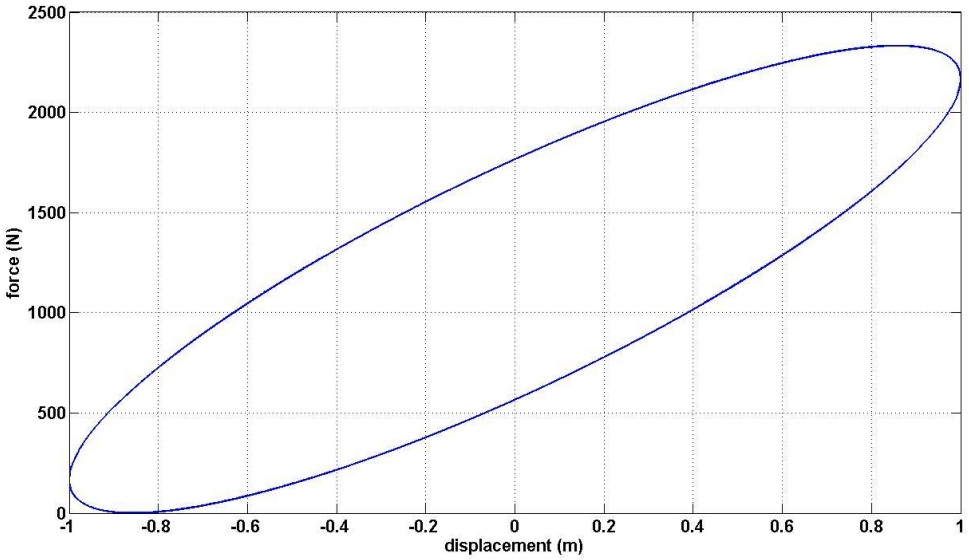

Figure 8.4: A typical hysteresis loop of sliding SDOF model, viscous damping makes a main contribution to energy dissipated (high friction coefficient).

At low friction coefficient, due to sliding, most damping is caused by friction force and the viscous damping is very small. The typical hysteresis loop can be seen in Figure 8.5 (friction coefficient is up to 0.2). It is a typical hysteresis loop from the lowest part of contour plot Figure 8.7.

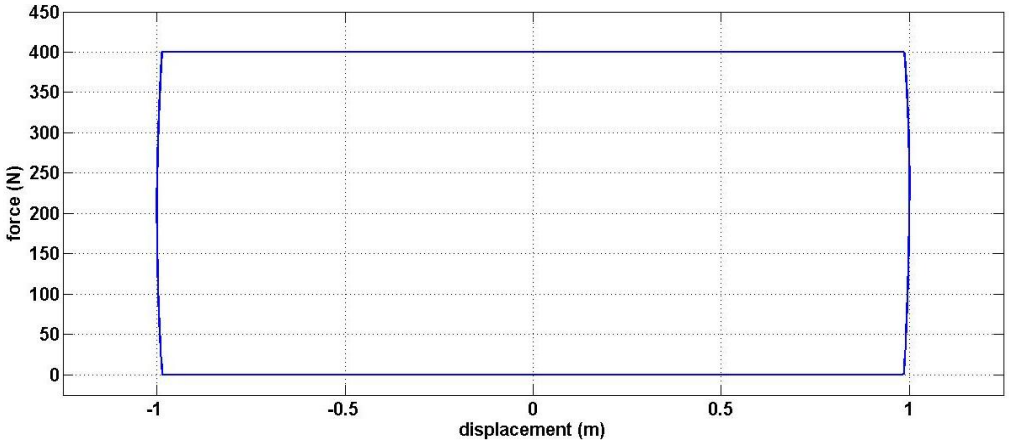

Figure 8.5: A typical hysteresis loop of sliding SDOF model, friction makes a main contribution to energy dissipated (at low friction coefficient).

Another typical hysteresis loop, where both friction and high loss factor are significant, is presented in Figure 8.6. In the case the hysteresis loops are a combination of both damping (viscous and friction). These cases are happened in the curve shapes of contour plot Figure 8.7.

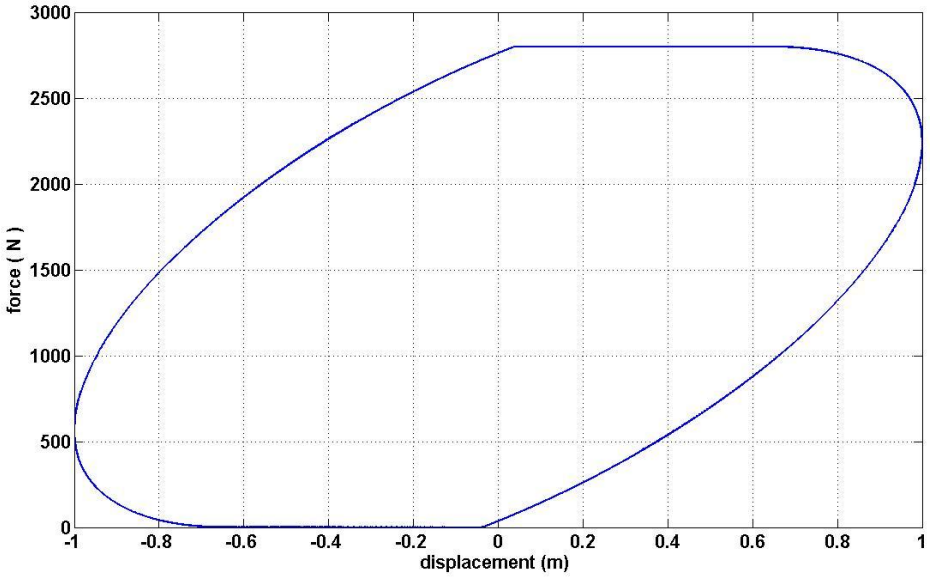

Figure 8.6: A typical hysteresis loop of sliding SDOF model, both friction and damping contribute to energy dissipated.

The total result of energy dissipation is shown in contour plot, Figure 8.7.

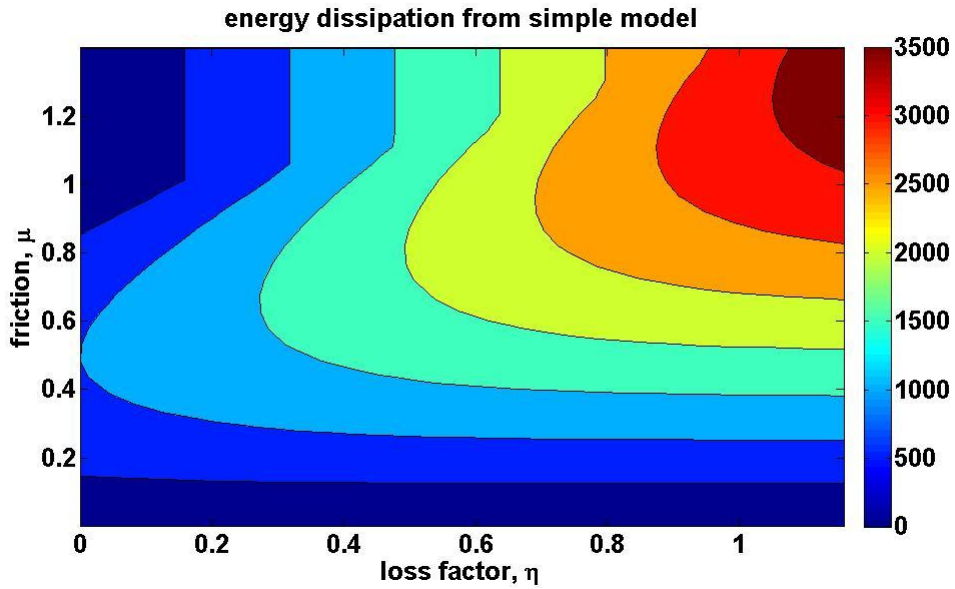

Figure 8.7: Variation of energy dissipated from loss factor and friction

As it can be seen in Figure 8.7, at very low values of friction coefficient the model shows more sensitivity to energy dissipation while at high friction coefficient it shows less sensitive because the particles are stickier due to friction. Also it can be seen that at lower friction coefficient the energy dissipated is less sensitive to loss factor. These phenomenons are also seen for granular medium.

8.3 Test Model and Sensitivity Analysis Procedure

In the previous section a simplified model was used to demonstrate the sensitivity for both the loss factor and the friction coefficient. In this section, this is now expanded to an MDOF system that is more representative of the actual system.

By assuming the model under study as,

$$Y = \sum_{i=1}^{r} \Omega_i Z_i \tag{8-1}$$

where the input factors are Z_i and Ω_i are weights as fixed coefficients, r stands for number of input variables and Y values are output parameters. The individual Z variables are characterized as independent and distributed normally with mean zero.

8.3.1 Scatter plots and Linear Regression

A typical scatter plot which obtained based from a Monte Carlo experiment has been shown in Figure 8.8. This example shows the scatter plots of Y versus input parameters Z_1, Z_2, Z_3, and Z_4 which distributed normally with mean zero. As it can be seen in Figure 8.8 parameter Z_4 both converges to a line and has a higher concentration of the data points (scatter points) than Z_3 and so on. Therefore the output Y is more sensitive to Z_4 than it is to Z_3 .The influence of input factor Z_4 on the output is more than the others. In this case the order of sensitivity is $Z_4>Z_3>Z_2>Z_1$.

Monte Carlo methods are based on sampling from the distribution of input. The inputs are independent and can be arranged in a Monte Carlo matrix,

$$M=\begin{bmatrix} Z_1^{(1)} & Z_2^{(1)} & \dots & Z_r^{(1)} \\ Z_1^{(2)} & Z_2^{(2)} & \dots & Z_r^{(2)} \\ \dots & \dots & \dots & \dots \\ Z_1^{(N-1)} & Z_2^{(N-1)} & \dots & Z_r^{(N-1)} \\ Z_1^{(N)} & Z_2^{(N)} & \dots & Z_r^{(N)} \end{bmatrix} \qquad (8\text{-}2)$$

These values have been substituted (for each row) to the model main Equation 8-1. The output values which are calculated from the model equation can be produced as a vector, Y.

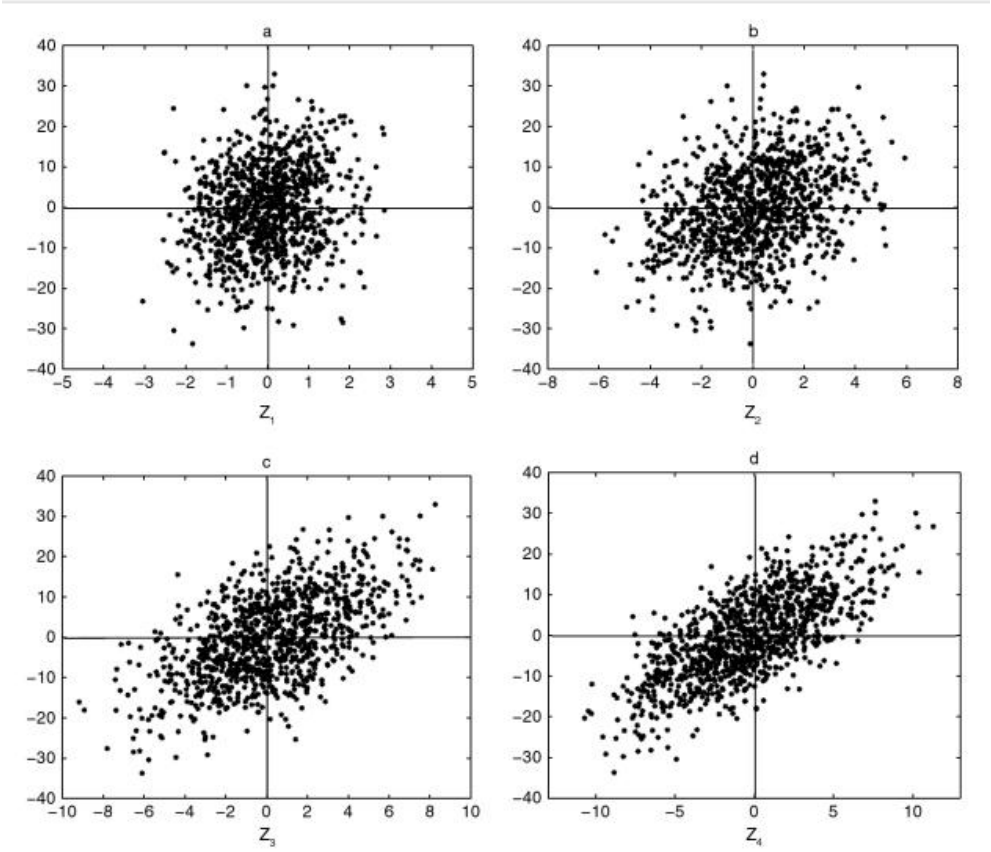

Figure 8.8: Scatter plots of Y versus $Z_{1,}\ldots, Z_4$ [120].

$$Y=\begin{bmatrix} Y^{(1)} \\ Y^{(2)} \\ \ldots \\ Y^{(n-1)} \\ Y^{(N)} \end{bmatrix} \qquad (8\text{-}3)$$

where each of the values for this vector e.g. $Y^{(N)}$, is calculated by Equation 8-1 and input values $Z_1^{(N)}, Z_2^{(N)}, \ldots, Z_r^{(N)}$. As a conclusion, by knowing the *r* number of input factors and *N* set values of input, one can obtain *N* values for the output. *N* is also the number of times that the model should be used for calculations which is the size of Monte Carlo experiments. The results show *r* number of scatter plots. Scatter plots are a useful way which enables the user to analyse the sensitivity of each input parameters to the output in a glance and summarise them.

This could be obtained by using a simple linear regression on the data of the input values of matrix and output vector values.

8.4 Sensitivity Analysis on the Granular Medium Model

The procedure which explained in previous section is applied for the granular material medium. For simulation, the model based on DEM which was used in Chapter 6 is conducted.

As a first step, an input file should be produced by randomness method within the specific defined range and evenly distributed. The input parameters are stiffness, friction coefficient and damping ratio (Table 8.1). In order to investigate the sensitivity of the power dissipated at different conditions a wide range of input parameters was considered. An amplitude excitation, 6*g* at 100Hz was used throughout.

Table 8.1: Input variable parameters to granular particles

Stiffness (N/m)		Damping ratio		Friction coefficient	
Lowest value	Highest value	Lowest value	Highest value	Lowest value	Highest value
6×10^{2}	6×10^{5}	0.025	025	0.1	1

8.4.1 LOOPFC Method

After generating the input data file, the method 'LOOPFC' is used. In this method a batch file is created which is containing a series of commands to be executed by the PFC3D code so that this script file is set up to automatically read the input data file, line by line. The process in the batch file is generating all walls with their properties, and then the input ASCII file which contains all information is read. The codes for calculating energy dissipated by friction and viscous were used. Figures 8.9 to 8.11 show the scatter plots for each of the stiffness and damping and friction coefficient versus power dissipated for high amplitude vibrations with 600 set values therefore the code runs for 600 times iteration.

In Figures 8.9 and 8.10 it can be seen that power dissipation is less sensitive to changing stiffness and damping ratio. In Figure 8.11, it can be seen that in very low friction coefficient there is a higher sensitivity to the output power dissipated, this is similar to what expected in chapter 7, Figure 7.8. Also in Figure 8.11, for an arbitrary stiffness and damping ratio equal to 229303 N/m and 0.08 respectively, the sensitivity to friction coefficient is shown (solid lines).

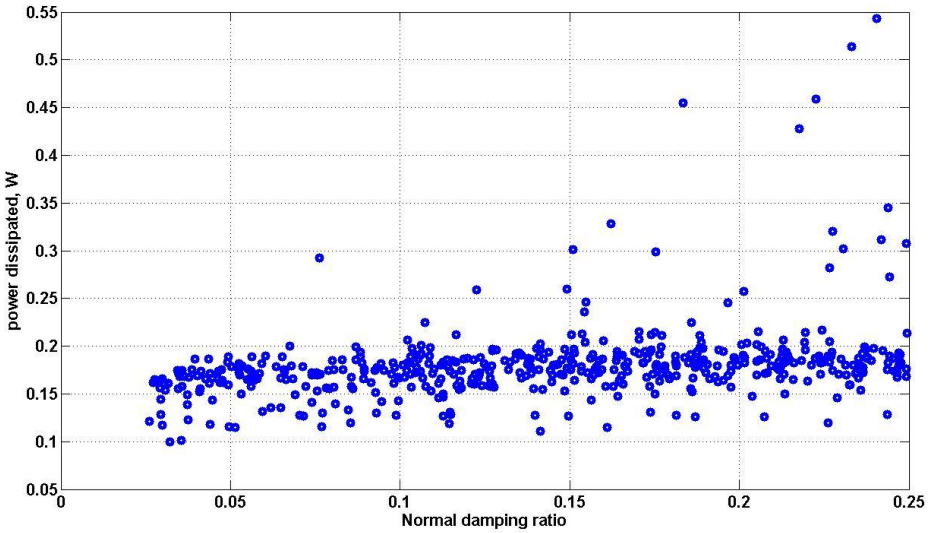

Figure 8.9: Scatter plot of damping ratio versus power dissipated.

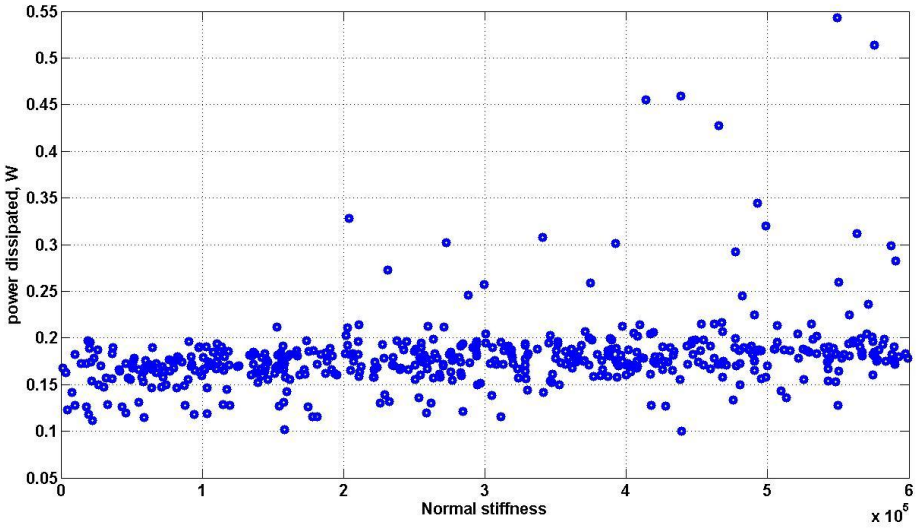

Figure 8.10: Scatter plot of stiffness versus power dissipated.

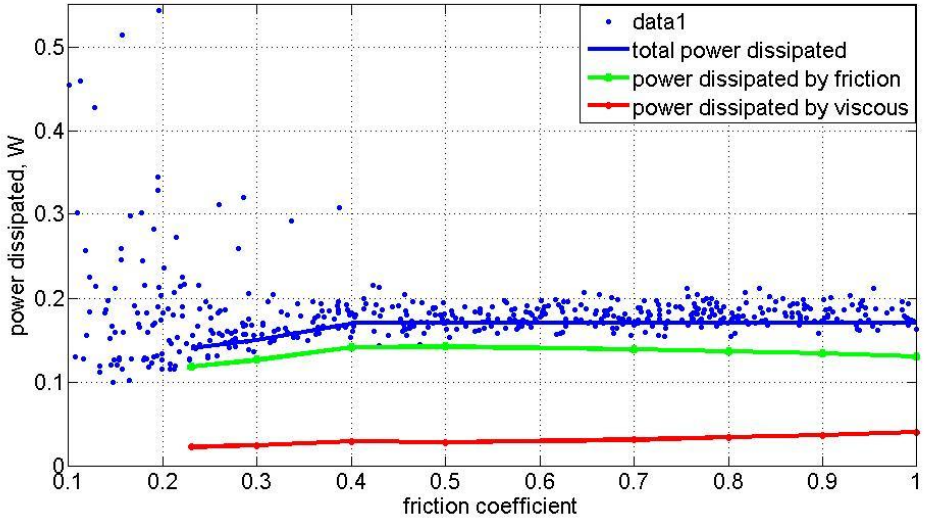

Figure 8.11: Scatter plot of friction coefficient versus power dissipated.

In order to compare the results with SDOF sliding model, the results were re-plotted for lower stiffness as used in SDOF model. Figures 8.12 and 8.13 show the sensitivity of power dissipated to friction coefficient and damping ratio. As it can be seen in Figure 8.12, the power dissipated is sensitive to friction coefficient at lower values and less sensitive at higher friction coefficients. This can be seen in Figure 8.7 at lower loss factor, however at higher loss factor there is a discrepancy and thought that it is because of constant normal force which assumed for sliding SDOF model. Figure 8.13 shows that the power dissipated is less sensitive to damping ratio and this also can be seen in Figure 8.6 so that the loss factor is less sensitive by moving from left to right.

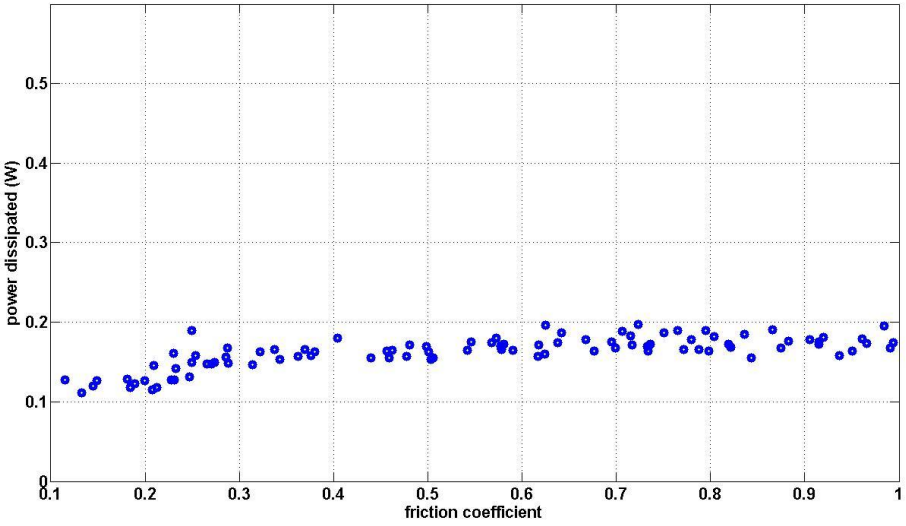

Figure 8.12: Scatter plot of friction coefficient versus power dissipated

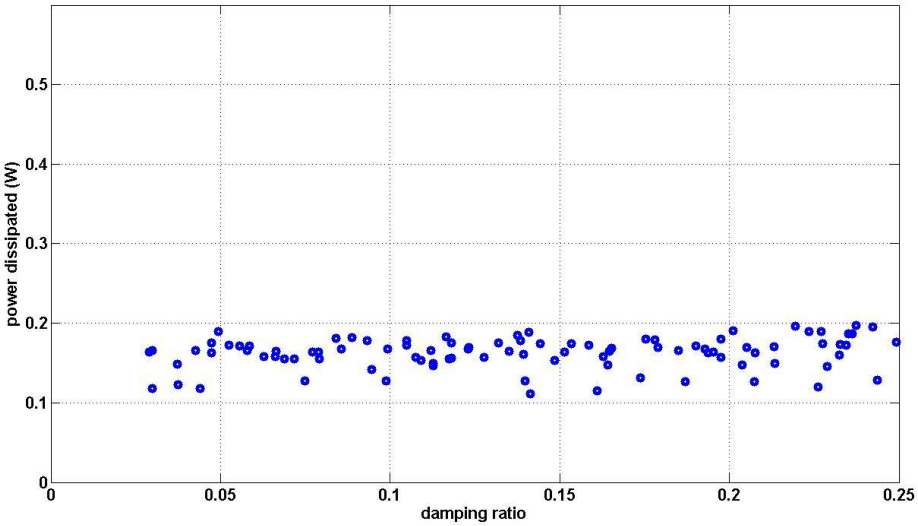

Figure 8.13: Scatter plot of damping versus power dissipated.

8.5 Chapter summary

In this chapter the sensitivity of granular medium to the stiffness, damping and friction coefficient variables were studied to help better understand the earlier chapters. As it was shown the power dissipated of the system is more sensitive to the very low friction coefficient and also in a very low damping ratio, however they are

less sensitive to higher value of those. A simple sliding model of SDOF sliding system was modelled and the behaviour of friction and damping were also studied. The comparison between two approaches is consistent and returns similar results at some cases. Discrepancies which are because of simplifications at SDOF model were also mentioned.

9 Conclusions and Future Work

9.1 Conclusions

This thesis has considered the energy dissipated in a granular medium composed of spherical polymeric particles whose properties change significantly over the frequency range considered. The work involved theoretical, numerical and experiment approaches. The excitation of granular medium in this work is both in vertical (same direction as gravity) and horizontal directions and as a sinusoidal vibration. Material and physical properties of individual viscoelastic particles were obtained by utilising visco-analyser test machine and also a designed test rig. A numerical model based on Discrete Element Method (DEM) in three dimensional was developed to simulate the behaviour of polymeric granular medium. As viscoelastic fillers are more effective for low-amplitude vibrations (where the particles are permanently in contact like as solid medium and do not slip relative to one another), the investigation on energy dissipation of granular medium in both low and higher amplitude vibrations were performed and in each case the corresponding theory approach was utilised. The sensitivity of parameters on power dissipation in granular medium was performed.

9.1.1 Main conclusions

- A numerical model that uses Discrete Element Method (DEM) was developed for prediction of energy dissipation in a viscoelastic granular medium. One simplification in the model was approximating viscoelastic behaviour using the Kelvin-Voigt model (spring and viscous damper in parallel) in order to provide acceptable calculation times. It provides a reasonable estimate to the curve at lower frequencies i.e. if the effective temperature is some way above the glass transition. Another simplification used was linear stiffness for small deformations. Despite the simplifications the model was found to be in good agreement with experiments (under vertical and horizontal vibrations with different number of particles) in a range of frequencies and amplitudes excitations (see Figures 6.3, 6.4, 6.11, 7.4).

- When the granular medium is subjected to low amplitude vibration, where particles do not collide and move relative to each other but are in permanent contact. In this case the medium behaves as a solid. Significant levels of energy can be dissipated by the generation of internal standing waves within the granular medium (see Figures 4.8, 6.14 zone *a*). As behaviour can be predicted using finite element analysis, it is easily applied for many complex structures. The Effectiveness of predictor method was demonstrated by comparison with experimental results (see Figures 4.8, 6.11).

- It was shown that changing the amplitude of vibration within the *low amplitude vibrations* zone does not change the damping as viscoelastic materials are generally amplitude-independent (see Table 4.1).

- Investigation using high-loss polymers used as granular dampers at *higher amplitudes* (the particles move relative to one another). In these higher amplitudes it is apparent that there are two main distinct phases: convection and gas (see Figure 6.14 zones *c* and *d*). These are not present during lower amplitudes. Granular dampers designed for low amplitude vibrations therefore may be used in high vibration environments too.

- At *higher amplitudes* and within convection zone (the particles start sliding and rolling on each other) while contact friction is a significant energy dissipation mechanism, overall power dissipation levels were found to be relatively insensitive to the friction coefficient (see Figure 7.8). It was found that at excitation above 1g and in convection zone, power dissipation is relatively insensitive to the damping of individual particles as increased loss through viscous/viscoelastic effects are balanced by reduced loss through friction (see Figure 6.14 zone *c*). This is different from the better-known low-amplitude case where system damping is directly proportional to the loss factor of the particles.
- A transition phase between completely solid and convection is appeared which has highest damping and is thought that this is because of friction due to spinning (see Figure 6.14 zone *b*).

- At extremely high amplitude vibrations particles spend more time out of contact with each other (the particles separated from each – gas region). It can be seen the particles with lower damping reach the gas region earlier because they are less sticky and more collisions can happen so although the damping for each individual particle it less but the total damping increases (see Figure 6.14, zone d).

- The power dissipation of the system is more sensitive to the very low friction coefficient (see Figure 8.11) and also in a very low damping ratio however they are less sensitive to higher values of them (see Figures 7.9, 8.11).

- Comparison between vertical and horizontal direction of vibrations for granular medium show that more total energy is dissipated in vertical vibrations. The actual amount of friction induced is nearly the same for both directions (see Figures 7.11, 7.12).

Granular particles have been shown to be a useful damping method. Therefore better understanding of how they can be utilised in practical applications is extremely important. Such as, the amplitude of vibrations in which they will be used, and the

parameters which affects the energy dissipation in the system, at that specific amplitude, should be considered. From the findings of this thesis, the phenomenological behaviours observed and presented can help pave the way for the effective use of viscoelastic particle damper damping technologies.

9.2 Recommended Future Work

The current research has helped to improve the understating of the performance of spherical viscoelastic particles. In this granular medium, the energy dissipation under various amplitudes and frequencies of excitations are studied. However, according to the author's opinion, the current research has the following limitations on the basis of which future work strategy can be defined.

- In the current work, the particle dampers are spherical in shape. For practical purposes it may be preferable to make shapes such as rods or irregular shapes by chopping or grinding bulk materials – making these shapes are easier to be produced. The effect of using these alternative shapes should be investigated. It is expected that such particles may display different characteristics but still follow the same fundamental behaviour outlined in this thesis. In order to model this medium in PFC3D a "clump" strategy should be used. A clump is a collection of spherical particles that behaves as a single rigid body.
- In the current work, relatively shallow granular medium at low amplitude vibrations considered, for deep particle dampers, the pressure within the granular medium has been shown to be less than would be with the hydrostatic assumption and reaches a saturation pressure; therefore the behaviour of energy dissipation for this deep medium can be investigated. It is expected that by further increasing in thickness of granular bed while the wave speed does not increase, therefore damping can be improved. In fact by increasing the thickness of granular medium as a result, thicknesswise resonance can then occur at lower frequencies.
- In the current research, the host structure was highly rigid to avoid interface with the flexural mode shapes of container. The behaviour of a flexible container should be investigated because in practical applications this could easily happen.

This is relatively simple to conduct experimentally. However, DEM simulation would be more complex. It seems that this would require the coupling of the DEM solver with the FE model of the container.

- The response of granular medium to non-sinusoidal excitation can be studied. This could be different with mono sinusoidal excitation as the material of viscoelastic granular medium is affected differently by a wide range of frequencies. Very little work on multi-frequency excitation is currently available.
- In order to change packing fraction and number of contact points between particles, mixed spherical particles with different sizes can be used. Although this could lead to the segregation phenomenon in the granular medium, it is however because of changing the diameter of particles, stiffness of particles on contact points between each other and the container could be different and the energy dissipation can be affected from this phenomenon.
- Granular particles can be used in a granular medium with different materials (different loss factors, stiffness and friction coefficients) which may be more suitable for different applications. Combinations of materials, as a mixture could be also used to investigate the effectiveness and improve the energy dissipation of the whole system at a wider range of amplitude excitations.

References

[1] Ungar E E, Kerwin E M, *Plate damping due to thickness deformations in attached viscoelastic layers*, Journal of the Acoustical Society of America, vol. 36(2), (1964), pp. 384-392.

[2] Els JDN, *The effectiveness of particle dampers under centrifugal loads*, PhD Thesis, University of Stellenbosch, South Africa, 2008.

[3] Pendleton S C *et al*, *Particle damping for launch vibration mitigation: Design and test validation*, Proceeding of the 49th AIAA/ASME/ASCE/AHS/ASC structures, structural Dynamics, and Material Conference, 2008. Schaumburg.

[4] Brennen C E, Ghosh S, Wassgren C R , *Vertical oscillation of a bed of granular material*, ASME Journal of Applied Mechanics, vol 63, pp 156-162.

[5] Poschel T *et al*, *Onset of fluidisation in vertically shaken granular*, material Physical Review E, vol. 62 (2000), pp. 1361-1367.

[6] House J R, *Vibration damping materials*, World Intellectual Property Organisation, International Patent Classification, F16F7/00, G10K11/16, International publication Number WO90/01645, (1990).

[7] Varanasi K K, Nayfeh S A, *Damping of flexural vibration using low-density foams and granular materials*, ASME, Design Engineering Technical Conference, September 2003.

[8] Saluena C, Poschel T and Esipov S.E, Dissipative *properties of vibrated granular material*, Phys. Rev. E vol. 59, (1999), pp. 4422-4425.

[9] Lu Z, Masri S F, Lu X. *Parametric studies of the performance of particle dampers under harmonic excitation*, Structural Control and Health Monitoring, vol. 18, (2011), pp. 79-98.

[10] Wong C X, Daniel M C, Rongong J A, *Energy dissipation prediction of particle dampers*, Journal of Sound and Vibration, vol. 319, (2009), pp. 91–118.

[11] Pamley R J, House J R, Brennan M J, *Comparison of passive damping treatments for hollow structures*, Proceedings of Smart Structures and Materials: Damping and Isolation, Newport Beach, SPIE 4331, (2001), pp. 455-467.

[12] Rongong J A, Tomlinson G R, *Vibration damping using granular viscoelastic materials*, Proceeding of ISMA 27, Noise and Vibration Engineering Conference, Leuven, Belgium, (2002), pp. 431-440.

[13] Oda M, Iwashita K, Mechanics of granular materials, Balkema Rotterdam, Netherlands, Brookfield, 1999.

[14] Janssen H A, *Experiments on grain pressure in silos*, Transactions of the Association of German Engineers 39 (1895), pp. 1045–1049.

[15] Sperl M, *Experiments on corn pressure in silo cells–translation and comment of Janssen's paper from1895*, Granular Matter, vol. 8 (2006), pp. 59–65.

[16] Duran J, Sands, powders and grains, Springer-Verlg, New York, 2000.

[17] Oyama Y, *Horizontal rotating cylinder*, Bull. Inst. Phys. Chem. Res. (Tokyo), Rep.18 (1939), 6001.

[18] Wassgren C R, Brennen C E and Hunt M L, *Vertical vibration of a deep bed of granular material in a container*, AMSE Journal of Applied Mechanics, vol. 63 (1996), pp. 712-719.

[19] Wassgren C R, *Vibration of Granular Materials*, PhD thesis, California Institute of Technology, Pasadena, California 1997.

[20] Liu S, Lia Pik-Yin, *Heaping of granular materials in a cylindrical vibrating bed*, Journal of Physics. A: Math. Gen, vol. 33,(2000), pp. 8241-8249.

[21] Renard S *et al*, *Vertically shaken column of spheres. Onset of fluidization* European Physical Journal E vol. 4, (2001), pp. 233-239.

[22] Eshuis P, *et al* , *Phase diagram of vertically shaken granular matter*, Physics of Fluid vol 19, (2007), 123301.

[23] Ristow G H, *Critical exponents for granular phase transitions*, Europhys. Lett., vol. 40(6), (1997), pp. 625-630.

[24] Saluena C , Poschel T, *Convection in horizontally shaken granular material*, Europhys. E1, (2000), pp. 55-59.

[25] Tennakoon S G K , Kondic L, Behringer R P, *Onset of flow in a horizontally vibrated granular bed: Convection by horizontal shearing*, Europhysics Letters, vol. 45, no.4, (1999), pp. 470-475.

[26] Metcalfe G, Tennakoon S G K, Kondic L, Schaeffer D G and Behringer R P, *Granular friction, Coulomb failure, and the fluid-solid transition for horizontally shaken granular materials*. Physical Review E, vol. 65, no.3, (2002), pp. 031302/1-031302/15.

[27] Tennakoon S G K, Behringer R P, *Vertical and horizontal vibration of granular materials: Coulomb friction and a novel switching state*, Physical Review Letters, vol. 81, no4, (1998), pp.794-797.

[28] King P J, Swift M R, Benedict K A, Routledge A, *Surface stability of granular systems under horizontal and vertical vibration: The applicability of coefficient of friction.* Physical Review E, vol. 62, no. 5, (2000), pp. 6982-6988.

[29] Torquato s, Random Heterogeneous Materials: Microstructure and macroscopic properties, Springer, New York, 2006.

[30] Conway J H,Sloane N J A, Spherical packing, Lattices and groups, Springer, New York, 1999.

[31] Song C, Wang P, Makse H.A, *A phase diagram for jammed granular matter* Nature, vol. 453, (2008), pp. 629-632.

[32] Zamponi F, *Packing close and loose* , Nature vol. 453 , (2008), pp. 606-607.

[33] Callister W, Materials Science and Engineering, John Wiley& Sons, 2007.

[34] Knight J B, Fandrich C G, Lau C N, Jaeger H M and Nagel S R, *Density relaxation in a vibrated granular materials* Physical Review E, vol. 51, no. 5, (1995), pp. 3957-3963.

[35] Nowak E R, Knight J B, Ben-Naim E, Jaeger H M and Nagel S R, *Density fluctuations in vibrated granular materials*, Physical Review E, vol. 57, no. 2, (1998), pp. 1971-1982.

[36] Zhang N, and Rosato A D, *Experiments and simulations on vibration induced densification of bulk solids*, Kona, vol. 24, (2006), pp. 93-103.

[37] Martin W T, Huntley J M, Wildman R D, *Hydrodynamics model for a vibrofluidized granular bed*, Journal of Fluid Mechanics, vol. 535, (2005), pp. 325-345.

[38] Ohtsuki T, Ohsawa, *Hydrodynamics for convection in vibrating beds of cohesionless granular materials*, Journal of Physical Society of Japan, vol. 72, no. 8, (2003), pp. 1963-1967.

[39] Goldhirsch I, *Rapid granular flow*, Annual Review of Fluid Mechanics, vol. 35, (2003), pp. 267-293.

[40] Yang M Y, *Development of master design curves for particle impact dampers*, PhD Thesis, The Pennsylvania State University, 2003.

[41] Papalou A, Masri S F, *Response of impact dampers with granular materials under random excitation*, Earthquake Engineering & Structural Dynamics, vol. 25, (1996), pp. 253-267.

[42] Panossian H V, *Structural damping enhancement via non-obstructive particle damping technique*, ASME Journal of Vibration and Acoustics vol. 114, (1992), pp. 101–105.

[43] Panossian H V, *Non-obstructive particle damping: new experiences and capabilities*, Proceedings of the 49th AIAA/ASME/ASCE/AHS/ASC, Structures, Structural Dynamics and Materials Conference, 2008.

[44] Ramachandran S, Lesieutre G, *Dynamics and performance of a harmonically excited vertical impact damper*, Journal of Vibration and Acoustic Transaction of the ASME, vol. 130(2):11, (2008), DOI: 10.1115/1.2827364.

[45] Popplewell N, Liao M, *A simple design procedure for optimum impact dampers*, Journal of Sound and Vibration, vol. 146(3), (1991), pp. 519-526.

[46] Li K, Darby A, *Experiments on the effect of an impact damper on a multiple-degree-of-freedom system*, Journal of Vibration and control, vol. 12(5), (2006), pp. 445-464.

[47] Wang B, Yang M, *Damping of honeycomb sandwich beams*, Journal of Material Processing Technology, vol. 105, (2000), pp. 67-72.

[48] Maley S, *Particulate Enhanced Damping of Sandwich Structures*, PhD Thesis, Purdue University, 2001.

[49] Simonian S S, Camelo V, and Sienkiewicz J, *Disturbance suppression using particle damping,* Proceeding of the 49th AIAA/ASME/ASCE/AHS/ASC Structures, Structural Dynamics and Materials Conference, April 2008.

[50] Simonian S S, Camelo V, and Sienkiewicz J, *Jitter suppression using particle damping*, Proceeding of the 48th AIAA/ASME/ASCE/AHS/ASC Structures, Structural Dynamics and Materials Conference, April 2007.

[51] Simonian S, Camelo V, Brennan S, Abbruaaese N, Gualta B, *Particle damping application for shock and acoustic environment attenuation*, 49th AIAA/ASME/ASCE/AHS/ASC Structures, Structural Dynamics and Materials Conference, April 2008.

[52] Bai X M, Shah B, Keer L M, Wang Q J, Sunrr R Q, *Particle dynamics simulations of a piston-based particle damper,* Powder Technology, vol. 189(1), (2009), pp. 115-125.

[53] Papalou A, Masri S.F, *Performance of particle dampers under random excitation,* Journal of Vibration and Acoustic Transactions of the ASME, vol. 118(4), (1996), pp. 614-621.

[54] Papalou A, Masri S F, *Response of impact dampers with granular materials under random excitation,* Earthquake Engineering and Structural Dynamics, vol. 25(3), (1996), pp. 253-267.

[55] Papalou A, Masri S F, *An experimental investigation of particle dampers under harmonic excitation*, Journal of Vibration and Control, vol. 4(4), (1998), pp. 361-379.

[56] Fowler B L, Flint E M, Olson S.E., *Design methodology for particle damping,* Proceeding of SPIE International Symposium on Smart Structure and Materials: Damping and Isolation, Newport Beach CA, vol. 4331, (2001), pp. 186-197.

[57] Ibrahim R.A, *Vibro-Impact Dynamics, Modelling, Mapping and Applications,* vol. 43, Springer. Berlin, Heidelberg, 2009.

[58] Lu Z, Lu X, Masri S F, *Studies of the performance of particle dampers under dynamic loads,* Journal of Sound and Vibration, vol. 329, (2010), pp. 5415-5433.

[59] Hollkamp J J, Gordon R W, *Experiments with particle damping,* Proceeding of SPIE International Symposium on Smart Structure and Materials: Damping and Isolation, vol. 3327, (1998), PP. 2-12.

[60] Friend R D, Kinra V K, *Measurement and analysis of particle impact damping* ,Proceeding of SPIE International Symposium on Smart Structure and Materials: Damping and Isolation, vol. 3672, (1999), pp. 20-31.

[61] Friend R D, Kinra V K, *Particle impact damping*, Journal of Sound and Vibration, vol. 233, no.1, (2000), pp. 93-118.

[62] Marhadi K S, Kinra V K, *Particle impact damping: effect of mass ratio, material, and shape,* Journal of Sound and Vibration, vol. 283, (2005), pp. 433-448.

[63] Liu W, Tomlinson G R., Rongong J A., *The dynamic characterisation of disk geometry particle dampers,* Journal of Sound and Vibration, vol. 280, (2005), pp. 849-861.

[64] Rongong J A., Tomlinson G R, *Amplitude dependent behaviour in the application of particle dampers to vibrating structures,* Proceedings of the 46thAIAA/ASME/ASCE/AHS/ASC Structures, Structural Dynamics, and Materials Conference, AIAA, 2005-2327 Austin, Texas, USA, 2005.

[65] Liu W, Tomlinson G R, Worden K, *Nonlinearity study of particle dampers*, International Conference on Noise and Vibration Engineering, ISMA Leuven Belgium, vol. I, (2002), pp. 495-499.

[66] Saeki M, *Analytical study of multi-particle damping*, Journal of sound and vibration, vol. 281, (2005), pp. 1133-1144.

[67] Witt B L, Kinra V K, *Particle impact damping in the horizontal plane,* Proceedings of the 47thAIAA/ASME/ASCE/AHS/ASC Structures, Structural Dynamics, and Materials Conference, AIAA, 2006-2209 Newport, Rhode Island, USA, 2006.

[68] Fowler B L, Flint E M, Olson S E, *Effectiveness and predictability of particle damping,* Proceeding of SPIE International Symposium on Smart Structure and Materials: Damping and Isolation, Newport Beach CA, vol. 3989, (2000), pp. 356-367.

[69] Poschel T, Schwager T, *Computational Granular Dynamics*, Springer, Berlin, 2005.

[70] Herrmann H J, Luding S, *Modelling granular media on the computer*, Continuum Mech. Thermodynamic, vol. 10, (1998), pp. 189-231.

[71] Cundall P Strack O, *A discrete numerical model for granular assemblies*, Geotechnique vol. 29, (1979), pp. 47–65.

[72] Cundall P, *Formulation of a three-dimensional Distinct Element Model–Part I. A scheme to detect and represent contacts in a system composed of many polyhedral blocks*, International Journal of Rock Mechanics and Mining Sciences&Geomechanics Abstracts, vol. 25 (3), (1988), pp.107–116.

[73] Matchett A J, Yanagida T, Okudaira Y, Kobayashi S, *Vibration powder beds: a comparison of experimental and distinct element method simulated data*, Powder Technology, vol. 107, no. 1-2, (2000), pp. 13-30.

[74] Saeki M, *Impact damping with granular materials in a horizontally vibrating system*, Journal of Sound and Vibration, vol. 251, no.1, (2002), pp.153-161.

[75] Saluena C, Esipov S E, Poschel T, Simonian S, *Dissipative properties of granular ensembles*, Proceeding of the SPIE conference on Smart Structures and Materials, Passive Damping and Isolation, vol. 3327, (1998), pp.19-26.

[76] Chen T, Mao K, Huang X, Wang M Y, *Dissipation mechanisms of non-obstructive particle damping using discrete element method*, Proceeding of SPIE International Symposium on Smart Structures and Materials: Damping and Isolation, Newport beach, CA, 2001.

[77] Mao K, Wang M Y, Xu Z, Chen T, *Simulation and characterization of particle damping in transient vibrations*, Transactions of the ASME, vol. 126, (2004), pp. 202–211.

[78] Masson S, Martinez J, *Effect of particle mechanical properties on silo flow and stresses from distinct element simulation*, Powder Technology, vol. 109,(2000), pp. 167-178.

[79] Gonzalez C, Montellano F, Ayuga J, Ooi J Y, *Discrete element modelling of grain flow in a planar silo: Influence of simulation parameters*, Granular Matter, vol. 13, (2011a), pp. 149-158.

[80] Gonzalez C M, Montellano F, Ramirez A, Gallego E, Ayuga F, *Validation and experimental calibration of 3D discrete element models for the simulation of the discharge flow in silos*, Chemical Engineering Science, vol. 66(21), (2011b), pp. 5116-5126 .

[81] Yang S-C, Hsiau S-S, *The simulation and experimental study of granular materials discharged from a silo with the placement of inserts,* Powder Technology, vol. 120(3), (2001), pp. 244-255.

[82] Ramirez A, Nelsen J, Ayuga F, *On the use of plate-type normal pressure cells in silos, Part 2: validation for pressure measurements,* Computer and Electronics in Agriculture, vol. 71(1), (2010), pp. 64-70.

[83] Hartl J, Ooi J Y, *Experiments and simulations of direct shear tests: porosity, contact friction and bulk friction,* Granular Matter, vol. 10(4), (2008), 263-271.

[84] Gonzalez C M, Fuentes J.M, Ayuga T.E, Ayuga F, *Determination of the mechanical properties of maize grains and olives required for use in DEM simulations,* Journal of Food Engineering, vol. 111, (2012), pp. 553-562.

[85] Ketterhagen W R, Curtis J S, Wassgren C.R, Hancock B.C, *Modelling granular segregation in flow from quasi-three-dimensional, Wedge-shaped hoppers,* Powder Technology, vol. 179(3), (2008), pp. 126-143.

[86] Owen P, Cleary P, *Prediction of screw conveyor performance using the discrete element method (DEM),* Powder Technology, vol.193(3), (2009), pp. 274-288.

[87] Boac J M, Maghirang R G, Casada M E, Wilson J D, Jung Y S, *Size distribution and rate of dust generated during grain elevator handling*, Applied Engineering in Agriculture, vol. 25(4), (2009), pp. 533-541.

[88] Van Zeebroeck M, Lombaert G, Dintwa E, Ramon E, Degrande G, Tijskens E, *The simulation of the impact damage to fruit during the passage of a truck over a speed bump by means of the discrete element method,* Biosystems Engineering , vol. 101(1), (2008), pp. 58-68.

[89] Van Zeebroeck, Tijskens E, Dintwa E, Kafashan J, Loodts J, Baerdemaeker J, Ramon J, *The discrete element method (DEM) to simulate fruit impact damage during transport and handling: model building and validation of DEM to predict bruise damage of apples, Post harvest Biology and Technology,* vol. 41 (1), (2006), pp. 85-91.

[90] Nashif A D, Jones D I, Henderson J P, Vibration Damping, Wiley-Interscience, 1985.

[91] Ferry J D, Viscoelastic properties of Polymers, John Wiely & Sons, 1980.

[92] Bourinet M J, Houedec L D, *A dynamic stiffness analysis of damped tubes filled with granular material,* Computer and structures, vol. 73, (1999), pp. 395-406.

[93] Oyadiji S O, *Damping of vibration of hollow beams using viscoelastic spheres,* Proceeding of Smart Structure and Materials, Damping and Isolation, San Diego, SPIE vol. 2720, (1996), pp. 89-98.

[94] Walton K, *The effective elastic moduli of a random packing of spheres,* Journal of Mech. Phys. Solids, vol. 35, no 2, (1987), pp. 213-226.

[95] Fricke J R, *Lodengraf damping- an advanced vibration damping technology,* Journal of Sound and Vibration, vol. 34(7), (2000), pp. 22-27.

[96] Cremer L, Heckel M, Structure-Borne Sound, Springer, Berlin, 1973.

[97] Richards E J, Lenzi A, *On the prediction of impact noise,* VII: the structural damping of machinery, Journal of Sound and Vibration, vol. 97(4), (1984), pp. 549-586.

[98] Varanasi K K, Nayfeh S A, *Damping of flexural vibration using low-density, low-wave-speed media,* Journal of Sound and Vibration, vol. 292, (2006), pp. 402-414.

[99] House J R, *Damping hollow tubular structures with lightweight spheres,* Polymeric Materil Science and Engineering, vol. 60, (1989), pp. 734-738.

[100] Tschoegl W, The phenomenological theory of linear viscoelastic behaviour, Springer-Verlag, 1989.

[101] Garibaldi O, Viscoelastic material damping technology, Printed Torino, Italy, 1996.

[102] DTA Dynamic testing Agency, Dynamic testing of Materials, vol. 1, UK, 1996

[103] Rao S S, Yap F.F, Mechanical vibration, Pearson Education, 2010.

[104] Johnson K L, Contact Mechanics, Cambridge University Press, Cambridge 1985.

[105] Stronge W.J, Impact Mechanics, Cambridge University Press, 2000.

[106] Coaplen J, Stronge W.J, Ravani B, *Work equivalent composite coefficient of restitution,* International Journal of Impact Engineering, vol. 30(6), (2004), pp. 581-591.

[107] ANSYS,Inc. Release 13.0, Manual, 2010.

[108] Mindlin R.D, Deresiewicz H, *Elastic spheres in contact under varying oblique forces,* ASME Journal of Applied Mechanics, vol. 20, (1953), pp. 327-344.

[109] Tsuji Y, Tanaka T, Ishida T, *Lagrangian numerical simulation of plug flow of cohesionless particles in a horizontal pipe,* Powder Technology, vol. 71, (1992), pp. 239-250.

[110] Vu-Quoc L, Zhang X, *An accurate and efficient tangential force-displacement model for elastic frictional contact in particle-flow simulation,* Mechanics of Materials, vol. 31, (1999), pp.235-269.

[111] Vu-Quoc L, Zhang X, Lesburg L, *Normal and tangential force displacement relations for frictional elasto-plastic contact of spheres,* Journal of Solids and Structures, vol. 38, (2001), pp. 6455-6489.

[112] Kenneth G, Mc Connell, Vibration testing, John Wiley&sons Inc, 1995.

[113] Snowdon J C, Vibration and Shock in Damped Mechanical Systems, Wiley, New York, 1968.

[114] Itasca Consulting Group INC, PFC 4D V4.0 manual, Minneapolis/ Minnesota/ USA, 2008.

[115] Tschoegl N W, Knauss W G, Emeri I*, Poisson's ratio in linear viscoelasticity-a critical review,* Mechanics of Time-Dependent Materials, vol. 6(1), (2002), pp. 3-51.

[116] Grosch K A, *The relation between the friction and visco-elastic properties of rubber,* Proceeding of the Royal Society of London Series A25, vol. 274, no. 1356, (1963), pp. 21-39.

[117] Saltelli A. *et al,* Global Sensitivity Analysis, John Wiley &sons Inc, 2008.

Appendix-A

Collected test data from viscoanalyser test machine for blue elastomer. (measurements at ±70°C)

```
-METRAVIB
\blue ball mast 16 9 2011.fva Version
Measurement date; 16/09/2011
Solicitation type: Tension-compression;
Dim. (mm): H = 13.64 E = 3.34 L = 3.92; 5;
T; °C
Dyn str.;sans
Freq;Hz
E';Pa
Tan delta;sans
Measurement n¦; 1
;-69.9;0.0008;1;2.44643e+009;0.265665
;-69.9;0.0008;1.50597;2.66698e+009;0.230579
;-69.9;0.0008;2.26793;2.84726e+009;0.205311
;-69.9;0.0008;3.41543;2.999e+009;0.186412
;-69.9;0.0008;5.14352;3.1562e+009;0.169379
;-69.9;0.0008;7.74597;3.2711e+009;0.160001
;-69.9;0.0008;11.6652;3.40182e+009;0.146325
;-69.9;0.0008;17.5673;3.52896e+009;0.135851
;-69.9;0.0008;26.4558;3.63472e+009;0.125075
;-69.9;0.0008;39.8415;3.71546e+009;0.115688
;-69.9;0.0008;60;3.69395e+009;0.114944
;-64.9;0.0008;1;1.40375e+009;0.486136
;-64.9;0.0008;1.50597;1.60918e+009;0.437725
;-64.9;0.0008;2.26793;1.77965e+009;0.399823
;-64.9;0.0008;3.41543;1.96379e+009;0.363617
;-64.9;0.0008;5.14352;2.13432e+009;0.332259
;-64.9;0.0008;7.74597;2.31994e+009;0.300683
;-64.9;0.0008;11.6652;2.53583e+009;0.266224
;-64.9;0.0008;17.5673;2.69916e+009;0.24489
;-64.9;0.0008;26.4558;2.85825e+009;0.221465
;-64.9;0.0008;39.8415;2.95966e+009;0.207167
;-64.9;0.0008;60;3.01827e+009;0.194268
;-59.9;0.0008;1;6.06679e+008;0.736142
;-59.9;0.0008;1.50597;7.27309e+008;0.691049
;-59.9;0.0008;2.26793;8.73025e+008;0.642162
;-59.9;0.0008;3.41543;1.02581e+009;0.59519
;-59.9;0.0008;5.14352;1.20084e+009;0.546503
;-59.9;0.0008;7.74597;1.38212e+009;0.50312
;-59.9;0.0008;11.6652;1.5629e+009;0.460799
;-59.9;0.0008;17.5673;1.78862e+009;0.413301
;-59.9;0.0008;26.4558;1.91078e+009;0.391011
;-59.9;0.0008;39.8415;2.1245e+009;0.346922
;-59.9;0.0008;60;2.21431e+009;0.329197
;-54.9;0.0008;1;2.73047e+008;0.911365
;-54.9;0.0008;1.50597;3.24644e+008;0.869827
;-54.9;0.0008;2.26793;3.90724e+008;0.829184
```

;-54.9;0.0008;3.41543;4.72912e+008;0.788237
;-54.9;0.0008;5.14352;5.81576e+008;0.742874
;-54.9;0.0008;7.74597;7.03753e+008;0.699722
;-54.9;0.0008;11.6652;8.15949e+008;0.66545
;-54.9;0.0008;17.5673;9.81745e+008;0.617972
;-54.9;0.0008;26.4558;1.11205e+009;0.58386
;-54.9;0.0008;39.8415;1.29693e+009;0.537825
;-54.9;0.0008;60;1.38824e+009;0.528594
;-49.9;0.0008;1;1.19387e+008;1.0526
;-49.9;0.0008;1.50597;1.47433e+008;1.01821
;-49.9;0.0008;2.26793;1.845e+008;0.977518
;-49.9;0.0008;3.41543;2.29028e+008;0.933145
;-49.9;0.0008;5.14352;2.86235e+008;0.88655
;-49.9;0.0008;7.74597;3.48387e+008;0.847517
;-49.9;0.0008;11.6652;4.29094e+008;0.806707
;-49.9;0.0008;17.5673;5.20658e+008;0.769469
;-49.9;0.0008;26.4558;5.99198e+008;0.745629
;-49.9;0.0008;39.8415;7.04084e+008;0.725115
;-49.9;0.0008;60;7.46738e+008;0.782487
;-44.9;0.0008;1;5.87394e+007;1.11211
;-44.9;0.0008;1.50597;7.29092e+007;1.09486
;-44.9;0.0008;2.26793;9.03784e+007;1.07669
;-44.9;0.0008;3.41543;1.13102e+008;1.05148
;-44.9;0.0008;5.14352;1.43315e+008;1.0142
;-44.9;0.0008;7.74597;1.81104e+008;0.975753
;-44.9;0.0008;11.6652;2.23976e+008;0.934203
;-44.9;0.0008;17.5673;2.7152e+008;0.901375
;-44.9;0.0008;26.4558;3.30401e+008;0.872766
;-44.9;0.0008;39.8415;3.7758e+008;0.888129
;-44.9;0.0008;60;3.95581e+008;1.09595
;-39.9;0.0008;1;3.15377e+007;1.08302
;-39.9;0.0008;1.50597;3.84753e+007;1.09048
;-39.9;0.0008;2.26793;4.70134e+007;1.09663
;-39.9;0.0008;3.41543;5.87215e+007;1.09645
;-39.9;0.0008;5.14352;7.25111e+007;1.09708
;-39.9;0.0008;7.74597;9.23256e+007;1.07417
;-39.9;0.0008;11.6652;1.15268e+008;1.05374
;-39.9;0.0008;17.5673;1.41725e+008;1.02699
;-39.9;0.0008;26.4558;1.71501e+008;1.02358
;-39.9;0.0008;39.8415;2.01537e+008;1.09884
;-39.9;0.0008;60;2.33128e+008;1.37728
;-34.9;0.0008;1;1.84718e+007;0.997828
;-34.9;0.0008;1.50597;2.21549e+007;1.04217
;-34.9;0.0008;2.26793;2.63076e+007;1.06105
;-34.9;0.0008;3.41543;3.20615e+007;1.08934
;-34.9;0.0008;5.14352;4.03557e+007;1.10027
;-34.9;0.0008;7.74597;5.00899e+007;1.11265
;-34.9;0.0008;11.6652;6.09124e+007;1.11479
;-34.9;0.0008;17.5673;7.53348e+007;1.1136
;-34.9;0.0008;26.4558;8.70853e+007;1.16912
;-34.9;0.0008;39.8415;9.8473e+007;1.44701
;-34.9;0.0008;60;1.49695e+008;1.34696
;-29.9;0.0008;1;1.1341e+007;0.877997
;-29.9;0.0008;1.50597;1.32578e+007;0.943222

;-29.9;0.0008;2.26793;1.55561e+007;0.989725
;-29.9;0.0008;3.41543;1.86135e+007;1.03356
;-29.9;0.0008;5.14352;2.27251e+007;1.07513
;-29.9;0.0008;7.74597;2.80084e+007;1.09685
;-29.9;0.0008;11.6652;3.38276e+007;1.12298
;-29.9;0.0008;17.5673;4.08555e+007;1.13212
;-29.9;0.0008;26.4558;4.62893e+007;1.26645
;-29.9;0.0008;39.8415;5.57249e+007;1.62415
;-29.9;0.0008;60;8.54059e+007;1.31886
;-26.9;0.0008;1;8.50986e+006;0.832947
;-26.9;0.0008;1.50597;9.83433e+006;0.884363
;-26.9;0.0008;2.26793;1.16703e+007;0.923923
;-26.9;0.0008;3.41543;1.36715e+007;0.979269
;-26.9;0.0008;5.14352;1.65908e+007;1.03777
;-26.9;0.0008;7.74597;2.0001e+007;1.07676
;-26.9;0.0008;11.6652;2.40823e+007;1.1073
;-26.9;0.0008;17.5673;2.91367e+007;1.12428
;-26.9;0.0008;26.4558;3.14576e+007;1.31592
;-26.9;0.0008;39.8415;4.16944e+007;1.55523
;-26.9;0.0008;60;6.10701e+007;1.32221
;-23.9;0.0008;1;6.79115e+006;0.729382
;-23.9;0.0008;1.50597;7.67625e+006;0.789417
;-23.9;0.0008;2.26793;8.95782e+006;0.855765
;-23.9;0.0008;3.41543;1.04522e+007;0.913116
;-23.9;0.0008;5.14352;1.24037e+007;0.980625
;-23.9;0.0008;7.74597;1.47447e+007;1.0332
;-23.9;0.0008;11.6652;1.76723e+007;1.08434
;-23.9;0.0008;17.5673;2.16301e+007;1.10302
;-23.9;0.0008;26.4558;2.28214e+007;1.32972
;-23.9;0.0008;39.8415;3.16778e+007;1.46338
;-23.9;0.0008;60;4.21121e+007;1.31995
;-20.9;0.0008;1;5.68933e+006;0.608988
;-20.9;0.0008;1.50597;6.18501e+006;0.691287
;-20.9;0.0008;2.26793;7.07827e+006;0.754482
;-20.9;0.0008;3.41543;8.01554e+006;0.830752
;-20.9;0.0008;5.14352;9.51105e+006;0.912708
;-20.9;0.0008;7.74597;1.10287e+007;0.97033
;-20.9;0.0008;11.6652;1.32623e+007;1.03127
;-20.9;0.0008;17.5673;1.60355e+007;1.06742
;-20.9;0.0008;26.4558;1.6194e+007;1.34109
;-20.9;0.0008;39.8415;2.35373e+007;1.36902
;-20.9;0.0008;60;3.02082e+007;1.30425
;-17.9;0.0008;1;4.72483e+006;0.530874
;-17.9;0.0008;1.50597;5.18304e+006;0.585285
;-17.9;0.0008;2.26793;5.8356e+006;0.66306
;-17.9;0.0008;3.41543;6.51319e+006;0.729575
;-17.9;0.0008;5.14352;7.591e+006;0.805177
;-17.9;0.0008;7.74597;8.67473e+006;0.881963
;-17.9;0.0008;11.6652;1.0212e+007;0.958289
;-17.9;0.0008;17.5673;1.21726e+007;1.0038
;-17.9;0.0008;26.4558;1.17727e+007;1.33188
;-17.9;0.0008;39.8415;1.78489e+007;1.27042
;-17.9;0.0008;60;2.21598e+007;1.26538
;-14.9;0.0008;1;4.26915e+006;0.424301

;-14.9;0.0008;1.50597;4.5928e+006;0.50102
;-14.9;0.0008;2.26793;5.04507e+006;0.564347
;-14.9;0.0008;3.41543;5.59097e+006;0.633238
;-14.9;0.0008;5.14352;6.26197e+006;0.701761
;-14.9;0.0008;7.74597;7.16906e+006;0.792271
;-14.9;0.0008;11.6652;8.17805e+006;0.861884
;-14.9;0.0008;17.5673;9.50814e+006;0.9206
;-14.9;0.0008;26.4558;9.15798e+006;1.28788
;-14.9;0.0008;39.8415;1.39433e+007;1.17238
;-14.9;0.0008;60;1.67894e+007;1.19811
;-11.9;0.0008;1;3.89749e+006;0.386476
;-11.9;0.0008;1.50597;4.1197e+006;0.427865
;-11.9;0.0008;2.26793;4.43438e+006;0.479843
;-11.9;0.0008;3.41543;4.87687e+006;0.555522
;-11.9;0.0008;5.14352;5.39529e+006;0.62115
;-11.9;0.0008;7.74597;6.06934e+006;0.69118
;-11.9;0.0008;11.6652;6.94542e+006;0.777293
;-11.9;0.0008;17.5673;7.93517e+006;0.840142
;-11.9;0.0008;26.4558;7.25948e+006;1.24718
;-11.9;0.0008;39.8415;1.11446e+007;1.06882
;-11.9;0.0008;60;1.30875e+007;1.11364
;-8.9;0.0008;1;3.65231e+006;0.304654
;-8.9;0.0008;1.50597;3.79586e+006;0.356337
;-8.9;0.0008;2.26793;4.06632e+006;0.408613
;-8.9;0.0008;3.41543;4.36586e+006;0.470014
;-8.9;0.0008;5.14352;4.84669e+006;0.547128
;-8.9;0.0008;7.74597;5.34673e+006;0.615336
;-8.9;0.0008;11.6652;5.98505e+006;0.69072
;-8.9;0.0008;17.5673;6.77448e+006;0.751286
;-8.9;0.0008;26.4558;6.26256e+006;1.1572
;-8.9;0.0008;39.8415;9.16477e+006;0.968058
;-8.9;0.0008;60;1.06758e+007;1.02925
;-5.9;0.0008;1;3.3647e+006;0.259482
;-5.9;0.0008;1.50597;3.54514e+006;0.309983
;-5.9;0.0008;2.26793;3.76869e+006;0.350661
;-5.9;0.0008;3.41543;4.06163e+006;0.410206
;-5.9;0.0008;5.14352;4.32456e+006;0.467725
;-5.9;0.0008;7.74597;4.76014e+006;0.540841
;-5.9;0.0008;11.6652;5.29206e+006;0.608432
;-5.9;0.0008;17.5673;5.84407e+006;0.672368
;-5.9;0.0008;26.4558;5.41821e+006;1.08258
;-5.9;0.0008;39.8415;7.88401e+006;0.883508
;-5.9;0.0008;60;9.00261e+006;0.954293
;-2.9;0.0008;1;3.23877e+006;0.241191
;-2.9;0.0008;1.50597;3.37458e+006;0.265928
;-2.9;0.0008;2.26793;3.51185e+006;0.301796
;-2.9;0.0008;3.41543;3.76998e+006;0.355434
;-2.9;0.0008;5.14352;4.00255e+006;0.407509
;-2.9;0.0008;7.74597;4.36365e+006;0.475708
;-2.9;0.0008;11.6652;4.77967e+006;0.535161
;-2.9;0.0008;17.5673;5.27828e+006;0.598639
;-2.9;0.0008;26.4558;4.79236e+006;1.00254
;-2.9;0.0008;39.8415;6.78097e+006;0.792165
;-2.9;0.0008;60;7.79383e+006;0.879095

;0;0.0008;1;3.07312e+006;0.203682
;0;0.0008;1.50597;3.2054e+006;0.237399
;0;0.0008;2.26793;3.35253e+006;0.269794
;0;0.0008;3.41543;3.54018e+006;0.306861
;0;0.0008;5.14352;3.73025e+006;0.358735
;0;0.0008;7.74597;4.05317e+006;0.414757
;0;0.0008;11.6652;4.3013e+006;0.468072
;0;0.0008;17.5673;4.68543e+006;0.527646
;0;0.0008;26.4558;4.40123e+006;0.941181
;0;0.0008;39.8415;6.04254e+006;0.716945
;0;0.0008;60;6.73702e+006;0.785848
;3;0.0008;1;2.98621e+006;0.185453
;3;0.0008;1.50597;3.11729e+006;0.215315
;3;0.0008;2.26793;3.20839e+006;0.235093
;3;0.0008;3.41543;3.36137e+006;0.270967
;3;0.0008;5.14352;3.50702e+006;0.309712
;3;0.0008;7.74597;3.7981e+006;0.35792
;3;0.0008;11.6652;4.02228e+006;0.419572
;3;0.0008;17.5673;4.32387e+006;0.470634
;3;0.0008;26.4558;4.02413e+006;0.872527
;3;0.0008;39.8415;5.37683e+006;0.644064
;3;0.0008;60;6.0488e+006;0.715888
;6;0.0008;1;2.92734e+006;0.18362
;6;0.0008;1.50597;2.97828e+006;0.19032
;6;0.0008;2.26793;3.10044e+006;0.214123
;6;0.0008;3.41543;3.24772e+006;0.240831
;6;0.0008;5.14352;3.41773e+006;0.276742
;6;0.0008;7.74597;3.52508e+006;0.314876
;6;0.0008;11.6652;3.77987e+006;0.36315
;6;0.0008;17.5673;4.01917e+006;0.41332
;6;0.0008;26.4558;3.83486e+006;0.791169
;6;0.0008;39.8415;4.87373e+006;0.571309
;6;0.0008;60;5.47007e+006;0.649953
;9;0.0008;1;2.84466e+006;0.160034
;9;0.0008;1.50597;2.90827e+006;0.176978
;9;0.0008;2.26793;3.00564e+006;0.19298
;9;0.0008;3.41543;3.1854e+006;0.213544
;9;0.0008;5.14352;3.28342e+006;0.246939
;9;0.0008;7.74597;3.38382e+006;0.274449
;9;0.0008;11.6652;3.62349e+006;0.323611
;9;0.0008;17.5673;3.79648e+006;0.367956
;9;0.0008;26.4558;3.64988e+006;0.731147
;9;0.0008;39.8415;4.53449e+006;0.514826
;9;0.0008;60;4.89636e+006;0.587181
;12;0.0008;1;2.75685e+006;0.155068
;12;0.0008;1.50597;2.84296e+006;0.163757
;12;0.0008;2.26793;2.95172e+006;0.176156
;12;0.0008;3.41543;3.07775e+006;0.191637
;12;0.0008;5.14352;3.12347e+006;0.221255
;12;0.0008;7.74597;3.33366e+006;0.252868
;12;0.0008;11.6652;3.45276e+006;0.28699
;12;0.0008;17.5673;3.6203e+006;0.32558
;12;0.0008;26.4558;3.53921e+006;0.659807
;12;0.0008;39.8415;4.23279e+006;0.459592

;12;0.0008;60;4.61801e+006;0.525084
;15;0.0008;1;2.74451e+006;0.144904
;15;0.0008;1.50597;2.78414e+006;0.162127
;15;0.0008;2.26793;2.86818e+006;0.169589
;15;0.0008;3.41543;2.99363e+006;0.178096
;15;0.0008;5.14352;3.06787e+006;0.198601
;15;0.0008;7.74597;3.17607e+006;0.230849
;15;0.0008;11.6652;3.35501e+006;0.256263
;15;0.0008;17.5673;3.48543e+006;0.290219
;15;0.0008;26.4558;3.39942e+006;0.622077
;15;0.0008;39.8415;3.99992e+006;0.412211
;15;0.0008;60;4.35385e+006;0.475641
;18;0.0008;1;2.71417e+006;0.137911
;18;0.0008;1.50597;2.7493e+006;0.143832
;18;0.0008;2.26793;2.81522e+006;0.156365
;18;0.0008;3.41543;2.90298e+006;0.168309
;18;0.0008;5.14352;3.03266e+006;0.182604
;18;0.0008;7.74597;3.12105e+006;0.200611
;18;0.0008;11.6652;3.21925e+006;0.231362
;18;0.0008;17.5673;3.39455e+006;0.263476
;18;0.0008;26.4558;3.30946e+006;0.582094
;18;0.0008;39.8415;3.85696e+006;0.366768
;18;0.0008;60;4.03073e+006;0.433242
;21;0.0008;1;2.52652e+006;0.140891
;21;0.0008;1.50597;2.63192e+006;0.133763
;21;0.0008;2.26793;2.733e+006;0.148455
;21;0.0008;3.41543;2.80771e+006;0.155385
;21;0.0008;5.14352;2.9035e+006;0.170651
;21;0.0008;7.74597;2.97661e+006;0.188567
;21;0.0008;11.6652;3.05072e+006;0.213275
;21;0.0008;17.5673;3.2351e+006;0.23804
;21;0.0008;26.4558;3.18614e+006;0.55824
;21;0.0008;39.8415;3.63523e+006;0.336049
;21;0.0008;60;3.77742e+006;0.394889
;24;0.0008;1;2.53708e+006;0.141422
;24;0.0008;1.50597;2.64344e+006;0.133058
;24;0.0008;2.26793;2.69842e+006;0.14377
;24;0.0008;3.41543;2.75773e+006;0.149353
;24;0.0008;5.14352;2.86633e+006;0.160287
;24;0.0008;7.74597;2.93272e+006;0.173461
;24;0.0008;11.6652;3.05536e+006;0.194115
;24;0.0008;17.5673;3.13732e+006;0.217481
;24;0.0008;26.4558;3.15818e+006;0.53569
;24;0.0008;39.8415;3.52213e+006;0.305557
;24;0.0008;60;3.65821e+006;0.357557
;27;0.0008;1;2.52735e+006;0.134121
;27;0.0008;1.50597;2.58627e+006;0.128316
;27;0.0008;2.26793;2.67887e+006;0.135929
;27;0.0008;3.41543;2.73839e+006;0.142166
;27;0.0008;5.14352;2.83108e+006;0.153474
;27;0.0008;7.74597;2.89663e+006;0.158194
;27;0.0008;11.6652;2.96387e+006;0.181748
;27;0.0008;17.5673;3.11709e+006;0.197836
;27;0.0008;26.4558;3.06024e+006;0.505526

;27;0.0008;39.8415;3.4408e+006;0.272397
;27;0.0008;60;3.51703e+006;0.322594
;30;0.0008;1;2.47393e+006;0.129554
;30;0.0008;1.50597;2.57977e+006;0.123908
;30;0.0008;2.26793;2.63585e+006;0.135715
;30;0.0008;3.41543;2.73753e+006;0.136171
;30;0.0008;5.14352;2.79622e+006;0.144789
;30;0.0008;7.74597;2.85494e+006;0.155185
;30;0.0008;11.6652;2.97655e+006;0.167969
;30;0.0008;17.5673;3.05117e+006;0.181551
;30;0.0008;26.4558;3.06937e+006;0.47678
;30;0.0008;39.8415;3.37193e+006;0.246628
;30;0.0008;60;3.44716e+006;0.29175
;33;0.0008;1;2.4876e+006;0.125113
;33;0.0008;1.50597;2.60068e+006;0.126989
;33;0.0008;2.26793;2.61885e+006;0.125502
;33;0.0008;3.41543;2.7317e+006;0.132572
;33;0.0008;5.14352;2.75677e+006;0.138911
;33;0.0008;7.74597;2.86597e+006;0.143872
;33;0.0008;11.6652;2.91616e+006;0.155931
;33;0.0008;17.5673;2.96795e+006;0.168576
;33;0.0008;26.4558;2.9129e+006;0.452275
;33;0.0008;39.8415;3.30868e+006;0.226339
;33;0.0008;60;3.356e+006;0.264642
;40;0.0008;1;2.37373e+006;0.124278
;40;0.0008;1.50597;2.40569e+006;0.130359
;40;0.0008;2.26793;2.50431e+006;0.125062
;40;0.0008;3.41543;2.58644e+006;0.122531
;40;0.0008;5.14352;2.70972e+006;0.13137
;40;0.0008;7.74597;2.75499e+006;0.140992
;40;0.0008;11.6652;2.78196e+006;0.142638
;40;0.0008;17.5673;2.9263e+006;0.147415
;40;0.0008;26.4558;2.87103e+006;0.418627
;40;0.0008;39.8415;3.14336e+006;0.192114
;40;0.0008;60;3.18074e+006;0.220106
;45;0.0008;1;2.36965e+006;0.110084
;45;0.0008;1.50597;2.43288e+006;0.128461
;45;0.0008;2.26793;2.49365e+006;0.122791
;45;0.0008;3.41543;2.56429e+006;0.121615
;45;0.0008;5.14352;2.61763e+006;0.127835
;45;0.0008;7.74597;2.73496e+006;0.129125
;45;0.0008;11.6652;2.76312e+006;0.131394
;45;0.0008;17.5673;2.83077e+006;0.135401
;45;0.0008;26.4558;2.89941e+006;0.399877
;45;0.0008;39.8415;3.10685e+006;0.175142
;45;0.0008;60;3.13182e+006;0.193202
;50;0.0008;1;2.35423e+006;0.111177
;50;0.0008;1.50597;2.3331e+006;0.109377
;50;0.0008;2.26793;2.41673e+006;0.108034
;50;0.0008;3.41543;2.50675e+006;0.115717
;50;0.0008;5.14352;2.56869e+006;0.120261
;50;0.0008;7.74597;2.66883e+006;0.122438
;50;0.0008;11.6652;2.68064e+006;0.130474
;50;0.0008;17.5673;2.72025e+006;0.134105

;50;0.0008;26.4558;2.72538e+006;0.39915
;50;0.0008;39.8415;3.02443e+006;0.161466
;50;0.0008;60;2.99318e+006;0.172941
;55;0.0008;1;2.3209e+006;0.0955062
;55;0.0008;1.50597;2.29311e+006;0.113515
;55;0.0008;2.26793;2.34012e+006;0.122267
;55;0.0008;3.41543;2.39203e+006;0.116723
;55;0.0008;5.14352;2.49011e+006;0.112016
;55;0.0008;7.74597;2.52259e+006;0.124094
;55;0.0008;11.6652;2.64268e+006;0.123335
;55;0.0008;17.5673;2.65244e+006;0.123799
;55;0.0008;26.4558;2.85375e+006;0.353614
;55;0.0008;39.8415;2.96623e+006;0.152058
;55;0.0008;60;2.85656e+006;0.161654
;60;0.0008;1;2.14955e+006;0.0968308
;60;0.0008;1.50597;2.26946e+006;0.10467
;60;0.0008;2.26793;2.30227e+006;0.121965
;60;0.0008;3.41543;2.42109e+006;0.114501
;60;0.0008;5.14352;2.39905e+006;0.125124
;60;0.0008;7.74597;2.51792e+006;0.11996
;60;0.0008;11.6652;2.53419e+006;0.124598
;60;0.0008;17.5673;2.65044e+006;0.1236
;60;0.0008;26.4558;2.6923e+006;0.385177
;60;0.0008;39.8415;2.85715e+006;0.144813
;60;0.0008;60;2.84221e+006;0.153063
;65;0.0008;1;2.21457e+006;0.0877976
;65;0.0008;1.50597;2.20698e+006;0.0983884
;65;0.0008;2.26793;2.29629e+006;0.0940718
;65;0.0008;3.41543;2.39751e+006;0.10848
;65;0.0008;5.14352;2.40376e+006;0.1188
;65;0.0008;7.74597;2.54231e+006;0.111586
;65;0.0008;11.6652;2.55422e+006;0.121792
;65;0.0008;17.5673;2.56205e+006;0.12277
;65;0.0008;26.4558;2.53309e+006;0.392058
;65;0.0008;39.8415;2.8686e+006;0.14141
;65;0.0008;60;2.75138e+006;0.145907
;70;0.0008;1;2.24252e+006;0.0831961
;70;0.0008;1.50597;2.21821e+006;0.107659
;70;0.0008;2.26793;2.21736e+006;0.100886
;70;0.0008;3.41543;2.29806e+006;0.1042
;70;0.0008;5.14352;2.34919e+006;0.107964
;70;0.0008;7.74597;2.44361e+006;0.112224
;70;0.0008;11.6652;2.46079e+006;0.117407
;70;0.0008;17.5673;2.49472e+006;0.122848
;70;0.0008;26.4558;2.46234e+006;0.380232
;70;0.0008;39.8415;2.76519e+006;0.140112
;70;0.0008;60;2.67953e+006;0.141457

Appendix-B

Natural frequencies and effective masses of solid viscoelastic material (used in Chapter 4).

MODE	FREQUENCY	EFFECTIVE MASS	MODE	FREQUENCY	EFFECTIVE MASS
1	67.03	3.02E-01	41	134.84	1.49E-28
2	70.91	5.82E-28	42	136.11	1.94E-27
3	77.54	2.33E-28	43	137.38	4.11E-26
4	78.15	2.63E-27	44	137.82	1.41E-04
5	82.73	4.21E-24	45	138.21	6.12E-26
6	83.10	1.55E-02	46	139.80	1.18E-29
7	85.87	2.89E-26	47	140.40	3.51E-06
8	87.60	1.10E-28	48	140.78	1.70E-29
9	89.81	8.71E-30	49	145.43	1.94E-27
10	90.25	3.06E-26	50	145.60	7.44E-29
11	93.51	2.44E-26	51	146.80	1.61E-29
12	94.63	2.64E-03	52	147.17	2.80E-05
13	95.65	7.34E-30	53	148.12	8.03E-04
14	100.35	1.45E-26	54	148.74	5.62E-05
15	101.50	6.01E-25	55	148.74	2.38E-27
16	101.79	2.46E-02	56	149.24	2.88E-26
17	102.64	3.52E-31	57	150.94	5.60E-31
18	105.11	3.95E-26	58	152.06	4.90E-25
19	106.09	2.19E-24	59	153.14	4.84E-24
20	106.66	8.92E-03	60	154.77	4.11E-26
21	108.33	1.15E-02	61	154.99	2.63E-23
22	108.90	5.61E-27	62	156.92	1.34E-02
23	110.44	2.66E-27	63	156.96	8.26E-26
24	113.87	2.68E-26	64	157.06	1.40E-23
25	115.27	7.59E-30	65	159.55	3.00E-25
26	115.72	1.99E-02	66	159.66	1.50E-04
27	117.39	6.99E-30	67	161.02	1.08E-30
28	117.57	1.64E-31	68	162.57	2.42E-23
29	118.38	4.48E-05	69	164.19	1.13E-23
30	120.09	4.51E-03	70	165.18	1.37E-02
31	122.60	1.35E-29	71	165.43	3.16E-02
32	122.80	3.81E-24	72	166.09	2.55E-05
33	123.50	3.18E-03	73	166.44	9.34E-29
34	126.05	1.16E-27	74	167.62	1.76E-27
35	127.48	1.09E-26	75	168.27	8.74E-27
36	128.35	1.28E-25	76	168.65	2.02E-30
37	130.64	1.25E-29	77	168.73	1.84E-28
38	131.21	1.16E-25	78	169.19	1.32E-25
39	132.97	2.25E-27	79	169.47	4.86E-29
40	133.79	4.52E-30	80	170.44	2.59E-07

MODE	FREQUENCY	EFFECTIVE MASS	MODE	FREQUENCY	EFFECTIVE MASS
81	171.81	6.59E-29	121	194.72	1.54E-04
82	172.06	4.74E-25	122	194.89	8.57E-24
83	172.90	5.65E-25	123	195.64	1.08E-23
84	173.36	8.88E-26	124	196.09	1.05E-03
85	173.71	1.18E-30	125	196.90	3.54E-23
86	174.52	1.36E-28	126	197.99	8.52E-26
87	174.68	8.15E-27	127	198.06	8.97E-29
88	175.33	2.61E-03	128	198.50	3.97E-27
89	175.59	1.16E-24	129	198.73	1.17E-04
90	176.78	3.92E-05	130	199.31	1.15E-04
91	177.41	3.57E-30	131	199.75	1.68E-25
92	178.11	5.20E-04	132	200.04	3.94E-29
93	179.03	8.37E-25	133	200.59	1.02E-04
94	180.41	1.77E-04	134	201.39	2.02E-26
95	180.42	9.85E-20	135	201.83	8.21E-29
96	181.04	2.11E-26	136	201.85	1.97E-26
97	181.14	1.09E-26	137	203.05	1.26E-28
98	182.93	1.95E-28	138	203.62	2.61E-25
99	183.06	8.20E-25	139	203.88	7.09E-25
100	183.37	1.99E-22	140	204.47	1.99E-28
101	183.44	3.38E-03	141	204.96	2.47E-05
102	184.87	3.15E-25	142	205.25	1.34E-29
103	185.14	9.89E-25	143	205.58	5.02E-26
104	185.91	7.27E-04	144	206.08	5.61E-25
105	186.46	2.55E-29	145	206.20	2.68E-28
106	186.63	1.57E-24	146	206.84	4.67E-03
107	187.01	5.19E-29	147	207.83	5.58E-27
108	187.31	4.22E-26	148	207.84	1.57E-25
109	187.86	1.90E-27	149	207.98	6.39E-05
110	189.40	1.88E-29	150	210.25	9.97E-27
111	189.89	6.55E-25	151	210.28	4.36E-25
112	189.90	6.59E-26	152	210.85	4.03E-24
113	190.31	1.92E-03	153	211.68	1.27E-04
114	191.47	2.42E-30	154	211.91	2.89E-23
115	191.94	2.49E-04	155	212.22	7.12E-23
116	193.15	4.26E-32	156	212.69	3.54E-21
117	193.30	2.47E-26	157	213.03	5.33E-22
118	193.60	1.41E-24	158	213.11	6.92E-05
119	194.47	3.39E-30	159	213.14	2.76E-21
120	194.57	1.53E-03	160	213.30	8.47E-22

MODE	FREQUENCY	EFFECTIVE MASS	MODE	FREQUENCY	EFFECTIVE MASS
161	213.34	3.58E-05	202	231.36	1.30E-05
162	213.40	4.25E-21	203	231.54	3.81E-22
163	213.92	3.58E-21	204	232.06	1.86E-04
164	214.64	1.17E-03	205	232.12	8.35E-22
165	215.69	1.08E-20	206	232.30	5.34E-23
166	217.85	1.99E-19	207	232.54	2.88E-21
167	217.97	1.96E-20	208	232.58	4.83E-22
168	218.32	1.53E-18	209	232.63	6.85E-04
169	218.77	4.10E-18	210	232.85	2.71E-22
170	219.56	8.90E-19	211	233.33	1.67E-22
171	219.89	1.24E-18	212	233.59	2.61E-23
172	220.57	6.03E-04	213	233.85	8.66E-22
173	220.75	3.85E-18	214	234.12	1.85E-06
174	222.01	5.65E-04	215	234.57	1.50E-21
175	223.16	5.44E-20	216	234.62	1.97E-21
176	223.47	7.97E-04	217	235.46	8.65E-06
177	223.77	3.69E-18	218	235.94	2.09E-22
178	223.85	2.71E-18	219	236.39	1.44E-22
179	223.98	3.12E-04	220	236.52	5.78E-22
180	224.39	1.55E-18	221	237.08	2.79E-21
181	224.83	6.16E-03	222	237.41	3.56E-22
182	225.24	3.92E-19	223	237.59	2.93E-22
183	225.51	1.26E-20	224	237.76	1.55E-21
184	225.55	1.54E-04	225	237.82	4.41E-06
185	225.84	5.39E-20	226	238.15	4.14E-22
186	225.98	4.32E-18	227	238.39	1.26E-22
187	226.37	1.88E-17	228	239.04	1.85E-04
188	226.50	1.55E-04	229	239.23	3.03E-22
189	227.25	1.48E-20	230	239.26	1.29E-23
190	227.83	4.82E-19	231	239.52	9.12E-22
191	227.86	5.43E-19	232	239.95	1.18E-07
192	228.59	1.76E-19	233	240.08	5.88E-22
193	228.80	2.27E-19	234	240.14	4.71E-22
194	229.38	1.15E-19	235	240.89	3.13E-21
195	229.40	3.73E-04	236	241.84	1.57E-24
196	229.46	1.00E-04	237	241.86	4.31E-20
197	229.67	1.94E-20	238	241.87	1.21E-03
198	229.88	2.79E-22	239	242.30	4.10E-22
199	230.11	1.53E-21	240	243.22	4.61E-22
200	230.11	2.93E-20	241	243.34	4.98E-21
201	230.81	2.05E-21	242	243.37	1.87E-21

MODE	FREQUENCY	EFFECTIVE MASS	MODE	FREQUENCY	EFFECTIVE MASS
243	243.65	1.04E-23	286	255.12	5.01E-22
244	243.68	5.78E-06	287	255.77	2.24E-21
245	244.20	7.17E-22	288	256.41	7.25E-06
246	245.29	2.15E-21	289	256.66	1.47E-05
247	245.44	4.18E-05	290	256.70	1.23E-21
248	245.54	2.52E-22	291	257.72	1.15E-22
249	245.80	2.63E-21	292	257.79	1.36E-21
250	246.32	3.98E-22	293	257.95	2.14E-05
251	246.33	1.27E-21	294	258.18	1.59E-21
252	246.55	8.73E-04	295	258.24	4.84E-21
253	246.97	9.45E-23	296	259.03	2.24E-05
254	247.14	5.00E-06	297	259.09	2.22E-21
255	247.61	2.73E-21	298	259.24	7.42E-21
256	247.79	4.46E-22	299	259.59	1.50E-04
257	248.06	1.45E-03	300	260.06	1.05E-04
258	248.15	4.63E-21	301	260.30	2.81E-22
259	248.36	7.96E-08	302	261.08	5.73E-22
260	248.46	1.37E-21	303	261.12	5.35E-21
261	248.65	9.49E-22	304	261.41	7.90E-21
262	249.03	1.28E-23	305	261.58	9.79E-05
263	249.06	4.33E-22	306	261.66	9.85E-21
264	249.77	1.11E-21	307	262.11	3.48E-22
265	250.02	8.02E-06	308	262.39	2.43E-04
266	250.20	9.77E-21	309	262.58	1.98E-21
267	250.64	1.10E-19	310	262.72	2.47E-21
268	250.65	5.66E-04	311	263.36	6.69E-04
269	251.12	3.01E-08	312	263.36	4.33E-20
270	251.18	3.82E-23	313	263.61	9.60E-21
271	251.21	1.03E-21	314	264.11	2.18E-19
272	251.49	3.50E-06	315	264.12	7.60E-04
273	251.61	2.33E-22	316	264.22	2.43E-22
274	252.78	7.45E-07	317	264.38	2.60E-21
275	252.80	2.82E-21	318	265.33	1.06E-04
276	253.31	4.61E-26	319	265.38	1.22E-21
277	253.44	4.65E-21	320	265.71	1.47E-21
278	253.63	7.06E-22	321	266.07	2.03E-04
279	253.79	4.03E-22	322	266.24	2.21E-21
280	253.82	1.49E-21	323	266.65	1.47E-20
281	253.90	1.20E-22	324	266.78	3.21E-21
282	254.02	3.44E-23	325	267.09	1.29E-21
283	254.32	8.33E-22	326	267.15	8.89E-21
284	254.52	9.29E-22	327	267.74	3.25E-22
285	255.09	6.79E-21	328	268.22	2.95E-20

MODE	FREQUENCY	EFFECTIVE MASS	MODE	FREQUENCY	EFFECTIVE MASS
329	268.26	4.35E-04	371	278.43	2.48E-20
330	268.66	5.72E-21	372	278.75	1.85E-21
331	268.74	6.68E-23	373	279.08	1.75E-03
332	268.90	3.40E-21	374	279.24	2.42E-21
333	269.28	1.44E-20	375	279.67	3.36E-20
334	269.53	1.94E-21	376	279.95	1.17E-04
335	270.08	1.41E-20	377	280.09	3.99E-20
336	270.24	6.57E-04	378	280.21	4.19E-20
337	270.27	2.61E-20	379	280.41	2.19E-21
338	270.50	5.90E-21	380	280.45	6.18E-23
339	270.55	5.22E-03	381	280.89	2.79E-21
340	270.71	4.53E-03	382	280.91	4.23E-20
341	271.16	5.21E-20	383	281.10	3.36E-04
342	271.41	1.36E-21	384	281.76	5.61E-05
343	271.83	5.51E-21	385	281.91	9.58E-20
344	272.18	3.78E-23	386	282.12	5.28E-21
345	272.40	2.10E-22	387	282.18	2.03E-18
346	272.69	1.80E-20	388	282.19	7.10E-21
347	272.74	1.25E-20	389	282.44	1.63E-03
348	273.08	1.84E-20	390	282.45	4.49E-19
349	273.10	1.44E-21	391	282.83	6.44E-20
350	273.32	1.13E-22	392	282.92	2.54E-04
351	273.54	2.43E-20	393	283.04	3.89E-21
352	274.30	1.31E-20	394	283.63	1.05E-19
353	274.50	2.57E-05	395	283.75	2.33E-19
354	274.54	3.71E-21	396	284.20	3.85E-20
355	274.74	5.55E-04	397	284.26	5.46E-19
356	275.10	5.99E-21	398	284.54	3.43E-06
357	275.36	3.87E-23	399	284.72	6.62E-20
358	275.71	1.91E-19	400	284.78	8.62E-19
359	275.72	2.92E-04	401	285.02	2.06E-22
360	275.96	4.25E-20	402	285.26	1.01E-04
361	276.21	2.63E-22	403	285.33	3.00E-19
362	276.42	1.66E-20	404	285.39	3.30E-03
363	276.65	1.18E-21	405	285.50	3.18E-18
364	276.83	1.98E-20	406	285.65	7.36E-05
365	276.84	3.06E-04	407	285.89	3.22E-20
366	277.11	2.95E-20	408	286.22	1.32E-18
367	277.51	2.25E-04	409	286.42	7.65E-06
368	277.77	3.00E-20	410	286.56	9.35E-19
369	277.80	5.31E-20	411	286.65	2.44E-20
370	278.11	2.64E-09	412	286.90	4.35E-19

MODE	FREQUENCY	EFFECTIVE MASS	MODE	FREQUENCY	EFFECTIVE MASS
413	286.92	3.96E-18	459	297.37	2.12E-22
414	287.13	2.65E-05	460	297.44	1.16E-04
415	288.23	5.30E-21	461	297.49	6.14E-25
416	288.28	8.83E-19	462	297.72	5.33E-25
417	288.87	1.80E-20	463	297.87	1.37E-24
418	288.92	5.93E-04	464	298.35	2.16E-07
419	289.13	1.00E-03	465	298.39	7.15E-24
420	289.20	5.91E-19	466	298.58	2.78E-26
421	289.33	2.86E-18	467	298.73	3.44E-23
422	289.64	5.90E-22	468	298.91	4.03E-23
423	289.72	3.95E-04	469	299.17	1.17E-24
424	289.94	1.98E-19	470	299.26	8.86E-24
425	289.95	1.04E-20	471	299.86	5.11E-05
426	290.27	4.20E-19	472	300.00	3.25E-05
427	290.46	1.83E-20	473	300.19	1.45E-23
428	291.01	6.46E-06	474	300.34	4.22E-24
429	291.07	1.01E-18	475	300.59	1.15E-26
430	291.72	7.16E-06	476	300.77	6.49E-23
431	291.92	5.71E-06	477	300.95	2.67E-04
432	292.01	7.51E-20	478	301.43	5.93E-24
433	292.41	6.81E-19	479	301.64	1.52E-06
434	292.47	1.56E-18	480	301.98	1.72E-23
435	292.69	8.05E-21	481	302.06	9.80E-27
436	292.89	3.09E-22	482	302.18	3.35E-25
437	293.22	3.69E-20	483	302.26	1.12E-24
438	293.39	4.75E-05	484	302.47	6.27E-25
439	293.51	2.02E-21	485	302.77	8.30E-24
440	293.58	6.11E-22	486	302.97	4.89E-24
441	293.90	3.59E-05	487	302.98	3.06E-24
442	294.19	5.16E-22	488	303.07	1.40E-23
443	294.37	1.69E-06	489	303.23	2.33E-24
444	294.58	2.26E-23	490	303.38	6.27E-06
445	295.38	7.70E-25	491	304.10	1.13E-23
446	295.53	1.63E-23	492	304.11	2.21E-24
447	295.60	6.39E-23	493	304.20	3.49E-24
448	295.65	1.06E-04	494	304.42	8.06E-06
449	295.73	3.71E-23	495	304.49	2.58E-24
450	295.81	4.07E-22	496	305.36	6.32E-23
451	296.17	7.47E-23	497	305.49	7.48E-05
452	296.48	7.75E-24	498	305.54	1.86E-23
453	296.53	4.50E-23	499	305.66	3.41E-25
454	296.76	5.41E-05	500	305.93	2.41E-23
455	296.89	2.33E-23			
456	297.07	2.17E-22			
457	297.11	1.63E-24			
458	297.20	1.20E-23			

Appendix-C

Prony series with twenty terms and 15°C temperature for viscoelastic spherical particle used in Chapter 5/Section 5.4.2.

n	Prony magnitude parameter g	Prony time τ
1	.10714039e-3	.89615050
2	.20354534e-4	.25395800
3	.77327841e-4	.71968567e-1
4	.10494517e-3	.20395005e-1
5	.18584611e-3	.57796929e-2
6	.27636839e-3	.16378937e-2
7	.61570041e-3	.46415888e-3
8	.11130345e-2	.13153691e-3
9	.23850055e-2	.37275937e-4
10	.47878474e-2	.10563541e-4
11	.10451431e-1	.29935773e-5
12	.19564354e-1	.84834290e-6
13	.39677276e-1	.24040992e-6
14	.59388326e-1	.68129207e-7
15	.96383875e-1	.19306977e-7
16	.12255661	.54713593e-8
17	.14716764	.15505158e-8
18	.15622526	.43939706e-9
19	.14081563	.12451971e-9
20	.19767986	.35287350e-10

Appendix-D

Drawing of lower and upper plates, used for designed test rig to measure particle properties. (Chapter 5/Section 5.5)

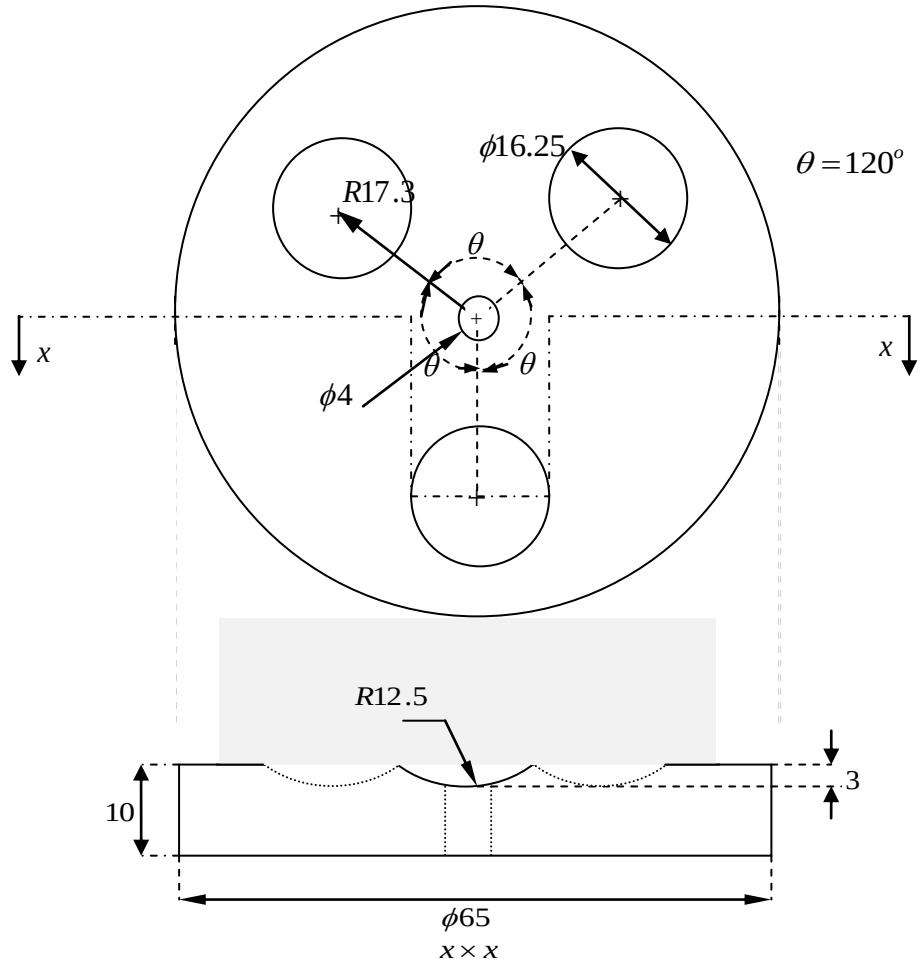

- Dimensions in mm
- Material: Aluminium

Lower plate of test rig

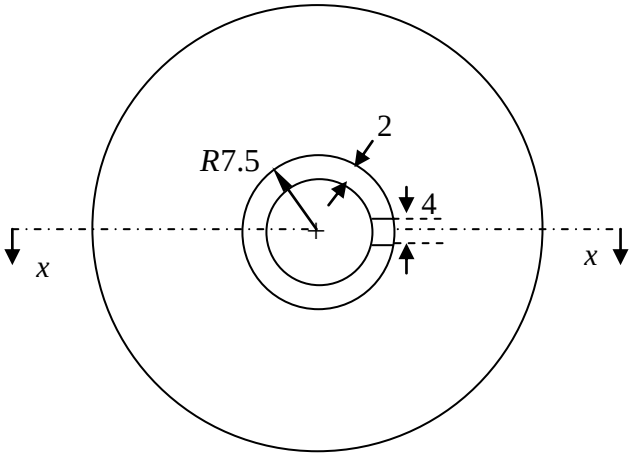

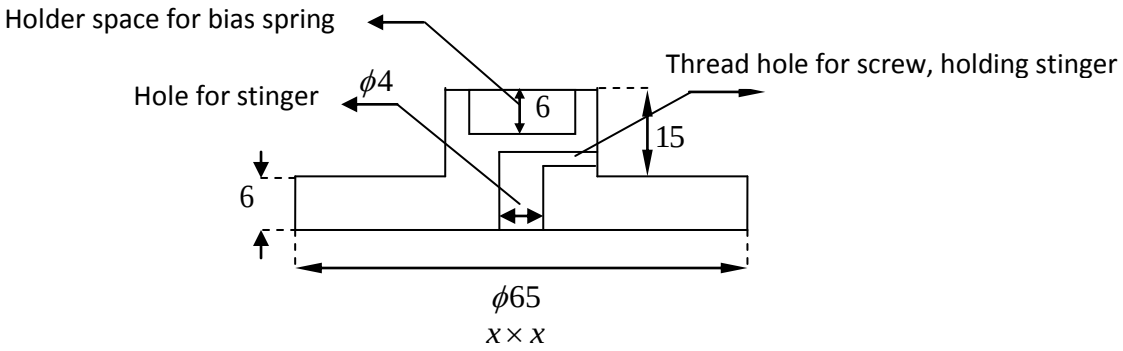

- Dimensions in mm
- Material: Aluminium

Upper plate of test rig

Appendix-E

Material properties for Sorbothane 60 and DC3120. (Chapter 5/Section 5.5)

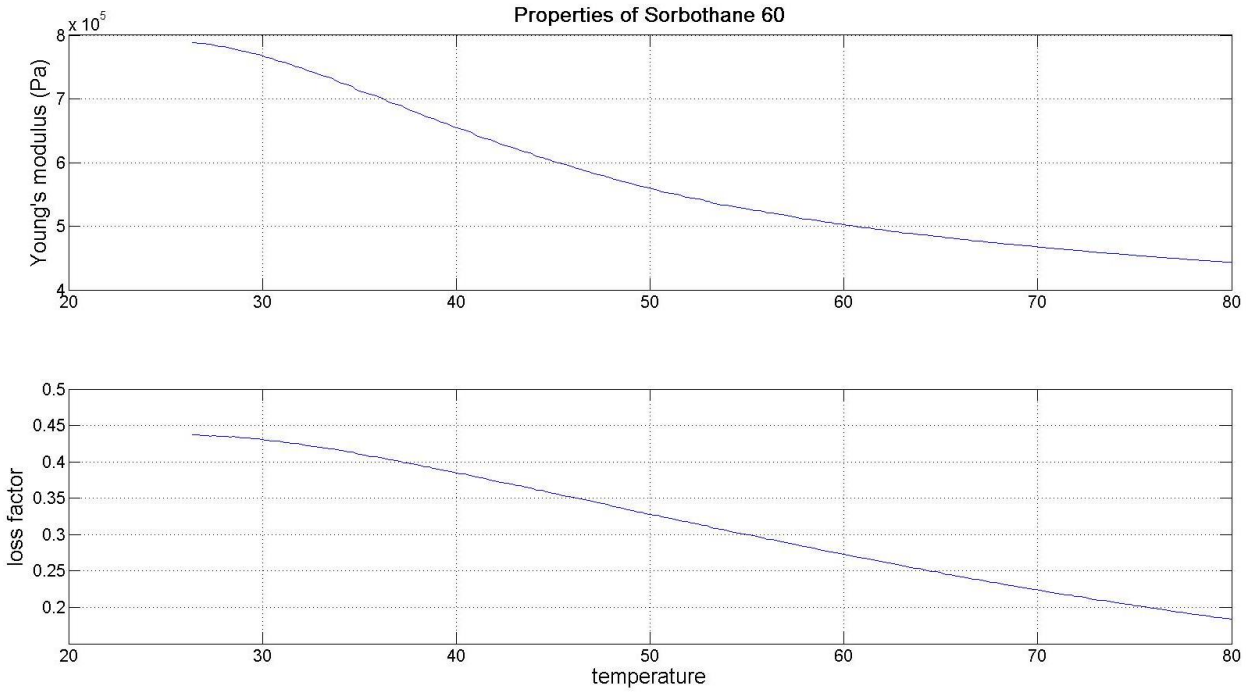

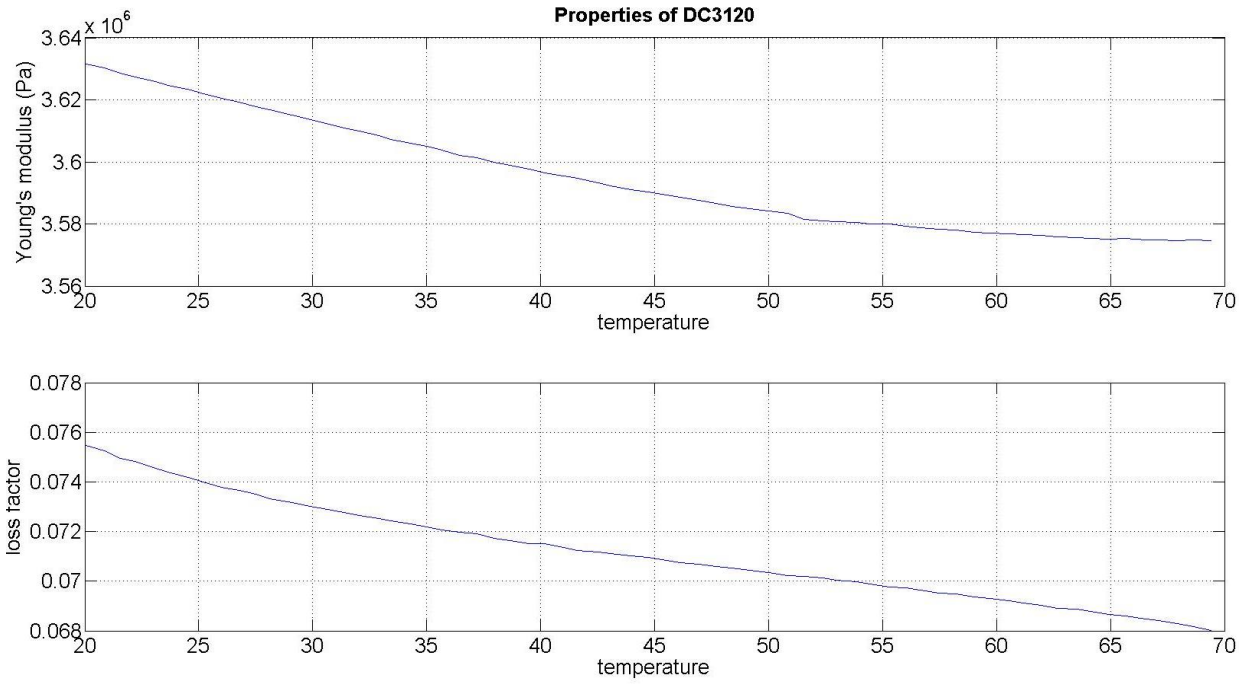

Appendix-F

Equilibrium situation (settling by gravity) for DEM model.

```
--- Previous file has been erased
Pfc3D>return
Pfc3D>call secondstep.dat.txt
Pfc3D>;.........................................(second part of
Pfc3D>;programme)the particles are allowed to fall from ;gravity loading and
Pfc3D>;settle within 60000 time steps   ..............................
Pfc3D>new
--- **************************************************
--- * All model specific information has been cleared *
--- **************************************************
Pfc3D>
Pfc3D>restore firststep.sav
File Created on 10:59:18 Wed Sep 05 2012
 By PFC3D version 4.00-182
 Registered to:

 Job Title:
Pfc3D>set grav 0 0 -9.81
Pfc3D>set time=0.0
Pfc3D>hist ball zvel .08 .06 0
--- History of Z-Velocity at ball 160 ( 7.569e-002, 6.714e-002, 1.365e-002)
Pfc3D>set dt auto
Pfc3D>set plot avi size 640 480
--- Hardcopy device set to AVI bitmap
Pfc3D>;movie avi_open file movie_step.avi
Pfc3D>;movie step 10 1 file movie_step.avi
Pfc3D>;.....................................................................
Pfc3D>
Pfc3D>
Pfc3D>ini rad mul 1.5
--- radius modified in 200 balls
Pfc3D>cycle 50000
 starting cycle:        0      av-unbal force:  0.000e+000
  starting time: 10:59:24     max-unbal force:  0.000e+000
  step      of    total  time-step       time   av-unbal  max-unbal
------ ------- -------- ---------- ---------- ---------- ----------
 50000   50000    50000 1.153e-004 5.793e+000 5.363e-009 1.281e-007
   ending cycle:    50000      av-unbal force:  5.363e-009
    ending time: 10:59:38     max-unbal force:  1.281e-007
Pfc3D>;movie avi_close  file  movie_step.avi
Pfc3D>plot set title text ' box_shaking'
Pfc3D>plot add ball blue
Pfc3D>plot add wall white
Pfc3D>plot add axes brown
Pfc3D>plot show
Pfc3D>save secondstep.sav
+++ File already exists!
--- Previous file has been erased
Pfc3D>return
```

Appendix-G

Loss factor versus Young's modulus, data from DMTA machine for 1-60 Hz frequency. (Chapter 3/Section 3.3.2)

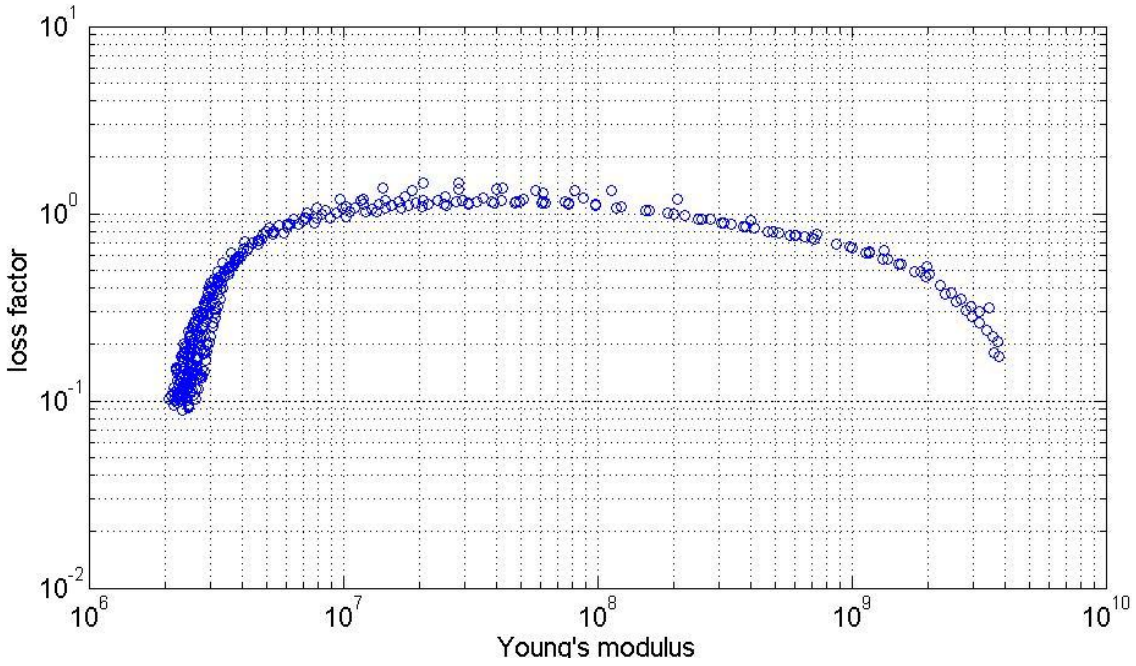

Publications

Darabi B, Rongong J.A, *Polymeric particle dampers under steady-state vertical vibrations,* Journal of Sound and Vibration, vol. 331(14), (2012), pp. 3304-3316.

Darabi B, Rongong J.A, *Amplitude dependent damping from granular viscoelastics,* Journal of Physics: Conference Series, Modern Practice in Stress and Vibration Analysis, MPSV, vol. 382, (2012), doi:10.1088/1742-6595/382/1/012026